
[All ETDs from UAB](#)

[UAB Theses & Dissertations](#)

2023

Development and Evaluation of a Nanomatrix Coated Stent Using a Vascular Sheet With Atherosclerosis Model

Xixi Zhang
University Of Alabama At Birmingham

Follow this and additional works at: <https://digitalcommons.library.uab.edu/etd-collection>

 Part of the [Engineering Commons](#)

Recommended Citation

Zhang, Xixi, "Development and Evaluation of a Nanomatrix Coated Stent Using a Vascular Sheet With Atherosclerosis Model" (2023). *All ETDs from UAB*. 23.
<https://digitalcommons.library.uab.edu/etd-collection/23>

This content has been accepted for inclusion by an authorized administrator of the UAB Digital Commons, and is provided as a free open access item. All inquiries regarding this item or the UAB Digital Commons should be directed to the [UAB Libraries Office of Scholarly Communication](#).

DEVELOPMENT AND EVALUATION OF A NANOMATRIX COATED STENT
USING A VASCULAR SHEET WITH ATHEROSCLEROSIS MODEL

by

XIXI ZHANG

HO-WOOK JUN, COMMITTEE CHAIR
BRIGITTA C. BROTT
JEONGA KIM
GANGJIAN QIN
PALANIAPPAN SETHU

A DISSERTATION

Submitted to the graduate faculty of The University of Alabama at Birmingham,
in partial fulfillment of the requirements for the degree of
Doctor of Philosophy

BIRMINGHAM, ALABAMA

2023

Copyright by
Xixi Zhang
2023

DEVELOPMENT AND EVALUATION OF A NANOMATRIX COATED STENT USING A VASCULAR SHEET WITH ATHEROSCLEROSIS MODEL

XIXI ZHANG

BIOMEDICAL ENGINEERING

ABSTRACT

While cardiovascular stent technology has considerable advances, there are hurdles to overcome due to the dysfunctional stented arteries which fail to maintain vascular homeostasis. Current stent designs ignored the significance of promoting functional artery healing (pro-healing). Therefore, we developed a pro-healing nanomatrix coating for stent. Previous studies investigated its effect on individual vascular cell type. In natural artery, there are multiple vascular cell types that strongly affect stent performance. Thus, an *in vitro* vascular double-layer (VDL) system was used to observe stent effects on different vascular cell types. And the pro-healing ability and mechanism of the nanomatrix coated stent were studied in the VDL and a rabbit model, compared to commercial bare metal stent (BMS) and drug eluting stent (DES). *In vitro* results indicated that this stent coating could 1) improve endothelialization and endothelial functions, 2) regulate smooth muscle cell phenotype to reduce the proliferation and migration, 3) suppress inflammation through a multifactorial manner, and 4) reduce foam cell formation, extracellular matrix remodeling, and calcification. Consistently, *in vivo* results demonstrated that compared with commercial BMS and DES, this pro-healing nanomatrix coated stent enhanced re-

endothelialization with negligible restenosis, inflammation, or thrombosis. Thus, these findings indicate the unique pro-healing feature of this nanomatrix stent coating with superior efficacy.

On the other side, *in vitro* atherosclerosis models are essential to evaluate vascular stent and therapeutics before *in vivo* and clinical studies, but significant limitations remain, such as the lack of three-layer vascular architecture and limited atherosclerotic features. Moreover, no scalable 3D atherosclerosis model is available for making high-throughput therapeutic evaluation. Herein, an *in vitro* 3D three-layer nanomatrix vascular sheet with critical atherosclerosis multi-features (VSA) was developed with endothelial dysfunction, monocyte recruitment, macrophages, extracellular matrix remodeling, smooth muscle cell phenotype transition, inflammatory cytokine secretion, foam cells, and calcification initiation. Notably, a high-throughput functional VSA assay was created and the use of these assays for evaluating atherosclerosis therapeutics was also performed including conventional drugs, therapeutic candidates, and a potential gene therapy. It demonstrated that VSA is a valuable *in vitro* platform for vascular therapeutics and device evaluation with high efficiency and flexibility.

Keywords: nanomatrix, stent, atherosclerosis, drug evaluation, 3D *in vitro* models, vascular sheet

TABLE OF CONTENTS

	Page
ABSTRACT.....	iii
LIST OF FIGURES	vii
LIST OF ABBREVIATIONS.....	x
INTRODUCTION	1
Background Research	1
Limitations of Current Cardiovascular Stents.....	1
Limitations of Stent Evaluation using Animal Model.	2
Significance of Vascular Sheet with Atherosclerotic Features.	2
Prohealing Nanomatrix Stent Coating.	3
Background Studies	4
Specific Aims.....	9
 PRO-HEALING NANOMATRIX COATED STENT ANALYSIS IN AN IN VITRO VASCULAR DOUBLE-LAYER AND IN A RABBIT MODEL	 13
 ATHEROSCLEROTIC THREE-LAYER NANOMATRIX VASCULAR SHEETS FOR HIGH-THROUGHPUT THERAPEUTIC EVALUATION	 68
 CONCLUSIONS.....	126
 FUTURE STUDIES	128

LIST OF REFERENCES	129
APPENDIX.....	132
A IACUC APPROVAL	132
B NON-GLP NON-CLINICAL STUDY PROTOCOL	133

LIST OF FIGURES

<i>Figure</i>	<i>Page</i>
INTRODUCTION	
1 HAEC migration on stent <i>in vitro</i>	6
2 Monocyte response to stent <i>in vitro</i>	7
3 HAEC migration in the microchannel assay	8
4 <i>Ex vivo</i> vessel dilation.....	8
PRO-HEALING NANOMATRIX COATED STENT ANALYSIS IN AN IN VITRO VASCULAR DOUBLE-LAYER AND IN A RABBIT MODEL	
1 Schematic diagram illustrating in vitro study using vascular double layer	19
2 PA-YKNO nanomatrix coating could promote endothelialization while reduce SMC migration <i>in vitro</i>	30
3 PA-YKNO nanomatrix coating could promote the transition of SMC to contractile phenotype <i>in vitro</i>	33

4	PA-YKNO nanomatrix coating could promote the transition of SMC to contractile phenotype <i>in vitro</i>	35
5	PA-YKNO nanomatrix coating could regulate inflammation <i>in vitro</i>	38
6	PA-YKNO nanomatrix coating could administer foam cell formation, ECM remodeling, and calcification <i>in vitro</i>	41
7	Summary of atherosclerotic gene expression in the VDL	42
8	PA-YKNO nanomatrix coating could accelerate stent coverage <i>in vivo</i>	44
9	PA-YKNO nanomatrix coating could improve endothelialization while suppress restenosis, and inflammation <i>in vivo</i>	46

ATHEROSCLEROTIC THREE-LAYER NANOMATRIX VASCULAR SHEETS FOR HIGH-THROUGHPUT THERAPEUTIC EVALUATION

1	Nanomatrix vascular sheet (VS), nanomatrix vascular sheet with atherosclerosis (VSA), and VSA functional assays for therapeutic evaluation	74
2	Development of single-layer nanomatrix VS using nanomatrix sheet technique.....	75
3	Development of double-layer nanomatrix vascular sheet using nanomatrix sheet technique, layer-by-layer assembly and cell-as-glue approach	79
4	Development of three-layer nanomatrix VS using nanomatrix sheet technique, layer-by-layer assembly and cell-as-glue approach	81
5	Induction of endothelial dysfunction and monocyte recruitment on the three-layer nanomatrix VS	83
6	Induction of macrophage formation, foam cell generation, and calcification initiation on the three-layer nanomatrix	

	vascular sheet	89
7	The development and use of VSA high-throughput functional assays for drug evaluation.....	92
8	Evaluation of Rosuvastatin and Sirolimus using VSA high-throughput functional assays	95
9	Evaluation of Curcumin and Colchicine using VSA high-throughput functional assays	98
10	Evaluation of miR146a-loaded liposomes (Lip-miR-146a) using VSA high-throughput functional assays	101

LIST OF ABBREVIATIONS

CD14	Cluster of Differentiation 14
CD68	Cluster of Differentiation 68
CDKN2A	Cyclin-dependent Kinase Inhibitor 2A
COL3A1	Collagen Type III Alpha 1
COL17A1	Collagen Type XVII Alpha 1
CVDs	Cardiovascular Diseases
DAF-FM	(4-Amino-5-Methylamino-2',7'-Difluorofluorescein) Diacetate
DCFH-DA	Dichlorofluorescein Diacetate
ECM	Extracellular Matrix
ELISA	Enzyme-Linked Immunosorbent Assay
eNOS	Endothelial Nitric Oxide Synthase
GM-CSF	Granulocyte-Macrophage Colony-Stimulating Factor
hAAF	Primary Human Aortic Adventitial Fibroblasts

hAEC	Human Aortic Endothelial Cells
hAoSMC	Human Aortic Artery Smooth Muscle Cells
HTS	High Throughput Drug Screening
ICAM-1	Intercellular Adhesion Molecule 1
IFN- γ	Interferon- γ
IL-1 α	Interleukin 1 α
IL-1 β	Interleukin 1 β
IL-4	Interleukin 4
IL-6	Interleukin 6
IL-8	Interleukin 8
IL-10	Interleukin 10
M-CSF	Macrophage Colony-Stimulating Factor
MCP-1	Monocyte Chemoattractant Protein-1
MYH-11	Muscle Myosin Heavy Chain 11
NOX4	Nicotinamide Adenine Dinucleotide Phosphate Oxidase 4

OOCC	Organ on a Chip
ox-LDL	Oxidized Low-Density Lipoprotein
PA	Peptide Amphiphile
PDGF-B	Platelet-derived Growth Factor Subunit B
PECAM-1	Platelet Endothelial Cell Adhesion Molecule-1
RNA	Ribonucleic Acid
ROS	Reactive Oxygen Species
RT-PCR	Real-Time Polymerase Chain Reaction
RUNX2	Runt-Related Transcription Factor 2
TCP	Tissue Culture Plate
TEBV	Tissue-engineered Blood Vessel
TGF- β 1	Transforming Growth Factor Beta 1
TNF- α	Tumor Necrosis Factor- α
VCAM-1	Vascular Cell Adhesion Molecule 1
VEGF-A	Vascular Endothelial Growth Factor A

VS Vascular Sheet

VSA Tissue-engineered Three-layer Vascular Sheet with Critical
Atherosclerosis Multi-features

INTRODUCTION

Background Research

Limitations of Current Cardiovascular Stents

Stents are implanted during the percutaneous treatment of narrowed arteries.¹ However, limitations and unresolved questions remain how to achieve optimal stent patency and safety.²⁻⁸ Bare metal stent (**BMS**) deployment remains limited by neointimal hyperplasia caused by vascular injury during stent implantation, leading to in-stent restenosis.⁹ To reduce restenosis, drug-eluting stents (**DES**), coated with anti-proliferative and/or immuno-suppressive agents targeting neointimal hyperplasia, have been developed.¹⁰ In general, these DES release sirolimus, everolimus, or paclitaxel and reduce the risk of restenosis by approximately 50% compared with BMS.¹¹⁻¹⁶ However, recent studies have revealed that the clinically used dose of those agents for DES cause serious adverse effects including 1) damage to the endothelium that delays re-endothelialization with impaired functions, 2) inflammation in response to the polymer coating, and 3) the persistent risk of late thrombosis.²⁻⁸ Additionally, patients are often required to take prolonged dual anti-platelet therapy.⁵ Thus, there remains a significant

clinical need for an innovative stent coating that can enhance re-endothelialization, while suppressing neointimal hyperplasia, thrombosis, and inflammation.

Limitations of Stent Evaluation using Animal Model

Another major issue in the stent industry is that outcomes from healthy animal model studies with or without balloon injury do not adequately predict problems found when stents are used in a large number of patients.^{17, 18} Balloon injury rabbit and swine models described by the FDA have been used to evaluate stent safety and efficacy.¹⁷ However, physical endothelial denudation by balloon injury does not reflect the complex clinical disease conditions such as endothelial dysfunction, inflammation, and foam cells that are observed in stent patients with atherosclerosis. The main reason leading to “overly optimistic” preclinical results is that the preclinical balloon injury rabbit or pig model lacks a disease-mimicking environment. These models are unable to predict clinically reported complications such as delayed re-endothelialization, excess inflammation, and late stent thrombosis.^{8, 18} In summary, the balloon injury healthy animal model does not reflect the disease conditions of stent patients with atherosclerosis. Therefore, there is a critical need to develop an innovative strategy for stent coating and stent evaluation in an atherosclerosis model in order to address **1)** adverse effects of current clinical dose of sirolimus and **2)** “overly optimistic” findings when evaluating stents in a healthy rabbit model.

Significance of Vascular Sheet with Atherosclerotic Features

In-stent restenosis, inflammation, and thrombosis continue to afflict the deployment of BMS and DES implanted in patients with atherosclerosis.¹⁹ However, the current balloon injury healthy animal models cannot provide atherosclerosis like environments to evaluate stent performance.²⁰ Therefore, it is imperative to develop *in vitro* and *in vivo* atherosclerosis mimicking environments. During atherosclerosis development and stent integration in the artery with plaque, vascular homeostasis greatly depends on the regulation of two primary vascular components- endothelium and tunica media, which are composed of endothelial cells, smooth muscle cells, and extracellular matrix (ECM).²¹ However, in most current *in vitro* atherosclerosis studies, a single type of cell of interest or simply mixing several types of cells on a tissue culture plate are commonly used, which do not replicate the proper pathogenesis of atherosclerosis. Thus, a 3-layered Vascular Sheets with Atherosclerotic features (**VSA**) should be developed with key pro-atherosclerotic cytokines, colony stimulating factors, monocytes, and Ox-LDL. The VSA will contain major features of atherosclerosis (endothelial dysfunction, sustained inflammation, and foam cell accumulation) that might stimulate in stent restenosis, thrombosis, and stent failure. Then, the VSA will be used to evaluate the efficacy of the prohealing nanomatrix coated stent compared with commercially available BMS and DES. Outcomes of stent evaluation with the VSA can provide valuable information about potential clinical stent performance on endothelial cells and smooth muscle cells with atherosclerosis features.

Prohealing Nanomatrix Stent Coating

Having a healthy endothelium is crucial to reduce complications, and an ideal stent coating should possess a multifunctional and biocompatible endothelium mimicking coating to facilitate re-endothelialization.^{22, 23} In nature, the healthy endothelium plays a critical role in regulating the function of the cardiovascular system: it 1) secretes the vascular tone modulator and vasodilator- nitric oxide (NO), 2) suppresses smooth muscle cell proliferation and regulates vessel remodeling, and 3) minimizes thrombosis and inflammation.²²⁻²⁴ Thus, an ideal stent coating strategy should focus on rapidly restoring the endothelium by use of a prohealing and multifunctional coating. In order to overcome the limitations of commercial BMS and DES, we successfully developed the prohealing multifunctional endothelium nanomatrix stent coating by incorporating nitric oxide (NO) producing peptide amphiphiles (PAs) capable of providing the chemical and biological properties of the endothelium as demonstrated in *Circulation*, *JACC*, *ACS Applied Materials & Interfaces*, *Acta Biomaterialia*, *Scientific Reports*, *Adv Drug Deliv Rev*, *Advanced Materials*, *ACS Nano*.²⁵⁻³⁶ (20 publications with 12 directly related, 8 supported, and 3 under review). Previous studies have evaluated improved effect of the prohealing nanomatrix on individual vascular cell type *in vitro* compared with commercial BMS and DES. Following this, the study here will further evaluate and study the therapeutic effect with the existence of all major vascular cell types under diseased condition *in vitro* and in a rabbit balloon injury model *in vivo*, with the hope to inspire upgraded stent coating design.

Background Studies

Synthesis and Characterization of Prohealing Multifunctional Endothelium

Mimicking Nanomatrix:³⁷ Two peptide amphiphiles (PAs) were successfully synthesized: PA-YIGSR [$\text{CH}_3(\text{CH}_2)_{14}\text{CONH-GTAGLIGQ-YIGSR}$] and PA-KKKKK [$\text{CH}_3(\text{CH}_2)_{14}\text{CONH-GTAGLIGQ-KKKKK}$]. The PAs contain enzyme-mediated degradable MMP-2 sensitive sequences along with either YIGSR or a polylysine (KKKKK) group to form NO donating residues. TEM images showed that PA-YK (90:10 mol/mol) and PA-YK-NO self-assembled into nanofibers with uniform diameters between 7-8 nm and several microns in length. PA-YK was reacted with NO gas to form PA-YKNO. The NO release profile from the PA-YKNO was evaluated using the Griess assay and instantaneous NO release was also confirmed using the Chemiluminescence assay. Successful NO release was found as a burst in the first 48 hours, followed by a slower sustained release over a period of 60 days, resulting in recovery of 90.8% of NO.^{27, 37}

Multifunctional effects of the NO releasing nanomatrix on endothelialization, smooth muscle cells, inflammatory responses, and platelet adhesion:^{31, 32} Importantly, the proliferation of smooth muscle cells, which is one of the key events in restenosis, begins as early as one day after stent-induced injury. Therefore, we showed highly desired release kinetics in that the 48 hour burst release of NO is critical to arrest neointimal hyperplasia. The following slow sustained release over a longer period is required to maintain the non-proliferative state of smooth muscle cells, anti-thrombogenicity of the vessel wall, and enhanced endothelialization during the recovery period, which may take a few weeks. HUVECs on the PA-YKNO nanomatrix showed significantly enhanced proliferation. Conversely, hAoSMCs showed a decreased proliferative response on PA-YKNO

nanomatrix. Platelet adhesion was dramatically reduced on the PA-YK and the PA-YKNO compared to Collagen I and stainless steel. This result indicates that the PA-YKNO nanomatrix prevents platelet adhesion which may contribute to limiting late thrombosis.³¹

In addition, PA-YKNO coated stents were deployed on a stable confluent monolayer of human aortic endothelial cells (hAECs) seeded on fibronectin-coated glass slides under an arterial physiological flow rate of 10 dyne/cm². The PA-YKNO coated stents greatly promoted hAEC migration on the stents and the migrated hAECs almost covered the complete surface of the stents after 7 days (**Figure. 1b**). However, a control group,

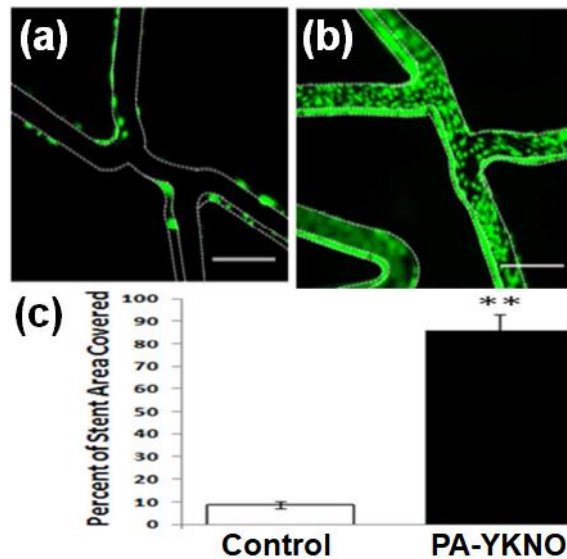


Figure 1. hAEC migration on (a) bare metal stent Control and (b) PA-YKNO coated stents at 7 days; Calcein Staining. (c) Percent stent area covered by hAECs at 7 days. Scale bar: 300 μ m, **p<0.001

uncoated bare metal stents, barely promoted hAEC migration and only a few hAECs covered the stent surface (**Figure. 1a**). These results demonstrate the prohealing ability of the PA-YKNO nanomatrix coated stent under physiological flow, indicating its potential for rapid re-endothelialization. The NO releasing nanomatrix also demonstrated the inhibition of inflammatory responses and platelet adhesion. Monocyte adhesion to TNF- α

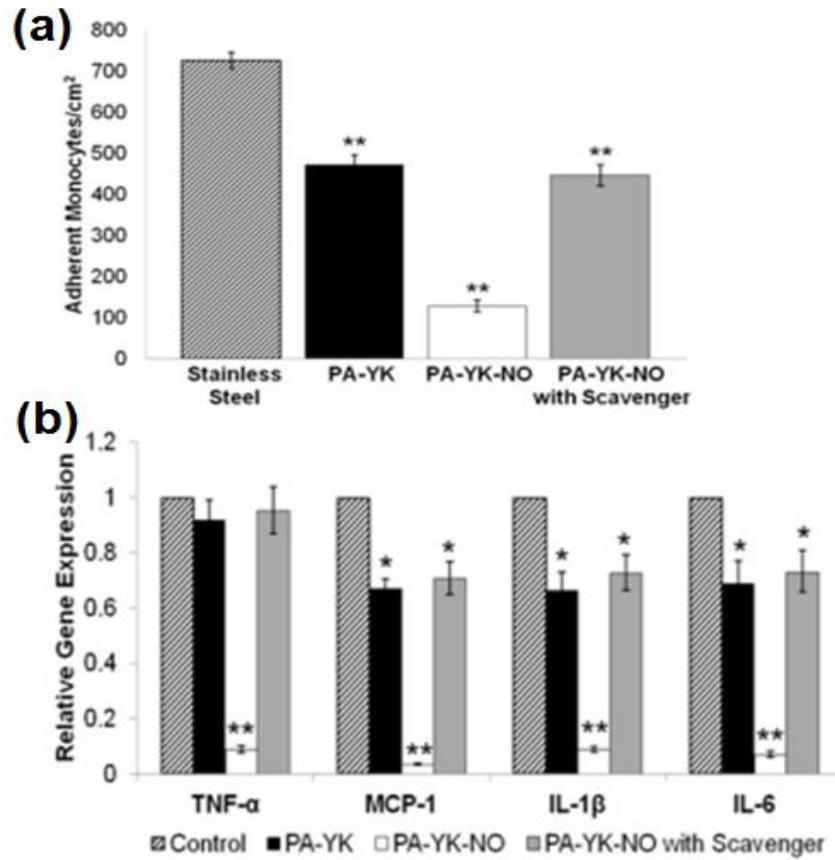


Figure 2. (a). Monocyte adhesion under physiological flow with TNF- α stimulation at 4 hours. (b). Monocyte inflammatory gene expression at 1 day. * $p < 0.01$. ** $p < 0.001$.

stimulated HUVECs cultured on stainless steel, PA-YK, and PA-YKNO nanomatrix was evaluated under arterial physiological flow rate of 10 dyne/cm² (**Figure. 2a**). Monocyte adhesion was significantly reduced on TNF- α stimulated HUVECs cultured on PA-YKNO; this exhibits the protective effects of NO against inflammatory cell adhesion to endothelial cells, even in an inflammatory environment. Monocyte inflammatory gene expression (TNF- α , MCP-1, IL-1 β , and IL-6) was further evaluated using qRT-PCR analysis (**Figure. 2b**). All four inflammatory gene expression levels were significantly decreased on PA-YKNO compared to both bare and PA-YK groups after 1 day, revealing the profound protective effects of NO against inflammatory responses.³² Cell migration was also

evaluated using a microchannel migration system (**Figure. 3**): Two polydimethylsiloxane (PDMS) chambers was connected by a narrow dual microchannel narrow system and then filled with media. In Figure 4, it was demonstrated that PA-YKNO promotes more migration of hAECs.

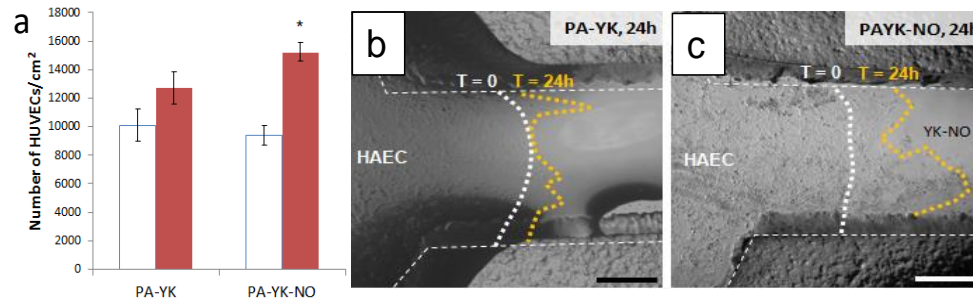


Figure 3. (a) hAEC proliferation after 1 (white line) and 4 (red line) days and microchannel migration assay of hAECs at 24 hours. (b) PA-YK control. (c) PA-YKNO.

Vasodilation effects of the NO releasing nanomatrix:³² NO is well-known for its role as a vasodilator and regulator of cardiovascular vessel diameter. The bioactivity of the

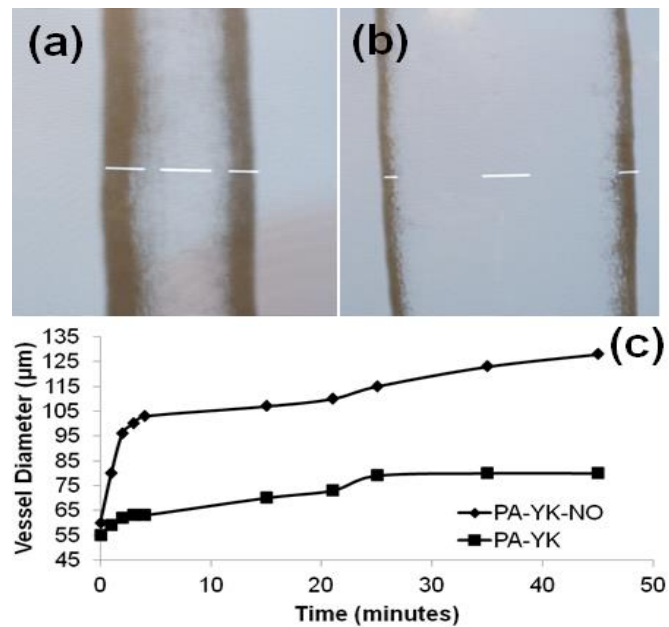


Figure 4. *Ex vivo* vessel dilation. (a) Vessel before and (b) after nanomatrix addition. (c) Vessel diameter after nanomatrix addition.

nanomatrix coating was evaluated *ex vivo* in vasoconstricted rat mesenteric arterioles (**Fig. 4**). Following arteriole excision, cannulation, and stable constriction with phenylephrine, PA-YKNO nanomatrix and PA-YK nanomatrix coated coverslips were added to the vessel

dilation chamber. The control PA-YK without NO did not elicit a vasodilatory response. The PA-YKNO nanomatrix coated coverslip quickly dilated the arteriole and maintained the dilated state, yielding an increase in diameter of 114% over its baseline constricted value (**Fig. 4b,c**).³²

Specific Aims

Stents are the most commonly implanted devices used in the treatment of cardiovascular diseases. Bare metal stent (BMS) use remains limited by high rates of in-stent restenosis that is a result of neointimal proliferation in response to vessel injury during stent deployment.⁹ To address this, drug-eluting stents (DES) coated with anti-proliferative agents such as everolimus have been developed to reduce restenosis by targeting the biochemical pathways of neointimal hyperplasia.^{2, 10} However, sirolimus released from DES is associated with a higher risk of endothelial apoptosis, incomplete re-endothelialization, and late stent thrombosis.^{2-9, 11, 38} Another major issue for the stent industry is that outcomes from the preclinical balloon induced healthy rabbit and juvenile pig models described by the FDA^{12, 17} do not adequately predict problems found when stents are used in patients with atherosclerosis.¹⁸ The main reason leading to “overly optimistic” preclinical results is that the balloon induced healthy rabbit and pig models do not reflect endothelial dysfunction, inflammation, and foam cell accumulation that are observed in stent patients with atherosclerosis. In order to overcome limitations of stents, we developed the prohealing endothelium mimicking nanomatrix stent coating by

incorporating nitric oxide (NO) producing peptide amphiphiles (PAs) as demonstrated *in vitro* and *ex vivo*, which showed that the prohealing nanomatrix coated stent exhibited improved endothelialization, reduced inflammation, and reduced smooth muscle cell proliferation with vessel dilation (**Fig. 1-4**). To explore the mechanism of therapeutic effect of PA-YKNO, the study here will further evaluate the prohealing nanomatrix coated stent in a layered vascular structure with endothelial cell, smooth muscle cell, monocytes, and foam cells *in vitro*, and in a balloon injured iliac artery model *in vivo*.

On the other side, *in vitro* atherosclerosis models are essential to evaluate therapeutics before *in vivo* and clinical studies, but significant limitations remain, such as the lack of three-layer vascular architecture and limited atherosclerotic features. Moreover, no scalable 3D atherosclerosis model is available for making high-throughput assays for therapeutic evaluation. Herein, we report an *in vitro* 3D three-layer nanomatrix vascular sheet with critical atherosclerosis multi-features (VSA), including endothelial dysfunction, monocyte recruitment, macrophages, extracellular matrix remodeling, smooth muscle cell phenotype transition, inflammatory cytokine secretion, foam cells, and calcification initiation. Notably, we also present the creation of high-throughput functional assays with VSAs and the use of these assays for evaluating therapeutics for atherosclerosis treatment. The therapeutics include conventional drugs (statin and sirolimus), candidates for treating atherosclerosis (curcumin and colchicine), and a potential gene therapy (miR-146a-loaded liposomes). The high efficiency and flexibility of the scalable VSA functional assays should facilitate drug discovery and development for atherosclerosis.

Therefore, our goals are to 1) explore the effect on PA-YKNO to vascular cells in the histological and molecular level *in vitro* and further evaluate *in vivo*; 2) address the

“overly optimistic” findings when evaluating stents in a healthy *in vitro* and *in vivo* environment.

Specific Aim 1: To evaluate PA-YKNO prohealing nanomatrix coated stent in a vascular double layer (VDL) *in vitro* and in a balloon injured rabbit iliac artery model *in vivo*. To investigate the performance of PA-YKNO coated stent under the existence of major vascular cell types, a vascular double layer (VDL) incorporating a bottom smooth muscle cell layer and a top endothelial layer together with monocytes and foam cells was used. The PA-YKNO coated stent compared with commercial BMS and DES was evaluated in the VDL and the stent effect on endothelial proliferation and function, smooth muscle cell proliferation and phenotype, monocyte recruitment, inflammation, and foam cell formation was studied in histological and molecular level. Then, the performance of PA-YKNO coated stent, commercial BMS and DES will be further evaluated in a balloon injured rabbit ilia artery model *in vivo*.

Specific Aim 2: To develop a vascular sheet with atherosclerotic features (VSA) suitable for stent and therapeutic evaluation under atherosclerotic conditions. There are no suitable *in vitro* models with atherosclerosis mimicking conditions for stent evaluation. Thus, we will develop the VSA consisting of 1) three layered structures of endothelial, smooth muscle, and fibroblast cells to model human blood vessels; and 2) the development of key features of atherosclerosis. Then, the nanomatrix coated stent will be compared with commercially available BMS and DES for endothelial function and proliferation, neointimal hyperplasia, inflammation, and foam cell formation.

PRO-HEALING NANOMATRIX COATED STENT ANALYSIS IN AN IN VITRO
VASCULAR DOUBLE-LAYER AND IN A RABBIT MODEL

by

XIXI ZHANG, JUN CHEN, BRIGITTA C. BROTT, PETER ANDERSON,
PATRICK HWANG, JENNIFER SHERWOOD, GILLIAN HUSKIN, YOUNG-SUP
YOON, RENU VIRMANI, AND HO-WOOK JUN

ACS Applied Materials & Interfaces 2022, 14, 46, 51728-51743.

Copyright

2018

by

ACS Publications

Used by permission

Format adapted for dissertation

Abstract

While cardiovascular stent technology has considerable advances, there are hurdles to overcome, including restenosis, thrombosis, inflammation, and delayed re-endothelialization. The cause for these issues is that the dysfunctional stented arteries are damaged by both disease and stent, which fail to maintain vascular homeostasis. However, current stent designs only targeted these issues but ignored the significance of promoting functional artery healing (pro-healing) to solve these concerns thoroughly. Therefore, we developed a pro-healing nanomatrix coating for stent. Previous studies investigated the effect of pro-healing nanomatrix coating on individual vascular cell type. In natural condition of stented artery, there are multiple vascular cell types and their cross talk could strongly affect stent performance. Thus, in this study, an *in vitro* vascular double-layer (VDL) system was used to observe stent effects on mutual communications among different vascular cell types. And the pro-healing ability and mechanism of the nanomatrix coated stent were studied in the VDL and a rabbit model, compared to commercial bare metal stent (BMS) and drug eluting stent (DES). *In vitro* results indicated that in a layered vascular structure, the pro-healing nanomatrix coated stent could 1) improve endothelialization and endothelial functions, 2) regulate smooth muscle cell (SMC) phenotype to reduce SMC proliferation and migration, 3) suppress inflammation through a multifactorial manner, and 4) reduce foam cell formation, extracellular matrix remodeling, and calcification. Consistently, *in vivo* results demonstrated that compared with commercial BMS and DES, this pro-healing nanomatrix coated stent enhanced re-endothelialization with negligible restenosis, inflammation, or thrombosis. Thus, these

findings indicate the unique pro-healing feature of this nanomatrix stent coating with superior efficacy over commercial BMS and DES.

Keywords: pro-healing, nanomatrix, stent, endothelial, smooth muscle cell, inflammation, rabbit

1. INTRODUCTION

Since the first implantation of a cardiovascular stent in 1986, stents have been a mainstay of cardiovascular medicine and percutaneous coronary intervention (PCI).³⁹ While stent technology has evolved from bare metal stents (BMS) to first- and second-generation drug-eluting stents (DES) and now looks to a future of bioabsorbable stents, issues and complications remain. Neointimal hyperplasia, restenosis, sustained inflammation, thrombosis, and the need for prolonged dual anti-platelet therapy all contribute to current stent shortcomings. Thus, the ideal stent technology has yet to be developed.

Healing of stented artery is critical to prevent stent-related complications. Specifically, endothelial recovery plays the leading role during the healing process after stent implantation. The healthy endothelium maintains vessel homeostasis and guides proper vessel reactions through tightly controlled and precise mechanisms.^{40, 41} Loss of or damage to this endothelium triggers an inflammatory cascade leading to neointimal hyperplasia, restenosis, sustained inflammation, and thrombosis.⁴⁰⁻⁴² Moreover, the function, and phenotype of another major component- smooth muscle cell (SMC) in the medial vascular layer- also play a significant role. Normal SMCs are contractile phenotypes

that are non-proliferative and responsive to endothelial regulations. Damage to the medial layer and stimulation of atherosclerosis would lead to the transition to a synthetic phenotype which would aggressively proliferate and produce extracellular matrix (ECM), leading to artery narrowing. However, current stents and therapies only target the stent-related complications while ignoring the significance of obtaining the functional artery to entirely solve these issues. For instance, DES could prevent the restenosis issue of BMS by targeting the mTOR pathway to inhibit SMC proliferation directly.⁴³ However, the anti-proliferative agent from DES negatively affects endothelial functions which increase the risk of thrombosis. And dual anti-platelet therapy was used to solve the thrombosis issue rather than repairing the damaged endothelium instead. Hence, the remained dysfunctional endothelium^{44, 45} by DES then leads to further stent issues of inflammation, late-stent thrombosis, and the late restenosis catch-up phenomenon.^{6, 7, 20, 46-51} Therefore, it is necessary to develop a stent coating that focuses on promoting the healing of functional stented arteries.

Nitric oxide (NO) is produced endogenously by the native endothelium and plays a significant role in the healthy arteries due to its capacity for vascular modulation, resulting in anti-inflammatory effects, prevention of platelet adhesion, and quiescence and regulation of SMCs.⁵²⁻⁵⁵ NO production is disrupted when the endothelium is damaged during cardiovascular disease and stent deployment. Thus, NO release from stent coating could compensate for this critical NO loss induced by endothelial dysfunction and improve vascular recovery.⁵⁶ In light of this, we developed a NO-releasing peptide amphiphile (PA)- based pro-healing nanomatrix stent coating (PA-YKNO).^{25, 29, 31, 32, 37, 57} PA has been widely used in biological applications because of the excellent biocompatibility.²⁵ The

nanomatrix coating, PA-YKNO, is composed of two types of PA nanofibers, several nanometers in diameter and microns in length, which can be deposited in a layered structure on the stent surface. Specifically, the first PA incorporates YIGSR, a peptide sequence derived from laminin that provides attachment sites for endothelial cells (ECs) and thus promotes re-endothelialization. The second PA contains a poly-lysine sequence, KKKKK, which can be charged with nitric oxide (NO), hence the name PA-YKNO for the nanomatrix coating. It is expected that this nanomatrix coating could promote the healing of functional arteries through the vascular modulator-NO, the endothelial adhesive ligand, and the biocompatible environment.

In our previous studies, the effect of nanomatrix coated stent on individual vascular cell type was evaluated, including ECs, SMCs, monocytes, and platelets in tissue culture plate.^{29, 31, 32, 37, 57} However, single cell type system is insufficient to advice the stent performance in arteries which include multiple cell types. In natural conditions, SMCs and ECs are the key vascular cells with mutual communications that affect atherogenesis. Moreover, during stent integration in an artery with plaque, vascular homeostasis greatly depends on the regulation of two primary vascular components- the tunica intima and tunica media, the main components of which are ECs and SMCs, respectively. In addition, the influence of EC-SMC cross-talk may exacerbate atherogenesis and lead to stent complications.⁵⁸⁻⁶⁰ Therefore, an *in vitro* EC-SMC vascular double layer (VDL) model was used to evaluate the “pro-healing” ability of the PA-YKNO nanomatrix to restore the functions of these two major vascular components and prevent stent-related complications.

Based on our knowledge, there was no thorough studies about how stent affect vascular cell recovery in terms of phenotype, function, inflammation, oxidative stress level,

and atherosclerotic features including foam cell formation, ECM remodeling and calcification. And these studies are critical to understand the stent coating working mechanism to advise future stent design. In particular, using the *in vitro* VDL, we investigated the pro-healing effect of PA-YKNO nanomatrix coating on the recovery of vascular cell function, phenotype, and regulation during atherosclerosis in 5 aspects at the histological and molecular level, 1) the migration of ECs and SMCs on the stent; 2) recovery of endothelial function; 3) transition of SMC phenotype; 4) regulation of inflammation and oxidative stress; and 5) other critical atherosclerotic features that might lead to stent-related complications, including foam cell formation, ECM remodeling, and calcification. Commercial BMS (REBEL™, Boston Scientific, US) and DES (Promus PREMIER™, Boston Scientific, US) were chosen as control (Figure 1). Then, the efficacy of the nanomatrix coated stents (PA-YKNO) was evaluated in a balloon injured rabbit iliac artery model and compared with commercial BMS and DES, the results of which were correlated with *in vitro* results. The results exhibited the remarkable pro-healing ability of PA-YKNO nanomatrix stent coating that could restore the impaired vascular functions to prevent potential stent complications with greatly promoted efficacy over commercial BMS and DES.

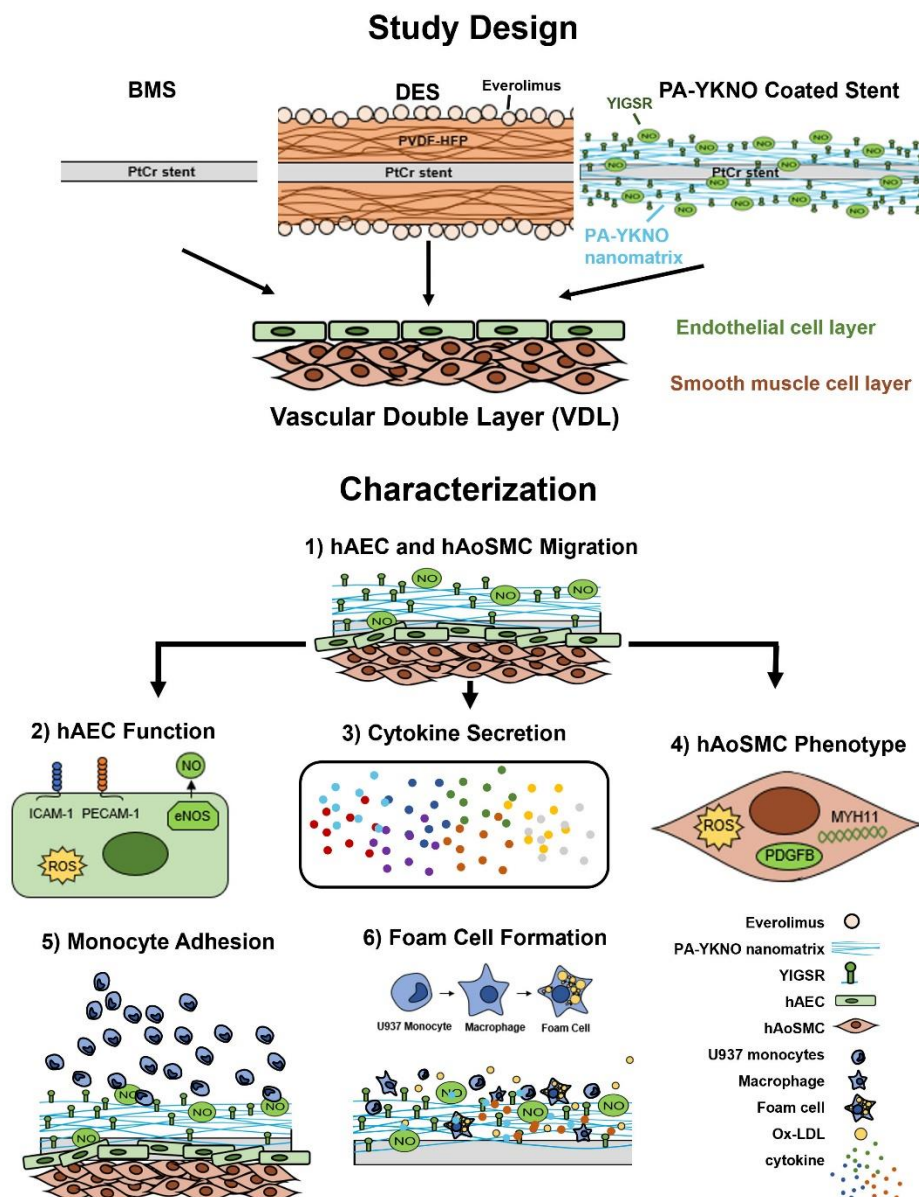


Figure 1. Schematic diagram illustrating in vitro study using vascular double layer (VDL).

2. MATERIALS AND METHODS

2.1 Preparation of the self-assembled peptide amphiphile nanomatrix.

Chemicals and resins for making PAs were purchased from Millipore-Sigma, US, Fisher Scientifics, US, or Sigma-Aldrich, US. The PA nanomatrix was synthesized as described

previously.^{29, 31, 32, 37, 57} Briefly, two discrete PAs were synthesized through Fluorenylmethoxycarbonyl (Fmoc) chemistry. The first PA was composed of an endothelial cell adhesive ligand (YIGSR) joined with a matrix metalloprotease-2 (MMP-2) degradable sequence (GTAGLIGQ) to form PA-YIGSR. The second PA (PA-KKKKK) consisted of the nitric oxide (NO) donor poly-lysine (KKKKK) linked to the MMP-2 degradable sequence. The two PAs were dissolved in deionized water at 1wt%, adjusted to pH 7 by adding NaOH, and mixed in a 9:1 molar ratio (YIGSR: KKKKK) to form PA-YK, which was subsequently reacted with scrubbed NO gas to form PA-YKNO. Self-assembly of the PA-YKNO nanomatrix coating on the stents was achieved by a water evaporation method as described below.^{31, 32, 57}

2.2 Water evaporation coating method for stents. Stent coating was prepared following previous established protocols.^{31, 32, 37} For the *in vitro* experiment, BMS (Rebel™, Boston Scientific, US) were cut open, flattened, and cut into pieces with identical surface areas. 20μL of PA-YKNO solution was dropped onto each stent piece, which were then placed in a chemical fume hood for 4 h to induce self-assembly of the nanofibers by solvent evaporation. This step was repeated 10 times. The stent pieces were further dried for another 48 h in a 37 °C incubator and sterilized under UV light for 4 h. For the *in vivo* experiments, stents were uniformly coated with PA-YKNO using a rotational coating technique through water evaporation-based self-assembly as described previously.^{31, 32, 57} Specifically, BMS (Rebel™, Boston Scientific, US) were mounted on a rotating mandrel attached to a motor and immersed in PA-YK-NO solution in an open top reservoir for 12 hours. After rotation in PA-YKNO solution for 12 h, the stents were allowed to continue rotating out of the solution to dry for a further 24 h. Stents were washed twice with sterile

DI water, crimped on the delivery balloon catheter, and ethylene oxide (EtO) sterilized before implantation.

2.3. Evaluation of stent effects on various biological functions

2.3.1. Development of the SMC-EC vascular double-layer (VDL) *in vitro* system. The *in vitro* VDL system that simulates the tunica media and tunica intima of the native vascular structure was created by seeding primary human aortic artery smooth muscle cells (hAoSMCs) on 48-well tissue culture plates at a seeding density of 2×10^4 cells per well and after the hAoSMC reached confluency, by seeding primary human aortic endothelial cells (hAECs) on top of the confluent hAoSMC layer at the same seeding density. The VDL, which was obtained after the hAEC layer reached confluency, mimicked the layered vascular structure of tunica media (hAoSMC layer) and tunica intima (hAEC layer). hAoSMCs and hAECs were purchased from ATCC, US. Mediums for culturing hAECs and hAoSMCs were purchased from Lifeline Cell Technology, US. Cells used for the VDL were at passage 5 or 6. Three stent groups were tested: BMS (Rebel™, Boston Scientific, US), DES (Promus Premier™, Boston Scientific, US), and PA-YKNO nanomatrix coated stents (coated Rebel™ stents, Boston Scientific, US). Stents (BMS, DES, or PA-YKNO) were flattened, cut into pieces with identical surface areas, placed in contact with the VDL, and cultured for 4 or 7 days.

2.3.2 Characterization of stent effect on endothelial function. Endothelial function was characterized by immunostaining (ICAM-1), DAF-FM, and rt-PCR (eNOS3, CD34, and PECAM-1). 1) Immunostaining. On days 4 and 7, the supernatant was replaced with 4% formaldehyde and incubated at room temperature for 10 min. Then, the VDL with

stent pieces was treated with PBS containing 0.25% Triton X-100 for 10 min. PBS with 0.1% Tween 20, 1% BSA, and 22.52 mg/mL glycine was used to treat VDL for 30 min to block the nonspecific binding of antibodies. Primary antibodies ICAM-1 (Abcam, US) were diluted 100 times in PBS with 0.1% Tween 20 and 1% BSA, added to the VDL, and incubated overnight at 4°C. Secondary antibodies (Abcam, US) for ICAM-1 were diluted 100 times in 1% BSA for 1h at room temperature in the dark, imaged, and quantified at 570nm/602nm immediately. The VDL was washed 3 times with PBS between each step.

2) DAF-FM Diacetate staining (Invitrogen, US). DAF-FM Diacetate is an indicator that detects nitric oxide secretion from endothelial cells. Briefly, 5mM stock solution was prepared by dissolving in DMSO. And 5µM working solution in PBS was prepared before the experiment. After removing the supernatant, the working solution was added, and the samples were incubated for 1h at 37°C in the dark. Then the probe was replaced with PBS, incubated for another 30 min, imaged by microscope (Nikon, US), and quantified at ex/em 485nm/528nm using a microplate reader (BioTek Synergy H1, Agilent, US).

3) rt-PCR. On day 7, the VDL was lysed using a RNeasy Plus Mini Kit (Qiagen, Hilden, Germany). RNA isolation was performed following the manufacturer's protocol. Then, the concentration of the RNA suspended in nuclease-free water was quantified using an ND-1000 UV spectrophotometer (Nanodrop, Wilmington, DE). The synthesis of complementary DNA was likewise conducted according to the manufacturer's protocol, using 500 ng RNA, which was reverse transcribed in a 2720 Thermo Cycler (Applied Biosystems, Foster City, CA) with a Verso cDNA Synthesis Kit (Thermo Fisher Scientific, Waltham, MA). Samples were then prepared in a 96-well PCR plate based on the TaqMan Master Mix protocol. For each sample, there were 2 µL cDNA solution, 10 µL 2x master

mix, 7 μ L RNA-free water, and 1 μ L gene primer (eNOS3, CD34, and PECAM-1, or GAPDH gene primer) from a TaqMan Gene Expression Assay kit (Applied Biosystems, Foster City, CA). The PCR plate was run in a LightCycler 480 (Roche Life Science, Indianapolis, IN) for the following cycles: pre-incubation at 50 °C for 2 min and 95 °C for 10 min; amplification for 45 cycles, at 95 °C for 15 s, and 60 °C for 1 min during each cycle; melting at 95°C for 5 s and 65 °C for 1 min, and cooling at 40°C for 30 s. Gene expression was normalized against the housekeeping gene, GAPDH. As described in a previous study, the $2^{-\Delta\Delta CT}$ method was used to assess gene expression.⁶¹ For eNOS3, CD 34, and PECAM-1 gene expression, data at each time point is expressed as a fold ratio relative to the data acquired for the VDL with BMS pieces at day 4. All experiments were performed with n=8.

2.3.3. Characterization of stent effect on SMC phenotype change. SMC phenotype change induced by the stents was characterized using rt-PCR. Like those described above, the gene primers for MYH11, PDGF-B, and GAPDH were from a TaqMan Gene Expression Assay kit (Applied Biosystems, Foster City, CA). Gene expression was normalized against the housekeeping gene, GAPDH, and data at each time point is expressed as a fold ratio relative to the data acquired for the VDL with BMS pieces at day 4. All experiments were performed with n=8.

2.3.4. Characterization of stent effect on inflammation. Inflammation of the stent treated VDL was characterized in 3 aspects: 1) monocyte adhesion, 2) cytokine secretion, and 3) oxidative stress. 1) Monocyte adhesion. On days 4 or 7, U937 cells

(ATCC, US) were incubated with Calcein Blue AM in the dark for 30 min and then washed with PBS to remove the excess. Then the stained U937 cells were added to the VDL with stent pieces and incubated for 30 min. Next, the VDL with stent pieces was washed with PBS to remove the unattached U937 cells and imaged (Nikon, US) and quantified at ex/em 322nm/435nm) Cytokine secretion. An ELISA-based quantitative array platform (RayBiotech, US) was used to measure the major inflammatory cytokine secretion- IL-1 α , IL-1 β , IL-4, IL-6, IL-8, IL-10, IL-13, INF- γ and MCP-1. Briefly, U937 cells were cultured with the VDL for 7 days, and the supernatant was collected for ELISA. After blocking, the diluted supernatant was added and incubated overnight at 4°C, followed by a wash step. The detection antibody cocktail for all the cytokines above was added and incubated for 2h at room temperature, followed by a wash step. Cy3 equivalent dye-conjugated streptavidin was added and incubated for 1h in the dark at room temperature. After thorough washing and drying, the signals were measured and analyzed via a laser scanner (GenePix® 4000B, Molecular Devices, US). 3) Oxidative stress. DCFH-DA which could measure reactive oxygen species (ROS) activity, was used to measure oxidative stress. A 5 mM DCFH-DA stock solution was prepared by dissolving in DMSO and stored at -20°C. Before the experiment, a 5 μ M working solution was also prepared by adding the stock solution to PBS. The VDL with stent pieces was gently washed with PBS, then DCFH-DA was added and incubated in the dark for 1h and imaged immediately by microscope (Nikon, US) and quantified at ex/em 485nm/528nm using a microplate reader (BioTek Synergy H1, Agilent, US). All experiments were performed with n=8.

2.3.5. Characterization of stent effect on ECM remodeling and calcification.

ECM remodeling and calcification were characterized using rt-PCR. Gene primers for MMP2, COL3A1, and COL17A1 for ECM remodeling, BMP2 and RUNX2 for calcification, and GAPDH were from a TaqMan Gene Expression Assay kit (Applied Biosystems, Foster City, CA). Gene expression was normalized against the housekeeping gene, GAPDH, and the data at each time point are expressed as a fold ratio relative to the data acquired for the VDL with BMS pieces on day 4. All experiments were performed with n=8.

2.4. Evaluation of stent effect on endothelialization and SMC migration.

To quantify the endothelialization and SMC migration on the stents, red fluorescent protein expressing hAoSMCs (RFP-hAoSMCs) and green fluorescent protein expressing hAEC (GFP-hAECs) were used to fabricate the VDL. RFP-hAoSMCs and GFP-hAECs were purchased from ANGIO-PROTEOMIE, US. Three stent groups were tested: BMS (Rebel™, Boston Scientific), DES (Promus Premier™, Boston Scientific), and PA-YKNO nanomatrix coated stents (coated Rebel™ stents, Boston Scientific). Stents (BMS, DES, or PA-YKNO) were flattened, cut into pieces with identical surface areas, and placed in contact with the VDL. On days 4 and 7, the VDL with stent pieces was imaged with microscope (Nikon, US) and quantified at ex/em 488nm/515nm for GFP-hAECs and 570nm/602nm for RFP-hAoSMCs using microplate reader (BioTek Synergy H1, Agilent, US). All experiments were performed with n=8.

2.5. Evaluation of stent effect on foam cell formation. Foam cells were induced from U937 cells. Firstly, macrophages were induced from U937 cells by adding Ox-LDL (50 μ g/mL), M-CSF (100 ng/mL), GM-CSF (25 ng/mL), and IFN- γ (100 ng/mL) to 1 million cells/mL in 48-well tissue culture plates and cultured for 7 days. Then, stent pieces were placed into the wells with the macrophages, and the foam cell formation was achieved by adding Ox-LDL (150 μ g/mL), M-CSF (100 ng/mL), GM-CSF (25 ng/mL), and IFN- γ (100 ng/mL). On day 7, foam cell formation was characterized by BODIPY staining (Fisher Scientific, US). Briefly, a 10 mM BODIPY stock solution was prepared by dissolving in DMSO and stored at -20°C. Before the experiment, a 100- times diluted BODIPY working solution was prepared by adding the stock solution to PBS. The supernatant was gently removed, and BODIPY was added after which the 48-well tissue culture plate was incubated in the dark for 30 min, imaged immediately at a microscope (Nikon, US), and quantified at ex/em 485nm/528nm using a microplate reader (BioTek Synergy H1, Agilent, US). All experiments were performed with n=8.

2.6. Balloon injured rabbit iliac arteries *in vivo*. Three stent cohorts were tested: BMS (Rebel™, Boston Scientific), DES (Promus Premier™, Boston Scientific), and PA-YKNO nanomatrix coated stents (coated Rebel™ stents, Boston Scientific). A total of seven rabbits (New Zealand white, male and female, one as extra) were used in this study. After pretreatment with aspirin, each rabbit underwent stent implantation and received two stents in each iliac artery via carotid access using standard catheterization techniques. At termination, stented vessel segments were fixed, extracted, and processed for post-mortem SEM and histological analysis.

2.6.1. Animals. This study was performed at Translation Testing and Training Laboratories (T3 Labs) in accordance with the requirements of the Animal Welfare Act and amendments and in conformance to the standards in the Guide for the Care and the Use of Laboratory Animals. T3 Labs is accredited by the Association for the Assessment and Accreditation of Laboratory Animal Care, International (AAALAC) and registered with the United States Department of Agriculture to conduct research in laboratory animals. All study protocols were reviewed and approved by the Institutional Animal Care and Use Committee (IACUC) prior to study initiation. Male and female New Zealand White rabbits were utilized for this study. Two rabbits were assigned to respective stent types, and each rabbit received two stents, with one in each iliac artery.

2.6.2. Surgical procedure. Rabbits were pretreated with aspirin (40 mg/day for 3 days) and sedated with ketamine (35 mg/kg) and xylazine (5 mg/kg) prior to stent implantation. Anesthesia was maintained with isoflurane (0.5-5%). The carotid access was then surgically prepared, and the animal was heparinized (150U/kg) to achieve an active clotting time above 250 seconds. Under fluoroscopic visualization, a guide catheter was placed in the carotid artery and advanced over the aortic arch into the abdominal aorta. A coronary guidewire was then placed in the iliac artery, followed by a PTCA balloon catheter (Emerge, Boston Scientific). The balloon catheter was inflated and deflated thrice for 30 seconds with 30-second reflow after each inflation to ensure balloon injury. Following denudation of the target segment, a stent mounted on a delivery balloon was advanced over the guidewire into the iliac artery and deployed over the injured area of the vessel. Stents were deployed as slightly oversized with a stent to artery ratio of 1.1:1. The carotid artery was ligated at the end of the procedure. The contralateral iliac artery

underwent stent implantation in a similar manner. Animals received daily anticoagulation treatment with aspirin (40 mg). At termination, animals were euthanized, and iliac arteries were perfusion rinsed with 0.9% saline and then perfusion fixed in situ with 10% neutral buffered formalin. Post perfusion, iliac treatment sites were carefully excised to include unstented areas (~2-3cm) proximal and distal to the stented segment. Adjacent muscle and downstream iliac artery segments were also harvested to evaluate for possible systemic inflammation and toxicity. Harvested specimens were immersion fixed in 10% neutral buffered formalin for a minimum of 24 hours prior to off-site shipping for further processing and analysis.

2.6.3. Histological Staining and analysis. After in situ perfusion fixation and iliac artery excision, tissue sections of the stented iliac arteries were taken. 2 stented arteries for each stent type were dehydrated and embedded in PMMA resin. Sections were made at 25%, 50%, and 75% segments of the stent and stained with hematoxylin and eosin (H&E) stain. Sections were then imaged and evaluated for evidence of balloon injury, toxicity, inflammatory responses, and endothelialization.

2.6.4. Scanning electron microscopy (SEM) and morphometric analysis. Stented segments (2 stented arteries for each stent type) were longitudinally bisected to expose the lumen and prepared for SEM observation. Stent halves were serially dehydrated in water, ethanol, and hexamethyldisilazane, desiccated overnight, and then sputter coated with gold and palladium prior to imaging. En faces SEM was performed on one-half of the bisected stents at 15x, 200x, and 600x magnifications. The 15x magnification SEM images were digitally assembled for a complete view of the entire luminal stent surface; 200x and 600x images were taken at the proximal, middle, and distal ends of the stented artery.

2.7. Scientific rigor and statistical analysis. Results for all experimental groups will be expressed as mean \pm standard deviation. Statistical comparisons were performed by ANOVA for multiple comparisons, with Tukey post hoc analysis for parametric data using the SPSS 15.0 software.

3. Results

3.1. PA-YKNO nanomatrix coating could promote endothelialization while reducing SMC migration *in vitro*. The effect of PA-YKNO on endothelialization and SMC migration compared with commercial BMS and DES were evaluated *in vitro* using the VDL on days 4 and 7. The VDL exhibited different responses among BMS, DES, and PA-YKNO coated stents (Figure 2). For BMS, on day 7, there was delayed endothelialization (Figure 2A) but the most SMC coverage (Figure 2B). For DES, on day 7, there was the least endothelialization (Figure 2C) and the most negligible SMC migration (Figure 2D). On the other hand, for the PA-YKNO coated stent, on day 7, there was almost complete endothelium (Figure 2E) and reduced SMC migration compared with BMS (Figure 2F). Notably, the data shown in Figure 2A-F was correlated with the quantitative results in Figure 2G-H. Figure 2G demonstrated that DES had the most delayed endothelialization on days 4 and 7 while PA-YKNO significantly improved the endothelialization. Specifically, the endothelium coverage on the PA-YKNO coated stents were 37.80 ± 0.012 and 12.92 ± 0.035 fold that of DES and BMS on day 4, respectively. In addition, PA-YKNO coated stents also demonstrated an excellent ability to suppress SMC migration similar to that of DES, with $8 \pm 3.8\%$ on day 4 and $43 \pm 7.1\%$ on day 7 relative to

BMS (Figure 2H). Therefore, the *in vitro* results indicated that the PA-YKNO coating could improve endothelialization while suppressing SMC migration.

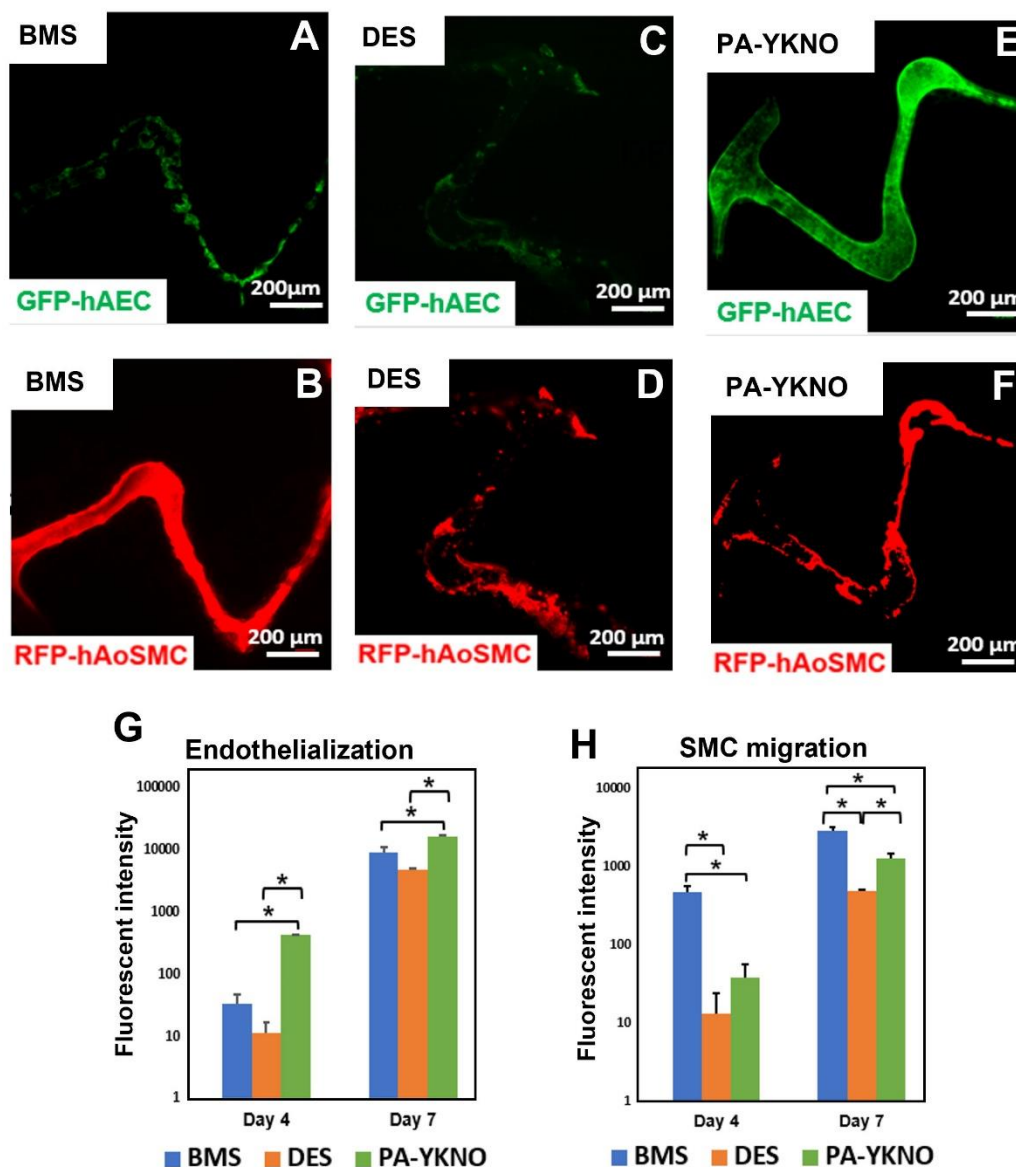


Figure 2. PA-YKNO nanomatrix coating could promote endothelialization while reduce SMC migration in vitro. (A), (C), and (E) Fluorescent image of GFP-hAEC migration on stent strut. (B), (D), and (F) Fluorescent image of RFP-hAoSMC migration on stent strut. (G) Quantification of the fluorescent intensity from GFP-hAECs on stent strut (PA-YKNO

vs BMS, 12.92 ± 0.035 fold on day 4 and 1.79 ± 0.13 on day 7; PA-YKNO vs DES, 37.80 ± 0.012 fold on day 4 and 3.35 ± 0.0078 fold on day 7). (H) Quantification of the fluorescent intensity from RFP-hAoSMCs on stent strut (DES vs BMS, 0.028 ± 0.022 fold on day 4, 0.16 ± 0.0062 fold on day 7; PA-YKNO vs BMS, 0.08 ± 0.038 fold on day 4, 0.43 ± 0.071 fold on day 7). (* $p < 0.05$)

3.2. PA-YKNO nanomatrix coating could improve endothelial functions *in vitro*. Endothelial function is significant in regulating the vascular environment and preventing stent-related complications.^{40, 42, 62} Therefore, the pro-healing effect of PA-YKNO coated stents on improving endothelial function recovery was evaluated. The endothelial functions were analyzed in 4 aspects: 1) nitric oxide (NO) secretion, 2) adhesion molecule expression (ICAM-1), 3) endothelial junction marker expression (PECAM-1), and 4) endothelial phenotype marker expression (CD34). As shown in Figure 3J, PA-YKNO coated stents induced significantly higher eNOS3 expression than BMS and DES on days 4 and 7, indicating that the PA-YKNO coating induces the more active NO secretion. This data agreed with the results obtained from the DAF-FM assay, which directly measures the secreted NO amount (Figure 3E-H). Figure 3H showed that PA-YKNO coated stents induced the highest NO secretion, with 1.20 ± 0.054 fold on day 4 and 1.30 ± 0.043 on day 7 compared with BMS as well as 1.30 ± 0.097 fold on day 4 and 2.49 ± 0.013 fold on day 7 compared with DES (Figure 3E-H). Moreover, the extent of endothelial dysfunction was evaluated by ICAM-1 gene expression⁶³ (Figure 3A-D). Notably, as shown by the quantified data in Figure 3D, PA-YKNO significantly reduced endothelial dysfunction, demonstrated by the remarkably lower ICAM-1 expression

compared with BMS and DES on both days 4 and 7 (Figure 3A-D). Additionally, the expression of the endothelial junction gene, PECAM-1, was also evaluated to demonstrate the endothelial ability to inhibit monocyte transmigration.⁶⁴ Figure 3K showed that PECAM-1 upregulation by PA-YKNO was 8.51 ± 0.037 times more than DES and 1.33 ± 0.28 times more than BMS on day 4. The most PECAM-1 upregulation by PA-YKNO coated stents were also observed on day 7, with 5.13 ± 0.041 times and 1.39 ± 0.28 times more than DES and BMS, respectively. We also evaluated the endothelial phenotype marker CD34⁶⁵ on days 4 and 7 and discovered that there was significantly more CD34 expression in the presence of PA-YKNO compared to BMS and DES, with 2.22 ± 0.11 and 19.33 ± 0.0080 fold, respectively, on day 7 (Figure 3I). Consequently, the PA-YKNO nanomatrix could effectively promote endothelial function compared with BMS and DES by increasing NO secretion and endothelial junction gene expression, maintaining endothelial phenotype while suppressing dysfunctional molecule, ICAM-1 expression.

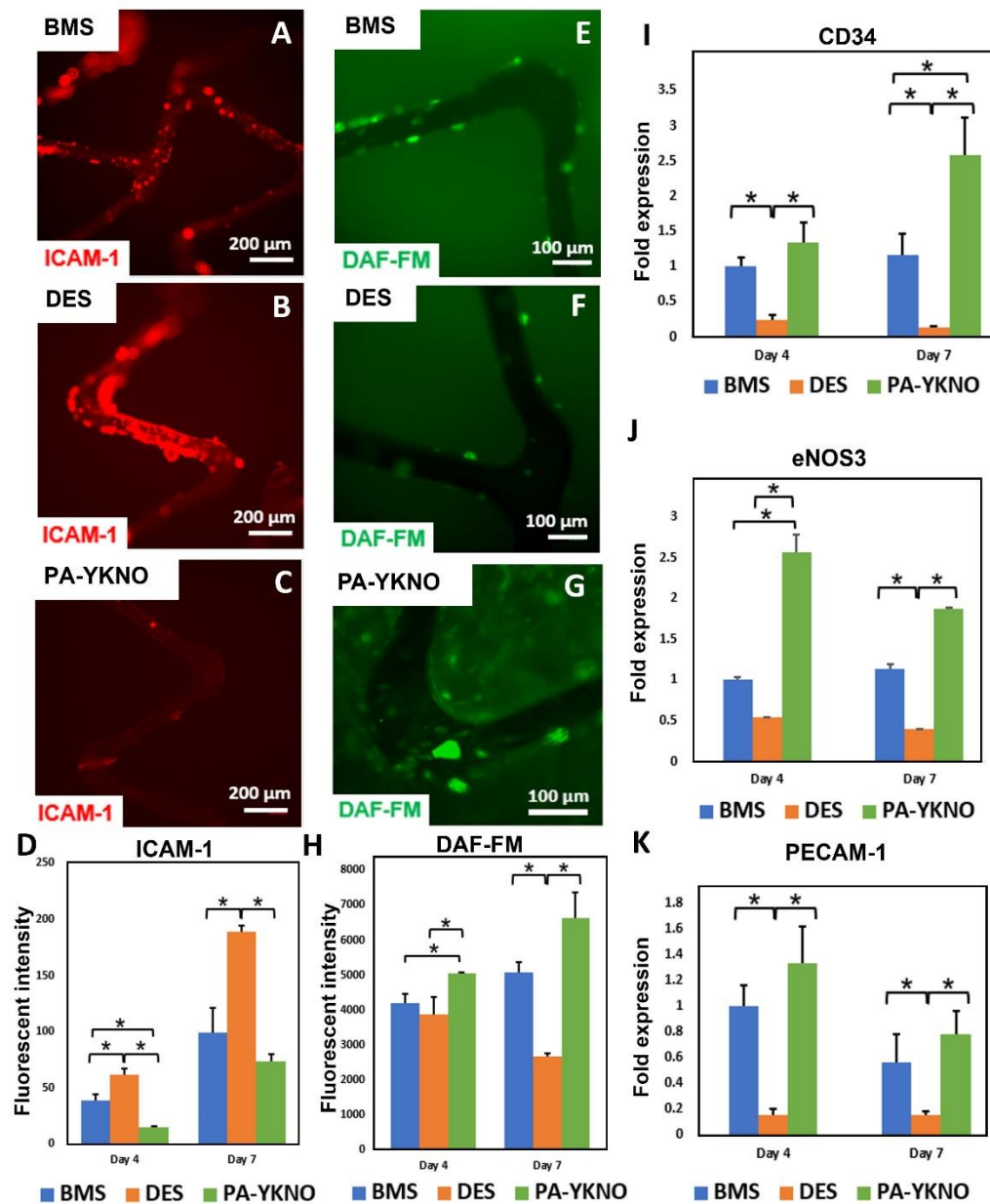


Figure 3. PA-YKNO nanomatrix coating could promote the endothelial functions in vitro.

(A)-(C) Immunostaining of ICAM-1 expressed by hAECs on stent strut. (D) Quantification of ICAM-1 fluorescent intensity on stent strut (PA-YKNO vs BMS: 0.38 ± 0.044 fold on

day 4, 0.74 ± 0.064 fold on day 7; PA-YKNO vs DES: 0.24 ± 0.028 fold on day 4, 0.39 ± 0.034 fold on day 7). (E)-(G) DF-FM staining of hAEC on stent strut. (H) Quantification of DAF-FM fluorescent intensity on stent strut (PA-YKNO vs BMS: 1.20 ± 0.054 fold on day 4 and 1.30 ± 0.043 on day 7; PA-YKNO vs DES: 1.30 ± 0.097 fold on day 4 and 2.49 ± 0.013 fold on day 7). (I) Gene expression of CD34 (I; PA-YKNO vs BMS: 1.34 ± 0.29 fold on day 4, 2.22 ± 0.11 fold on day 7; PA-YKNO vs DES: 5.49 ± 0.048 fold on day 4, 19.33 ± 0.0080 fold on day 7). (J) Gene expression of eNOS3 (J; PA-YKNO vs BMS: 2.57 ± 0.22 fold on day 4, 1.65 ± 0.035 fold on day 7; PA-YKNO vs DES: 4.73 ± 0.0038 fold on day 4, 4.67 ± 0.0010 fold on day 7). (K) Gene expression of PECAM-1 (K; PA-YKNO vs BMS: 1.33 ± 0.28 fold on day 4, 1.39 ± 0.28 fold on day 7; PA-YKNO vs DES: 8.51 ± 0.037 fold on day 4, 5.13 ± 0.041 fold on day 7) of hAEC on stent strut. (* $p < 0.05$)

3.3. PA-YKNO nanomatrix coating could promote the transition of SMC to contractile phenotype *in vitro*. It has been widely reported that normal vascular SMCs are quiescent contractile phenotypes.⁶⁶ However, during atherosclerosis, SMCs switch to a proliferative and synthetic phenotype, produce ECM, and significantly contribute to neointimal hyperplasia. Hence, reversing the synthetic to the quiescent contractile phenotype is critical for SMC recovery, thereby preventing neointimal hyperplasia.⁶⁷⁻⁷¹ Therefore, we investigated the effect of PA-YKNO coated stents on the expression of the typical contractile phenotype marker- MYH11^{72, 73} and the potent synthetic phenotype inducer- PDGFB⁷⁴⁻⁷⁷ on days 4 and 7. *In vitro* results demonstrated that compared with BMS and DES, PA-YKNO significantly suppressed the expression of a synthetic gene- PDGF-B ($32 \pm 5.6\%$ on day 4, $24 \pm 11\%$ on day 7, relative to BMS; 26 ± 4.5 fold on day 4,

25±3.5% on day 7, relative to DES) (Figure 4A). On the other hand, PA-YKNO promoted the expression of a contractile gene- MYH11^{67, 78-80} (PA-YKNO vs BMS: 3.57±0.18 fold on day 4, 1.84±0.046 fold on day 7; PA-YKNO vs DES: 6.22±0.025 fold on day 4, 28.91±0.035 fold on day 7) (Figure 4B). In particular, these data showed that for DES, even though everolimus released from the DES has significantly reduced SMC amount (Figure 2), the SMCs on DES maintained their synthetic phenotype that is often found in atherosclerotic plaque (Figure 4).

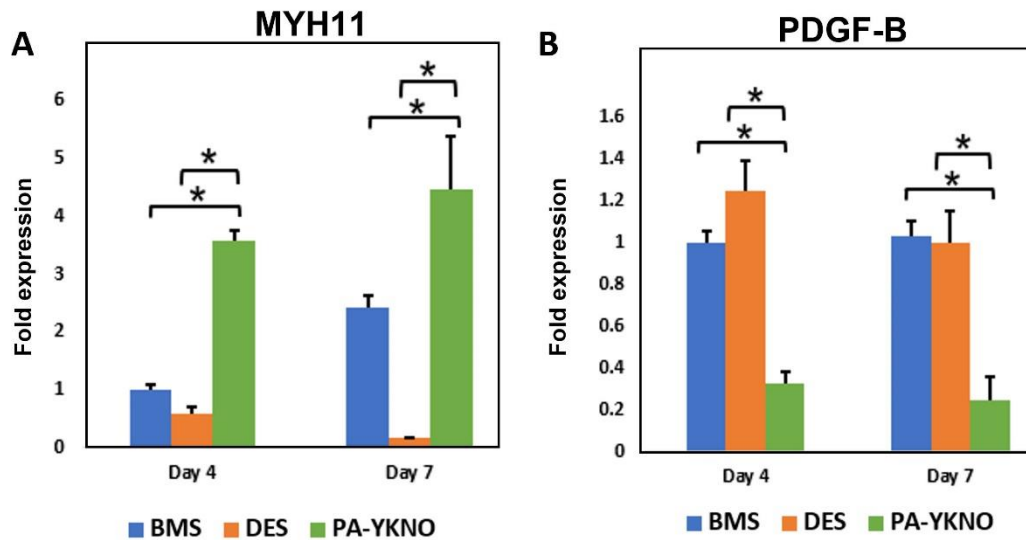


Figure 4. PA-YKNO nanomatrix coating could promote the transition of SMC to contractile phenotype in vitro. (A) Gene expression of MYH11 (PA-YKNO vs BMS: 0.32±0.056 fold on day 4, 0.24±0.11 fold on day 7; PA-YKNO vs DES: 0.26±0.045 fold on day 4, 0.25±0.035 fold on day 7). (B) Gene expression of PDGFB (PA-YKNO vs BMS: 3.57±0.18 fold on day 4, 1.84±0.046 fold on day 7; PA-YKNO vs DES: 3.57±0.18 fold on day 4, 1.84±0.046 fold on day 7) of hAoSMC on stent strut. (*p<0.05, PDGFB- PDGF-B)

3.4. PA-YKNO nanomatrix coating could regulate inflammation *in vitro*.

Atherosclerosis is an inflammatory disease; thus, the occurrence of stent-related complications greatly depends on the local inflammation and its regulation by the stents. Here, we comprehensively evaluated the inflammation regulation by PA-YKNO nanomatrix coating *in vitro* in 3 significant aspects, 1) monocyte recruitment, 2) inflammatory cytokine secretion, and 3) oxidative stress level. Figure 5A-C exhibited that monocyte adhesion on the stents was the most pronounced on DES, but the least on the PA-YKNO coated stent. These observations correlated with the quantitative data in Figure 5D, which showed that PA-YKNO coating significantly reduced monocyte recruitment compared with BMS and DES on days 4 and 7. Then, inflammatory cytokine secretion was studied using an ELISA array for six critical pro-inflammatory cytokines (IL-1 α , IL-1 β , IL-6, IL-8, IFN- γ , and MCP-1) and three critical anti-inflammatory cytokines (IL-4, IL-10, and IL-13)⁸¹⁻⁸³. Figure 5E exhibited that PA-YKNO coating could reduce pro-inflammatory cytokine expression and especially induced significantly stronger suppression of two potent pro-inflammatory cytokines, IL-1 β and IFN- γ , than DES and BMS. In particular, the IL-1 β secretion by VDL in the presence of PA-YKNO coated stents was $34\pm6.4\%$ and $59\pm11\%$ compared with the IL-1 β secretion induced by DES and BMS, respectively. In addition, an enhanced suppression effect for IFN- γ secretion compared to other stent types was also observed, in which the IFN- γ secretion by the VDL with PA-YKNO was 17 ± 14 and $32\pm25\%$ of that by VDL relative to DES and BMS, respectively.

On the other hand, for the critical anti-inflammatory cytokines, PA-YKNO has a significant promotive effect; for example, PA-YKNO induced significantly more IL-13 and IL-10 production than DES and BMS. Specifically, the VDL with PA-YKNO coated

stents secreted 7.43 ± 0.010 fold times and 3.68 ± 0.048 folds more IL-13 than the VDL with DES and BMS, respectively. In addition, the secretion of IL-10 by VDL after interaction with PA-YKNO coated stents was significantly greater than that of BMS and doubled compared with that of DES. Furthermore, PA-YKNO demonstrated better suppression of NOX4 expression compared with DES and BMS ($11 \pm 3.9\%$, $74 \pm 26\%$ vs BMS on day 4, $5.2 \pm 0.88\%$ vs DES, and $39 \pm 6.6\%$ vs BMS on day 7, Figure 5E). NOX4 is a gene marker closely related to oxidative stress⁸⁴, and this result was consistent with the data obtained DCFH-DA assay that was used to quantify the reactive oxygen species level. Figure 5F showed that DES strongly enhanced the oxidative stress on day 7 (3.50 ± 0.029 fold vs PA-YKNO and 2.16 ± 0.038 fold vs BMS); in contrast, PA-YKNO reduced oxidative stress on day 7 ($62 \pm 6.3\%$ vs BMS, $29 \pm 2.9\%$ vs DES). These results strongly indicated that PA-YKNO could significantly regulate inflammation through a multifactorial approach in the stented area.

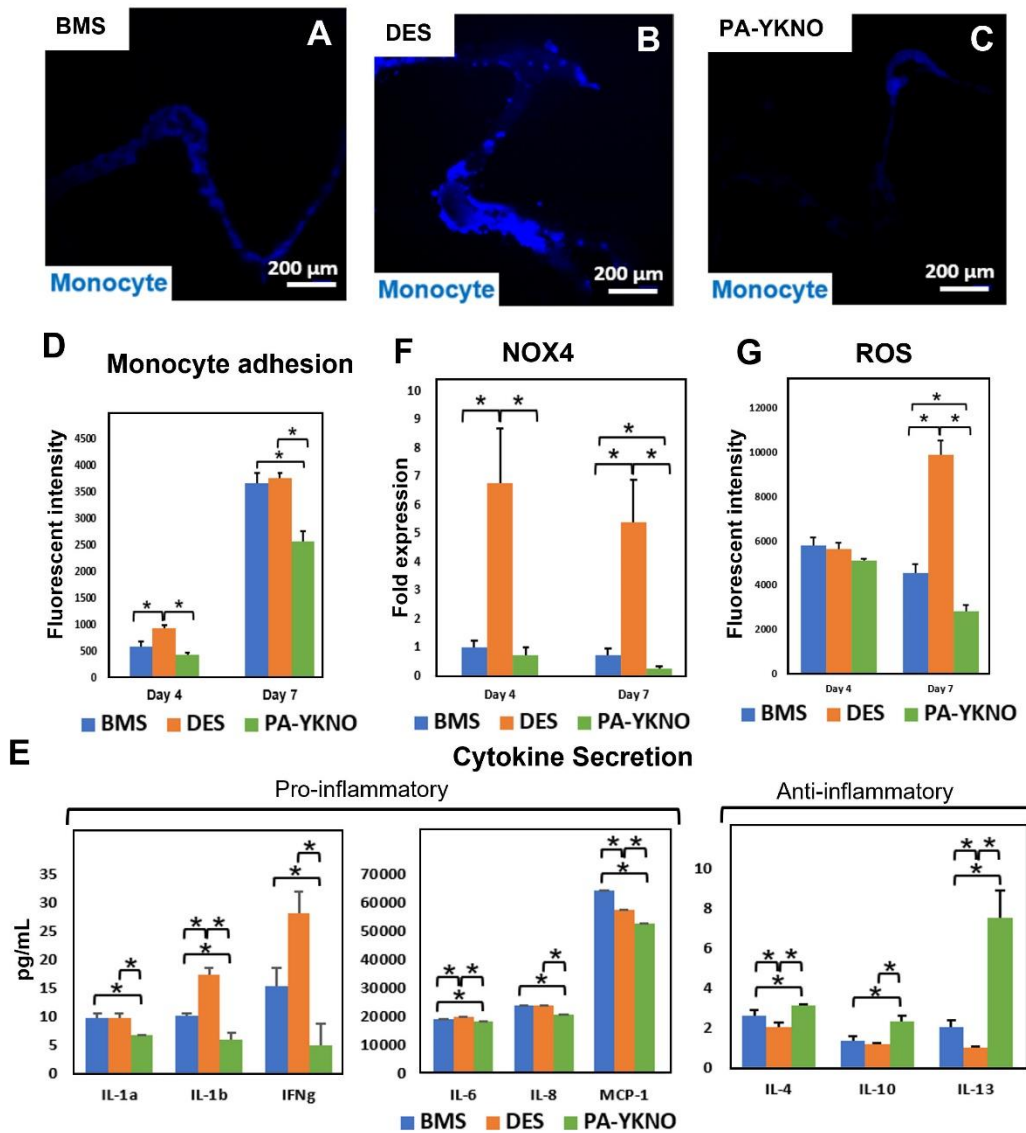


Figure 5. PA-YKNO nanomatrix coating could regulate inflammation in vitro. (A), (B), and (C) Calcein AM Blue stained monocytes adhered on stent strut. (D) Quantification of the fluorescent intensity from Calcein AM Blue stained monocytes on stent strut (PA-YKNO vs BMS: 0.47 ± 0.038 fold on day 4, 0.68 ± 0.055 fold on day 7; PA-YKNO vs DES: 0.74 ± 0.060 fold on day 4, 0.70 ± 0.056 fold on day 7). (E) Inflammatory cytokine secretion from VDLs after being treated with BMS, DES or PA-YKNO coated stents on day 7. (IL-

1α : PA-YKNO vs BMS: 0.70 ± 0.013 fold; PA-YKNO vs DES: 0.69 ± 0.013 fold. IL- 1β : PA-YKNO vs BMS: 0.59 ± 0.11 fold; PA-YKNO vs DES: 0.34 ± 0.064 fold. IFN- γ - PA-YKNO vs BMS: 0.32 ± 0.25 fold; PA-YKNO vs DES: 0.17 ± 0.14 fold. IL-6: PA-YKNO vs BMS: 0.96 ± 0.015 fold; PA-YKNO vs DES: 0.92 ± 0.015 fold. IL-8: PA-YKNO vs BMS: 0.87 ± 0.029 fold; PA-YKNO vs DES: 0.86 ± 0.02 fold. MCP-1: PA-YKNO vs BMS: 0.82 ± 0.00024 fold; PA-YKNO vs DES: 0.92 ± 0.00027 fold. IL-4- PA-YKNO vs BMS: 1.18 ± 0.090 fold; PA-YKNO vs DES: 1.52 ± 0.074 fold. IL-10- PA-YKNO vs BMS: 1.72 ± 0.10 fold; PA-YKNO vs DES: 2.01 ± 0.26 fold. IL-13- PA-YKNO vs BMS: 3.68 ± 0.048 fold; PA-YKNO vs DES: 7.43 ± 0.010 fold. (F) NOX4 expression of cells on stent strut (PA-YKNO vs BMS: 0.74 ± 0.26 fold on day 4, 0.39 ± 0.066 fold on day 7; PA-YKNO vs DES: 0.11 ± 0.039 fold on day 4, 0.052 ± 0.0088 fold on day 7). (G) Quantification of oxidative stress using DCFH-DA assay (DES vs PA-YKNO: 3.50 ± 0.029 fold; DES vs BMS: 2.16 ± 0.038 fold; PA-YKNO vs BMS: 0.62 ± 0.063 fold; PA-YKNO vs DES: 0.29 ± 0.029 fold). (* $p<0.05$)

3.5. PA-YKNO nanomatrix coating could reduce foam cell formation, calcification, and ECM remodeling *in vitro*. In addition to evaluating vascular cells and inflammation, the stent effects on foam cell formation, ECM remodeling, and calcification were investigated because they are also major atherosclerosis-related elements that strongly contribute to stent-related complications. Firstly, BODIPY staining was used to quantify the number of foam cells. Figure 6A showed that PA-YKNO could significantly reduce foam cell formation, with the foam cell number only $56\pm6.5\%$ and $46\pm5.3\%$ that of BMS and DES, respectively. Interestingly, rt-PCR results demonstrated that PA-YKNO also inhibited the expression of RUNX2 and BMP2, two typical gene markers for

calcification.⁸⁵⁻⁸⁷ In particular, on day 7, a significant downregulation of RUNX2 was induced by PA-YKNO coated stent, as demonstrated by the result that the RUNX2 expression was $1.3 \pm 0.4\%$ and $6.4 \pm 1.9\%$ that of BMS and DES, respectively. In addition, a more robust suppression for BMP2 by PA-YKNO coated stent than BMS and DES were observed (Figure 6B-6C). Moreover, PA-YKNO also downregulated the expression of typical gene markers for ECM remodeling- MMP2, COL3A1, and COL17A1⁸⁸⁻⁹⁰ on days 4 and 7. Significantly, it was found that PA-YKNO downregulated MMP2 and COL3A1 expression by up to 5 times compared with BMS on day 7. Furthermore, the reduction of COL17A1 by PA-YKNO was more evident- the expression in the presence of PA-YKNO coated stents was merely $0.13 \pm 0.12\%$ and $1.1 \pm 0.99\%$ compared with that of BMS and DES, respectively, on day 4. (Figure 6F). These results indicated that PA-YKNO has a therapeutic effect on lessening potential foam cell formation, ECM remodeling, and calcification, which could further prevent stent-related atherosclerotic complications. Up to here, the pro-healing effect of PA-YKNO coated stent was comprehensively studied using the in vitro VDL system, especially on molecular level in terms of cytokine secretion and gene expression, as summarized in Figure 5E and Figure 7.

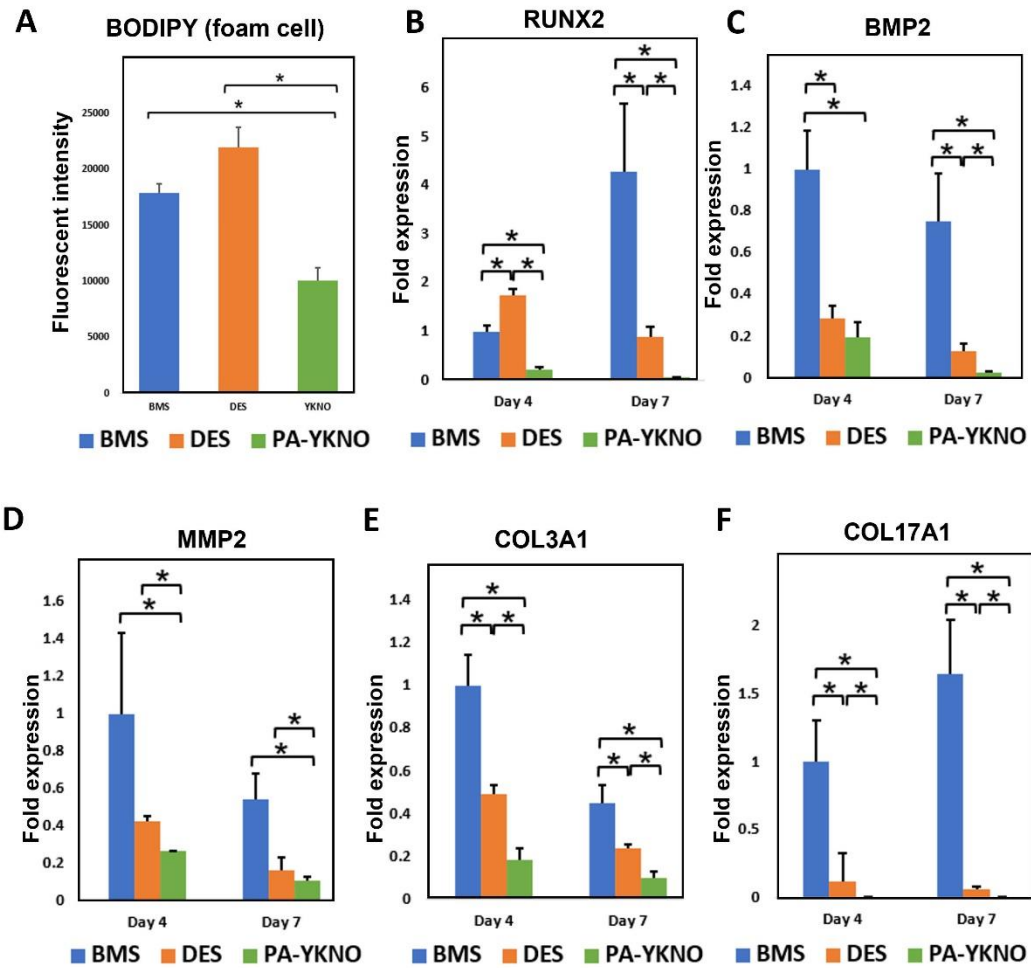


Figure 6. PA-YKNO nanomatrix coating could administer foam cell formation, ECM remodeling, and calcification in vitro. (A) Quantification of fluorescent intensity of BODIPY stained foam cell (PA-YKNO vs BMS: 0.56 ± 0.065 fold; PA-YKNO vs DES: 0.46 ± 0.053 fold). (B) Gene expression of RUNX2 (PA-YKNO vs BMS: 0.21 ± 0.061 fold on day 4, 0.013 ± 0.0040 fold on day 7). (C) Gene expression of BMP2 (PA-YKNO vs BMS: 0.20 ± 0.072 fold on day 4, 0.039 ± 0.0080 fold on day 7; PA-YKNO vs DES: 0.69 ± 0.26 fold on day 4, 0.23 ± 0.047 fold on day 7). (D) Gene expression of MMP2 (PA-YKNO vs BMS: 0.27 ± 0.0041 fold on day 4, 0.20 ± 0.034 fold on day 7; PA-YKNO vs DES: 0.62 ± 0.0092

fold on day 4, 0.66 ± 0.11 fold on day 7). (E) Gene expression of COL3A1 (E; PA-YKNO vs BMS: 0.19 ± 0.050 fold on day 4, 0.23 ± 0.062 fold on day 7; PA-YKNO vs DES: 0.37 ± 0.10 fold on day 4, 0.43 ± 0.12 fold on day 7). (F) Gene expression of COL17A1 (PA-YKNO vs BMS: 0.0013 ± 0.0012 fold on day 4, 0.0043 ± 0.0014 fold on day 7; PA-YKNO vs DES: 0.011 ± 0.0099 fold on day 4, 0.11 ± 0.036 fold) of cells on stent strut. (* $p < 0.05$)

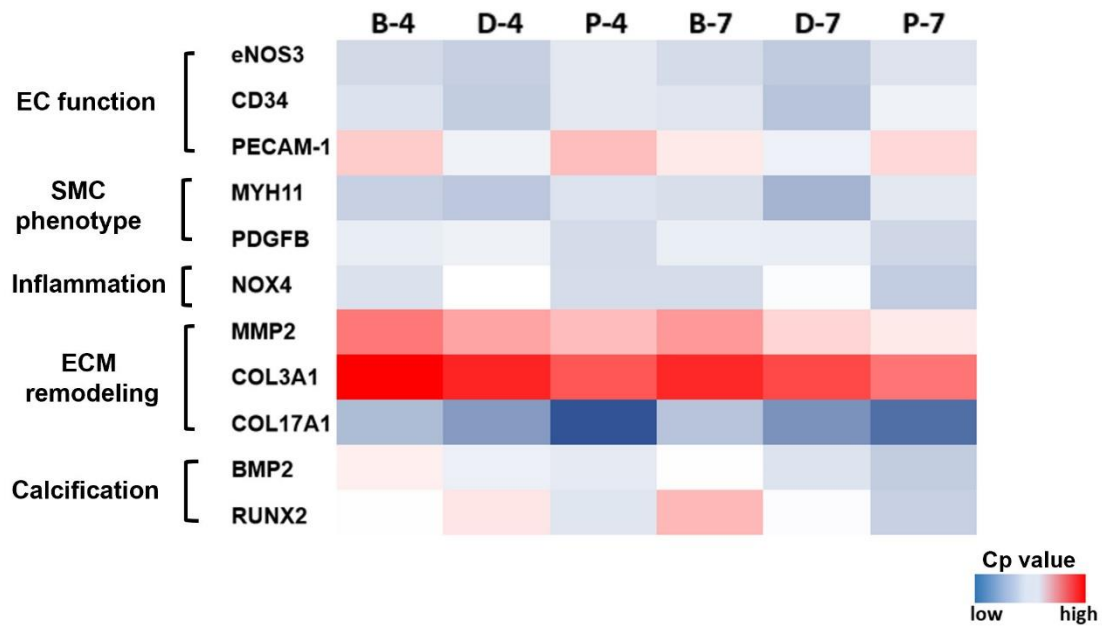


Figure 7. Summary of atherosclerotic gene expression in the VDL. (* $p < 0.05$) (PDGFB-PDGF-B). B-4: BMS on day 4; D-4: DES on day 4; P-4: PA-YKNO on day 4; B-7: BMS on day 7; D-7: DES on day 7; P-7: PA-YKNO on day 7.

3.6. PA-YKNO nanomatrix coating could accelerate stent coverage and improve endothelialization while suppressing restenosis and inflammation *in vivo*.

Representatives for the SEM images of the entire luminal stent surface (15x, left column) and detailed images of the proximal, middle, and distal stent areas (200x, middle column;

and 600x, right column) were depicted. As shown in Figure 8, the nanomatrix-coated stents demonstrated rapid stent coverage on day 4 ($57.47 \pm 5.44\%$) compared with DES ($4.03 \pm 2.71\%$) and BMS ($15.07 \pm 3.91\%$) (Figure 8G). Significantly, on day 28, BMS and PA-YKNO coated stented arteries obtained almost full coverage (BMS- $97.85 \pm 1.38\%$, PA-YKNO- $99.67 \pm 0.14\%$), while delayed coverage was observed in DES stented arteries ($82.09 \pm 5.56\%$) (Figure 8G). Interestingly, detailed SEM (200X) images demonstrated significantly different cell morphology on the stent coverage among BMS, DES and PA-YKNO coated stents. Specifically, for BMS stented arteries, a few sphere-shaped inflammatory cells were observed on day 4 (Figure 9A, highlighted with a red circle), while the elongated SMC-covered stent strut was seen on day 28 (Figure 9B, highlighted by red arrows). For DES, clusters of sphere-shaped inflammatory cells adhered to the stent strut on both days 4 and 28 (Figure 9D and E, highlighted by red circles and red arrows), indicating the sustained inflammation induced by DES. In contrast, Figure 9H exhibited PA-YKNO coated stent strut fully covered by a smooth endothelium layer with aligned spindle-shaped endothelial cells on day 28 (Figure 9H, pointed out by white arrows).

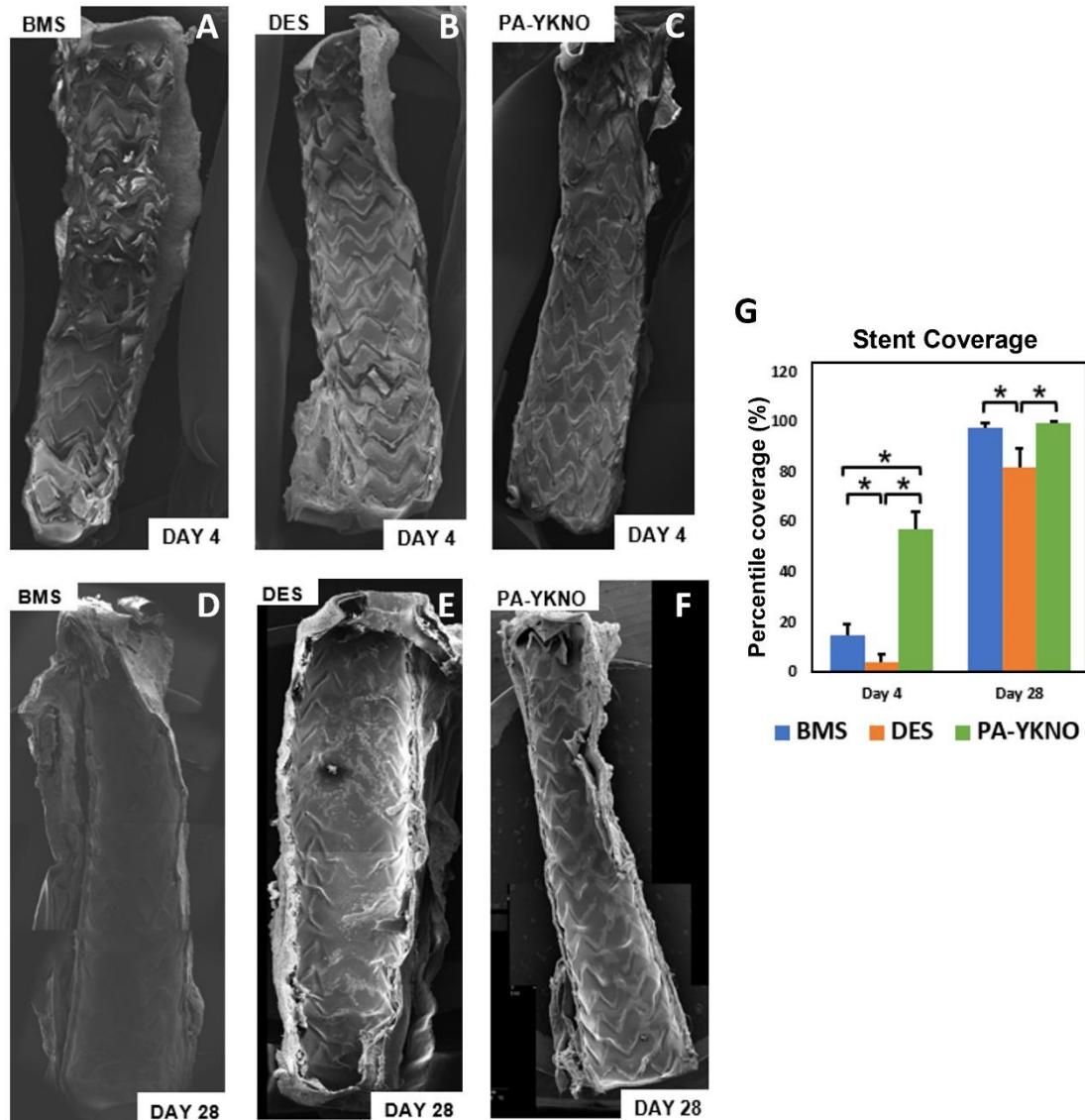


Figure 8. PA-YKNO nanomatrix coating could accelerate stent coverage in vivo. (A)-(F) Representative SEM images of BMS, DES, and PA-YKNO coated stent at day 4 and 28. (G) Quantification of stent coverage on day 4 and 28. (*p<0.05)

For histological analysis, there was no evidence of local inflammation, toxicity, or necrosis in any artery sample, indicating no biocompatible issue for PA-YKNO coated stents. Moreover, the histological analysis results were consistent with the SEM analysis.

Representative histology images demonstrated successful stent implantation within the arterial layers and different responses of the arteries to the stents. Specifically, BMS stented arteries showed significantly more neointimal hyperplasia above the stent strut (Figure 9C, pointed out by a double-head red arrow). DES stented arteries showed reduced neointimal hyperplasia but significant inflammation with monocytes aggregation around the stent strut (Figure 9F, pointed out by red arrows), which was consistent with what was shown in SEM images (Figure 9D and E). On the other hand, PA-YKNO coated stented arteries showed compromised neointima compared with BMS while negligible inflammatory cells (Figure 9I). This result may indicate greater and faster re-endothelialization, demonstrating the nanomatrix coating's pro-healing ability.

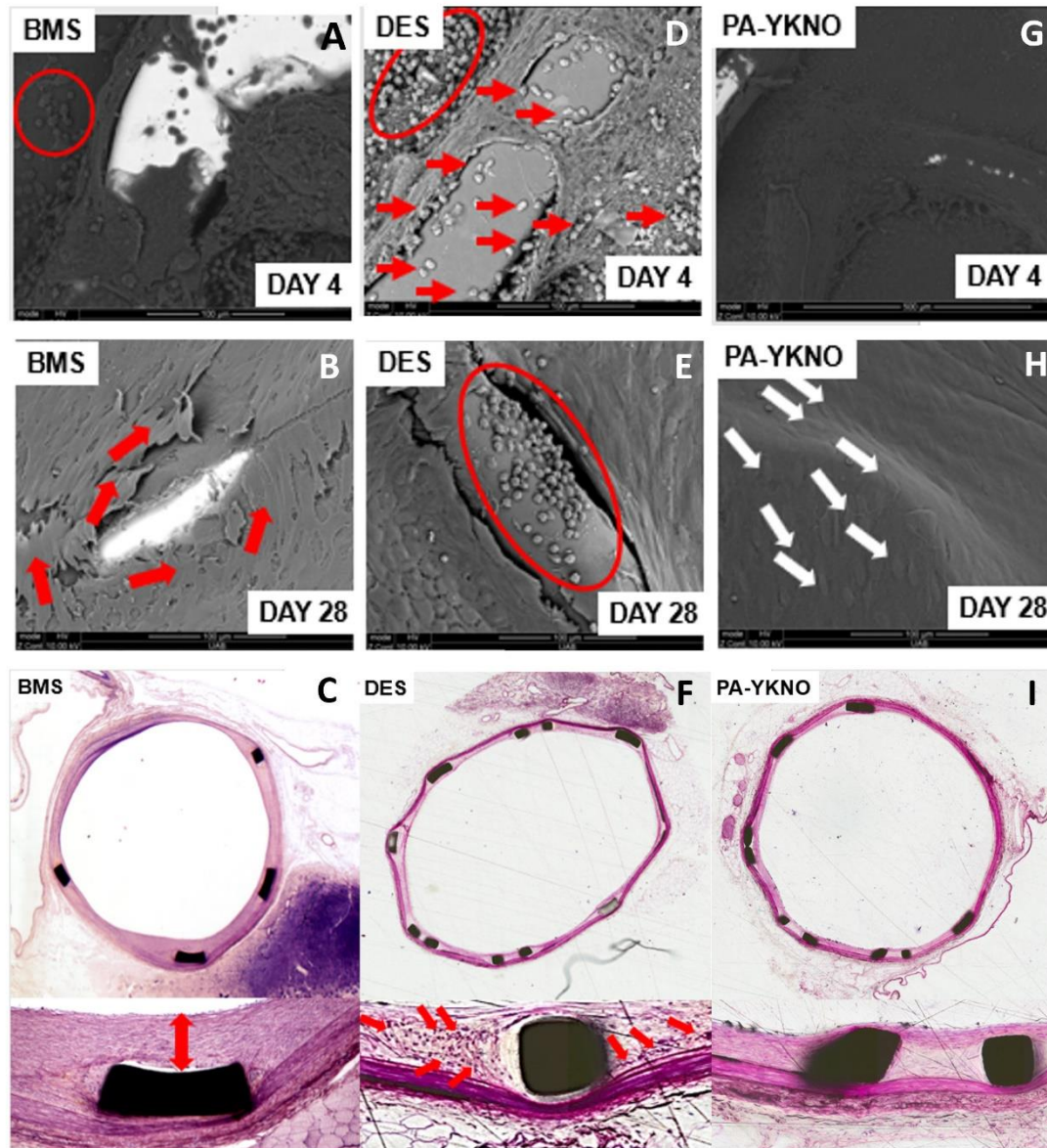


Figure 9. PA-YKNO nanomatrix coating could improve endothelialization while suppress restenosis, and inflammation in vivo. (A)-(B), (D)-(E), (G)-(H): Representative SEM images of BMS, DES, and PA-YKNO coated stent on day 4 and 28. (C), (F), and (I) Representative images for H&E staining of arteries after stented with BMS, DES and PA-YKNO coated stents on day 28. (* $p < 0.05$)

4. Discussion

In previous studies, we successfully developed the pro-healing nanomatrix stent coating composed of PAs with a NO-releasing and an endothelial adhesive ligand. The current study evaluated the "pro-healing" effect of PA-YKNO, defined as an ability to promote vascular healing and recover a functional vascular environment, using a VDL *in vitro* (Figure 1) and a balloon injury healthy rabbit iliac artery model *in vivo*. In addition, the effect of PA-YKNO coated stents were compared with commercial BMS and DES. Specifically, the *in vitro* VDL enables a comprehensive evaluation for the ability and mechanism of pro-healing nanomatrix coated stent at molecular level (Figure 5E and Figure 7). The *in vitro* and *in vivo* results comprehensively exhibited that PA-YKNO coating can successfully promote vascular healing; moreover, they addressed the critical questions regarding the function of PA-YKNO coating in four significant aspects.

1) **PA-YKNO coated stents could improve endothelium coverage and function.**

It was reported that an intact and functional endothelium could maintain vessel homeostasis through tightly controlled and precise mechanisms¹⁰⁻¹¹ and thus, is critical to preventing stent issues. Thus, firstly, we explored if PA-YKNO coating could promote or show better endothelium coverage compared with DES and BMS. Promisingly, the *in vitro* and *in vivo* results exhibited that PA-YKNO coated stents induced more excellent endothelial cell coverage, indicating faster endothelialization than DES and BMS, which agrees with the result in our previous study that PA-YKNO induced more hAEC migration. As reported, endothelial functions maintain vascular homeostasis by 1) secreting vascular modulator-NO to suppress inflammation, regulate SMC phenotype, reduce platelet adhesion and direct

vessel contraction/dilation; and 2) inhibiting inflammatory cell adhesion and transmigration. Furthermore, during endothelial regulation of inflammatory cell behaviors, PECAM-1 plays a significant role in preventing inflammatory cell transmigration⁶⁴, while ICAM-1 could arrest inflammatory cells.⁶³ Moreover, the maintenance of endothelial phenotype marker-CD34 is closely related to endothelial healing⁶⁵. Thus, in addition to endothelium coverage, we also compared the effect of PA-YKNO coated stents on endothelial function with that of DES and BMS by analyzing these markers mentioned above. As demonstrated in Figure 3, compared with DES and BMS, VDL treated with PA-YKNO coated stents secreted more vascular modulator-NO and expressed more PECAM-1 and CD34 but less ICAM-1. These exciting results strongly indicate that PA-YKNO coating improved endothelial function in VDL compared to DES and BMS, which has not been found in previous studies. Furthermore, the enhanced endothelial function by PA-YKNO coated stents may lead to inflammatory cell adhesion and transmigration.

2) PA-YKNO could improve smooth muscle cell differentiation towards an athero-protective contractile phenotype to reduce proliferation. Besides endothelium, SMCs play a significant role in atherosclerosis development and stenosis. Specifically, normal arterial SMCs often maintain their quiescent contractile phenotype; however, SMCs can dedifferentiate into proliferative synthetic phenotype during atherosclerosis progression and significantly contribute to neointimal hyperplasia. In atherosclerotic plaque, it was reported that PDGF-B could induce the dedifferentiation of SMCs from the contractile to the synthetic phenotype⁷⁷. And thus, the dedifferentiation leads to decreased SMC phenotype marker expression, such as myosin heavy chain 11- MYH11^{72, 73}. Figure

4B showed that VDL treated with PA-YKNO decreased the expression of synthetic phenotype inducer- PDGF-B while upregulating the contractile phenotype marker MYH11 expression. Moreover, reduced SMC migration by PA-YKNO coated stents were also observed *in vitro* and *in vivo*, as demonstrated in Figures 2 and 9. These results exhibited that PA-YKNO nanomatrix could direct differentiation of SMC to quiescent contractile phenotype, possibly resulting from the NO released from the PA-YKNO coating and the recovered endothelium. Other studies also reported similar results, showing that NO could direct SMC differentiation to contractile phenotype⁹¹. Importantly, we also explored the effect of DES on SMC phenotype- although everolimus on DES inhibited SMC proliferation via mTOR pathway⁹², it did not modulate the SMC phenotype. Instead, the SMCs with DES maintained a synthetic phenotype similar to that observed with BMS. This critical finding might explain why the late restenosis catch-up is observed in patients when the everolimus of DES is exhausted⁹³.

3) PA-YKNO could achieve inflammation resolution in a multifactorial manner. It is known that atherosclerosis is a chronic inflammatory disease, and the sustained inflammation responses caused by anti-proliferative drugs released from stent coating or byproducts of the drug carrier significantly impair vascular healing. Therefore, proper inflammation regulation by stent coating could strongly support vascular healing and prevent stent-related complications. In the current work, we studied stent-regulated inflammation resolution by characterizing 1) inflammatory cell adhesion on the stents, 2) inflammatory cytokine secretion by VDL, and 3) oxidative stress level within VDL after stent interaction with the VDL. These three factors are interrelated and strongly influence

inflammation progression. Interestingly, we observed significantly more reduced monocyte adhesion in PA-YKNO coated stent group than BMS and DES in Figure 5A-D *in vitro* and Figure 9 *in vivo*, which may be because PA-YKNO coated stents promoted better endothelium coverage and function, as discussed earlier. We also quantified the secretion of nine major inflammatory cytokines, which showed the resolved inflammation by PA-YKNO coating, as summarized in Figure 5E. Among these pro-inflammatory cytokines investigated by PA-YKNO, MCP-1 is known to promote monocyte penetration⁹⁴, and IFN- γ can direct pro-inflammatory M1 macrophage differentiation, which could, in turn, induce IL-1 and IL-8 secretions to further promote the inflammation in the plaque. Thus, reducing IFN- γ production by PA-YKNO indicates that PA-YKNO can alleviate inflammation by reducing primary inflammatory cytokine production. In addition, as shown in Figure 5E, increased production of anti-inflammatory cytokines- IL-4, IL-10, and IL-13^{81-83, 95, 96}, resulting from PA-YKNO, suggests that PA-YKNO might direct macrophage phenotype change from M1 to M2, thereby leading to inflammation resolution. Moreover, the *in vivo* results are correlated with the obtained *in vitro* results; the detailed *in vivo* SEM and H&E staining images exhibited reduced inflammatory cell aggregation around the strut of PA-YKNO coated stent, indicating less inflammation generated. In addition, *in vivo* histological results revealed no systemic inflammation, toxicity, or necrosis within the walls of PA-YKNO coated stented arteries. Also, the oxidative stress level was characterized. Figures 5E and F demonstrated that PA-YKNO significantly downregulated NOX4 expression and reduced ROS production compared with BMS and DES. It is reported that the differentiated macrophage and inflamed ECs and SMCs can generate NOX-4-derived ROS that can increase pro-inflammatory cytokine

secretion and other atherosclerotic symptoms. Thus, the downregulation of NOX-4 and the decrease of ROS by PA-YKNO may also contribute to the inflammation resolution observed in the PA-YKNO coated stent group. In short, it can be concluded that PA-YKNO could regulate inflammation in a multifactorial manner by controlling monocyte behavior, cytokine secretion, and redox balance.

4) PA-YKNO could prevent stent complications by controlling foam cell formation, calcification, and ECM remodeling. There are increasing reports about the strong relation between stent failure, including late restenosis/thrombosis and neo-atherosclerosis¹⁹, of which one of the significant features are foam cell aggregation. In the VDL here, it is disclosed that PA-YKNO could effectively reduce foam cell formation compared with commercial BMS and DES. Moreover, calcification is another concern that leads to stent fracture and thrombosis^{97,98}. RUNX2 and BMP2 are two typical gene markers indicating the calcification in the atherosclerotic lesion. Figure 6B-C showed that PA-YKNO could suppress RUNX2 and BMP2 expression in vascular cells. Furthermore, calcification is also related to vascular remodeling, which might lead to restenosis, during which ECM remodeling is the primary process.^{97,99} Thus, we evaluated three genes (MMP-2, COL3A1, and COL17A1) that are reported to relate to ECM remodeling. MMP-2 is one member of the matrix metalloproteinase family, strongly related to ECM degradation leading to plaque instability and rupture¹⁰⁰⁻¹⁰³. Figure 6D showed that PA-YKNO coating could significantly reduce MMP-2 expression. On the other hand, COL3A1 and COL17A1 are associated with ECM remodeling, leading to restenosis. The gene downregulation of COL3A1 and COL17A1 in Figures 6E and F suggested that PA-YKNO coating might

reduce ECM production. In addition, more robust downregulation results by PA-YKNO compared with DES and BMS suggested that PA-YKNO coated stents may better suppress ECM production than commercial BMS and DES.

5. Conclusion

This study demonstrated the significance of promoting functional arterial healing to prevent stent-related complications, which was widely neglected in the stent industry. Moreover, it is the first time we demonstrated the "pro-healing" capacity of PA-YKNO nanomatrix coated stent on EC recovery, SMC regulation, inflammation resolution, foam cell formation, calcification, and EC remodeling, using *in vitro* VDL system or a balloon injured rabbit iliac artery model. Instead of individual cell type in other *in vitro* systems, the VDL system featured with the layered structure with major vascular components- EC and SMC- on respective layer. And thus, VDL enabled the comprehensive *in vitro* evaluation of stents' effect on vascular cells with mutual communications, at the molecular level, especially for gene expression and cytokine secretion. In addition, using VDL, we compared the effects of PA-YKNO coated stents with commercially available BMS and DES from four perspectives. *In vitro* and *in vivo* results demonstrated that compared with BMS and DES, PA-YKNO nanomatrix coating could 1) improve endothelial recovery, 2) suppress SMC migration and neointimal hyperplasia, 3) reduce inflammation, 4) suppress potential stent complications including foam cell formation, calcification, and ECM remodeling. Therefore, this PA-YKNO nanomatrix stent coating merits further investigation for long-term efficacy and potential clinical viability. This study also provided vital information to guide future stent coating design.

Supporting Information. The following files are available free of charge.

P value summary for data presented in Figure 2-6, and 8. (DOC)

Abbreviation

BMS, bare metal stent; DES, drug-eluting stent; RFP-hAoSMC, red fluorescent protein expressing human aortic smooth muscle cell; GFP-hAEC, green fluorescent protein expressing human aortic endothelial cell; ECM, extracellular matrix; PCI, percutaneous coronary intervention; PA, peptide amphiphile; VDL, vascular double layer; GM-CSF: Granulocyte-macrophage colony-stimulating factor; ox- LDL: oxidized low density lipid; NO: nitric oxide; TNF- α : tumor necrosis factor- α ; IFN- γ : interferon- γ ; M-CSF: macrophage colony-stimulating factor

References

1. Doenst T, Haverich A, Serruys P, Bonow Robert O, Kappetein P, Falk V, Velazquez E, Diegeler A, Sigusch H. PCI and CABG for Treating Stable Coronary Artery Disease. *Journal of the American College of Cardiology*. 2019;73:964-976.
2. Rajendran P, Rengarajan T, Thangavel J, Nishigaki Y, Sakthisekaran D, Sethi G, Nishigaki I. The Vascular Endothelium and Human Diseases. *International Journal of Biological Sciences*. 2013;9:1057-1069.
3. Anne Krüger-Genge AB, Ralf-Peter Franke, Friedrich Jung. Vascular Endothelial Cell Biology: An Update. *International Journal of Molecular Sciences*. 2019;20.
4. Yau JW, Teoh H, Verma S. Endothelial Cell Control of Thrombosis. *BMC Cardiovascular Disorders*. 2015;15:130.
5. Im E, Hong M-K. Drug-Eluting Stents to Prevent Stent Thrombosis and Restenosis. *Expert Review of Cardiovascular Therapy*. 2016;14:87-104.
6. Inoue T, Croce K, Morooka T, Sakuma M, Node K, Simon Daniel I. Vascular Inflammation and Repair. *JACC: Cardiovascular Interventions*. 2011;4:1057-1066.
7. Nakazawa G. Stent Thrombosis of Drug Eluting Stent: Pathological Perspective. *Journal of Cardiology*. 2011;58:84-91.
8. Otsuka F, Nakano M, Ladich E, Kolodgie FD, Virmani R. Pathologic Etiologies of Late and Very Late Stent Thrombosis following First-Generation Drug-Eluting Stent Placement. *Thrombosis*. 2012;2012:608593.
9. Nakamura D, Attizzani GF, Toma C, Sheth T, Wang W, Soud M, Aoun R, Tummala R, Leygerman M, Fares A, Mehanna E, Nishino S, Fung A, Costa M, Bezerra HG. Failure Mechanisms and Neoatherosclerosis Patterns in Very Late Drug-Eluting and Bare-Metal Stent Thrombosis. *Circulation: Cardiovascular Interventions*. 2016;9:e003785.
10. Fuentes L, Gómez-Lara J, Salvatella N, Gonzalo N, Hernández-Hernández F, Fernández-Nofrerias E, Sánchez-Recalde Á, Alfonso F, Romaguera R, Ferreiro JL, Roura G, Teruel L, Gracida M, Marcano A, Lucrecia GH, Joan A. IVUS Findings in Late and Very Late Stent Thrombosis. A Comparison Between Bare-metal and Drug-eluting Stents. *Revista Española de Cardiología (English Edition)*. 2018;71:335-343.
11. Kereiakes Dean J, Yeh Robert W, Massaro Joseph M, Driscoll-Shempp P, Cutlip Donald E, Steg PG, Gershlick Anthony H, Darius H, Meredith Ian T, Ormiston J, Tanguay JF, Windecker S, Garratt N, Kandzari E, Lee P, Simon I, Iancu C, Trebacz J, Mauri L. Stent Thrombosis in Drug-Eluting or Bare-Metal Stents in Patients Receiving Dual Antiplatelet Therapy. *JACC: Cardiovascular Interventions*. 2015;8:1552-1562.

12. Alraies MC, Darmoch F, Tummala R, Waksman R. Diagnosis and Management Challenges of In-Stent Restenosis in Coronary Arteries. *World J Cardiol.* 2017;9:640-651.
13. Kuramitsu S, Shirai S, Ando K. Mechanism of In-Stent Restenosis after Second-Generation Drug-Eluting Stents (DES): Is It Different from Bare-Metal Stents and First-Generation DES? *J Thorac Dis.* 2015;7:E599-602.
14. Godo S, Shimokawa H. Divergent Roles of Endothelial Nitric Oxide Synthases System in Maintaining Cardiovascular Homeostasis. *Free Radical Biology and Medicine.* 2017;109:4-10.
15. Wise SGAUWAMPNMKCTI. Extracellular Matrix Molecules Facilitating Vascular Biointegration. *Journal of Functional Biomaterials.* 2012;3.
16. Hinsbergh VWMv. Endothelium—Role in Regulation of Coagulation and Inflammation. *Seminars in Immunopathology.* 2012;34:93-106.
17. Richards J, El-Hamamsy I, Chen S, Sarang Z, Sarathchandra P, Yacoub MH, Chester AH, Butcher JT. Side-Specific Endothelial-Dependent Regulation of Aortic Valve Calcification: Interplay of Hemodynamics and Nitric Oxide Signaling. *The American Journal of Pathology.* 2013;182:1922-1931.
18. Farah C, Michel LYM, Balligand J-L. Nitric Oxide Signalling in Cardiovascular Health and Disease. *Nature Reviews Cardiology.* 2018;15:292-316.
19. Kushwaha M, Anderson JM, Bosworth CA, Andukuri A, Minor WP, Lancaster JR, Anderson PG, Brott BC, Jun H-W. A Nitric Oxide Releasing, Self Assembled Peptide Amphiphile Matrix that Mimics Native Endothelium for Coating Implantable Cardiovascular Devices. *Biomaterials.* 2010;31:1502-1508.
20. Andukuri A, Minor WP, Kushwaha M, Anderson JM, Jun H-W. Effect of Endothelium Mimicking Self-Assembled Nanomatrices on Cell Adhesion and Spreading of Human Endothelial Cells and Smooth Muscle Cells. *Nanomedicine: Nanotechnology, Biology and Medicine.* 2010;6:289-297.
21. Andukuri A, Min I, Hwang P, Alexander G, Marshall LE, Berry JL, Wick TM, Joung YK, Yoon Y-S, Brott BC, Han D-K, Jun H-W. Evaluation of the Effect of Expansion and Shear Stress on a Self-Assembled Endothelium Mimicking Nanomatrix Coating for Drug Eluting Stents In Vitro and In Vivo. *Biofabrication.* 2014;6:035019.
22. Alexander GC, Vines JB, Hwang P, Kim T, Kim J-a, Brott BC, Yoon Y-S, Jun H-W. Novel Multifunctional Nanomatrix Reduces Inflammation in Dynamic Conditions in Vitro and Dilates Arteries ex Vivo. *ACS Applied Materials & Interfaces.* 2016;8:5178-5187.

23. Alexander GC, Hwang PTJ, Chen J, Kim J, Brott BC, Yoon YS, Jun HW. Nanomatrix Coated Stent Enhances Endothelialization but Reduces Platelet, Smooth Muscle Cell, and Monocyte Adhesion under Physiologic Conditions. *ACS Biomaterials Science & Engineering*. 2018;4:107-115.
24. Jun HW, Yuwono V, Paramonov SE, Hartgerink JD. Enzyme-Mediated Degradation of Peptide-Amphiphile Nanofiber Networks. *Advanced Materials*. 2005;17:2612-2617.
25. Li M, Qian M, Kyler K, Xu J. Endothelial–Vascular Smooth Muscle Cells Interactions in Atherosclerosis. *Frontiers in Cardiovascular Medicine*. 2018;5.
26. Tuttolomondo A, Di Raimondo D, Pecoraro R, Arnao V, Pinto A, Licata G. Atherosclerosis as an Inflammatory Disease. *Current Pharmaceutical Design*. 2012;18:4266-4288.
27. Jia L-X, Zhang W-M, Li T-T, Liu Y, Piao C-M, Ma Y-C, Lu Y, Wang Y, Liu T-T, Qi Y-F, Du J. ER Stress Dependent Microparticles Derived from Smooth Muscle Cells Promote Endothelial Dysfunction during Thoracic Aortic Aneurysm and Dissection. *Clinical Science*. 2017;131:1287-1299.
28. Anderson JM, Vines JB, Patterson JL, Chen H, Javed A, Jun H-W. Osteogenic Differentiation of Human Mesenchymal Stem Cells Synergistically Enhanced by Biomimetic Peptide Amphiphiles Combined with Conditioned Medium. *Acta Biomaterialia*. 2011;7:675-682.
29. Gimbrone MA, García-Cardena G. Vascular Endothelium, Hemodynamics, and the Pathobiology of Atherosclerosis. *Cardiovascular Pathology*. 2013;22:9-15.
30. Reed DM, Foldes G, Harding SE, Mitchell JA. Stem Cell-Derived Endothelial Cells for Cardiovascular Disease: a Therapeutic Perspective. *British Journal of Clinical Pharmacology*. 2013;75:897-906.
31. Chistiakov DA, Orekhov AN, Bobryshev YV. Vascular Smooth Muscle Cell in Atherosclerosis. *Acta Physiologica*. 2015;214:33-50.
32. Liu R, Leslie KL, Martin KA. Epigenetic Regulation of Smooth Muscle Cell Plasticity. *Biochimica et Biophysica Acta (BBA) - Gene Regulatory Mechanisms*. 2015;1849:448-453.
33. Yurdagul A, Jr., Finney AC, Woolard Matthew D, Orr AW. The Arterial Microenvironment: the Where and Why of Atherosclerosis. *Biochemical Journal*. 2016;473:1281-1295.
34. Wang G, Jacquet L, Karamariti E, Xu Q. Origin and Differentiation of Vascular Smooth Muscle Cells. *The Journal of Physiology*. 2015;593:3013-3030.

35. Durgin BG, Straub AC. Redox Control of Vascular Smooth Muscle Cell Function and Plasticity. *Laboratory Investigation*. 2018;98:1254-1262.
36. Frismantiene A, Philippova M, Erne P, Resink TJ. Smooth Muscle Cell-Driven Vascular Diseases and Molecular Mechanisms of VSMC Plasticity. *Cellular Signalling*. 2018;52:48-64.
37. Liu M, Gomez D. Smooth Muscle Cell Phenotypic Diversity. *Arteriosclerosis, Thrombosis, and Vascular Biology*. 2019;39:1715-1723.
38. Shi X, Xu C, Li Y, Wang H, Ma W, Tian Y, Yang H, Li L. A Novel Role of VEPH1 in Regulating AoSMC Phenotypic Switching. *Journal of Cellular Physiology*. 2020;235:9336-9346.
39. Boersema M, Katta K, Rienstra H, Molema G, Nguyen TQ, Goldschmeding R, Navis G, van den Born J, Popa ER, Hillebrands JL. Local Medial Microenvironment Directs Phenotypic Modulation of Smooth Muscle Cells After Experimental Renal Transplantation. *American Journal of Transplantation*. 2012;12:1429-1440.
40. Mammoto A, Hendee K, Muyleart M, Mammoto T. Endothelial Twist1-PDGFB signaling mediates hypoxia-induced proliferation and migration of α SMA-positive cells. *Scientific Reports*. 2020;10:7563.
41. Zhang Y, Zhang WD, Wang KQ, Li T, Song SH, Yuan B. Expression of Platelet-Derived Growth Factor in the Vascular Walls of Patients with Lower Extremity Arterial Occlusive Disease. *Exp Ther Med*. 2015;9:1223-1228.
42. Alexander MR, Murgai M, Moehle CW, Owens GK. Interleukin-1 β Modulates Smooth Muscle Cell Phenotype to a Distinct Inflammatory State Relative to PDGF-DD via NF- κ B-Dependent Mechanisms. *Physiological Genomics*. 2012;44:417-429.
43. Negishi K, Aizawa K, Shindo T, Suzuki T, Sakurai T, Saito Y, Miyakawa T, Tanokura M, Kataoka Y, Maeda M, Tomida S, Morita H, Takeda N, Kumorro I, Kario K, Nagai R, Imai Y. An Myh11 Single Lysine Deletion Causes Aortic Dissection by Reducing Aortic Structural Integrity and Contractility. *Scientific Reports*. 2022;12:8844.
44. Liu R, Jin Y, Tang WH, Qin L, Zhang X, Tellides G, Hwa J, Yu J, Martin KA. Ten-Eleven Translocation-2 (TET2) Is a Master Regulator of Smooth Muscle Cell Plasticity. *Circulation*. 2013;128:2047-2057.
45. Goikuria HFMDAUVMRSMEELAVKAI. Characterization of Carotid Smooth Muscle Cells during Phenotypic Transition. *Cells*. 2018;7.
46. Zhao XN, Li YN, Wang YT. Interleukin-4 Regulates Macrophage Polarization via the MAPK Signaling Pathway to Protect against Atherosclerosis. *Genet Mol Res*. 2016;15.

47. Tse K, Tse H, Sidney J, Sette A, Ley K. T Cells in Atherosclerosis. *Int Immunol*. 2013;25:615-622.
48. Maiuri MC, Grassia G, Platt AM, Carnuccio R, Ialenti A, Maffia P. Macrophage Autophagy in Atherosclerosis. *Mediators of Inflammation*. 2013;2013:584715.
49. Chen F, Haigh S, Barman S, Fulton D. From Form to Function: the Role of Nox4 in the Cardiovascular System. *Frontiers in Physiology*. 2012;3.
50. Zhang M, Sara JD, Wang F-l, Liu L-P, Su L-X, Zhe J, Wu X, Liu J-h. Increased Plasma BMP-2 Levels are Associated with Atherosclerosis Burden and Coronary Calcification in Type 2 Diabetic Patients. *Cardiovascular Diabetology*. 2015;14:64.
51. Durham AL, Speer MY, Scatena M, Giachelli CM, Shanahan CM. Role of Smooth Muscle Cells in Vascular Calcification: Implications in Atherosclerosis and Arterial Stiffness. *Cardiovascular Research*. 2018;114:590-600.
52. Sun Y, Byon CH, Yuan K, Chen J, Mao X, Heath JM, Javed A, Zhang K, Anderson PG, Chen Y. Smooth Muscle Cell-Specific Runx2 Deficiency Inhibits Vascular Calcification. *Circulation Research*. 2012;111:543-552.
53. Grootaert MOJ, Moulis M, Roth L, Martinet W, Vindis C, Bennett MR, De Meyer GRY. Vascular Smooth Muscle Cell Death, Autophagy and Senescence in Atherosclerosis. *Cardiovascular Research*. 2018;114:622-634.
54. Kini Annapoorna S, Vengrenyuk Y, Shameer K, Maehara A, Purushothaman M, Yoshimura T, Matsumura M, Aquino M, Haider N, Johnson Kipp W, Readhead B, Kidd A, Feig E, Krishnan P, Sweeny J, Milind M, Moreno P, Mehran R, Kovacic C, Baber U, Dudley T, Narula J, Sharma S. Intracoronary Imaging, Cholesterol Efflux, and Transcriptomes After Intensive Statin Treatment. *Journal of the American College of Cardiology*. 2017;69:628-640.
55. Lim W-W, Corden B, Ng B, Vanezis K, D'Agostino G, Widjaja AA, Song W-H, Xie C, Su L, Kwek X-Y, Tee N, Dong J, Ko N, Wang M, Pua CJ, Jamal MH, Soh B, Viswanathan S, Schafer S, Cook SA. Interleukin-11 is Important for Vascular Smooth Muscle Phenotypic Switching and Aortic Inflammation, Fibrosis and Remodeling in Mouse Models. *Scientific Reports*. 2020;10:17853.
56. Farrell K, Simmers P, Mahajan G, Boytard L, Camardo A, Joshi J, Ramamurthi A, Pinet F, Kothapalli CR. Alterations in Phenotype and Gene Expression of Adult Human Aneurysmal Smooth Muscle Cells by Exogenous Nitric Oxide. *Experimental Cell Research*. 2019;384:111589.
57. Saran U, Foti M, Dufour J-F. Cellular and Molecular Effects of the MTOR Inhibitor Everolimus. *Clinical Science*. 2015;129:895-914.

58. Buccheri D, Piraino D, Andolina G, Cortese B. Understanding and Managing In-Stent Restenosis: a Review of Clinical Data, from Pathogenesis to Treatment. *Journal of Thoracic Disease*. 2016;8:E1150-e1162.
59. Bianconi V, Sahebkar A, Atkin SL, Pirro M. The Regulation and Importance of Monocyte Chemoattractant Protein-1. *Current Opinion in Hematology*. 2018;25:44-51.
60. Gao S, Zhou J, Liu N, Wang L, Gao Q, Wu Y, Zhao Q, Liu P, Wang S, Liu Y, Guo N, Shen Y, Wu Y, Yuan Z. Curcumin Induces M2 Macrophage Polarization by Secretion IL-4 and/or IL-13. *Journal of Molecular and Cellular Cardiology*. 2015;85:131-139.
61. Hofmann U, Knorr S, Vogel B, Weirather J, Frey A, Ertl G, Frantz S. Interleukin-13 Deficiency Aggravates Healing and Remodeling in Male Mice After Experimental Myocardial Infarction. *Circulation: Heart Failure*. 2014;7:822-830.
62. Park S-J, Kang S-J, Virmani R, Nakano M, Ueda Y. In-Stent Neoatherosclerosis. *Journal of the American College of Cardiology*. 2012;59:2051-2057.
63. Borovac JA, D'Amario D, Vergallo R, Porto I, Bisignani A, Galli M, Annibali G, Montone RA, Leone AM, Niccoli G, Crea F. Neoatherosclerosis after Drug-Eluting Stent Implantation: a Novel Clinical and Therapeutic Challenge. *European Heart Journal - Cardiovascular Pharmacotherapy*. 2019;5:105-116.
64. Shi X, Gao J, Lv Q, Cai H, Wang F, Ye R, Liu X. Calcification in Atherosclerotic Plaque Vulnerability: Friend or Foe? *Frontiers in Physiology*. 2020;11.
65. Halwani DO, Anderson PG, Brott BC, Anayiotos AS, Lemons JE. The Role of Vascular Calcification in Inducing Fatigue and Fracture of Coronary Stents. *Journal of Biomedical Materials Research Part B: Applied Biomaterials*. 2012;100B:292-304.
66. McDonald Robert A, Halliday Crawford A, Miller Ashley M, Diver Louise A, Dakin Rachel S, Montgomery J, McBride Martin W, Kennedy S, McClure John D, Robertson Keith E, Douglas G, Channon M, Oldroyd G, Baker H. Reducing In-Stent Restenosis. *Journal of the American College of Cardiology*. 2015;65:2314-2327.
67. Palomino-Morales R, Torres C, Perales S, Linares A, Alejandre MJ. Inhibition of Extracellular Matrix Production and Remodeling by Doxycycline in Smooth Muscle Cells. *Journal of Pharmacological Sciences*. 2016;132:218-223.
68. Freitas-Rodríguez S, Folgueras AR, López-Otín C. The Role of Matrix Metalloproteinases in Aging: Tissue Remodeling and Beyond. *Biochimica et Biophysica Acta (BBA) - Molecular Cell Research*. 2017;1864:2015-2025.
69. Olejarz WŁDK-TG. Matrix Metalloproteinases as Biomarkers of Atherosclerotic Plaque Instability. *International Journal of Molecular Sciences*. 2020;21

ATHEROSCLEROTIC THREE-LAYER NANOMATRIX VASCULAR SHEETS FOR
HIGH-THROUGHPUT THERAPEUTIC EVALUATION

by

**JUN CHEN[†], XIXI ZHANG[†], GILLIAN HUSKIN, WILL EVANS, PATRICK
TAEJOON HWANG, JEONG-A KIM, BRIGITTA C. BROTT, HANJOONG JO,
AND HO-WOOK JUN**

Submitted to *Nature Communication*

Format adapted for dissertation

Abstract

In vitro atherosclerosis models are essential to evaluate therapeutics before *in vivo* and clinical studies, but significant limitations remain, such as the lack of three-layer vascular architecture and limited atherosclerotic features. Moreover, no scalable 3D atherosclerosis model is available for making high-throughput assays for therapeutic evaluation. Herein, we report an *in vitro* 3D three-layer nanomatrix vascular sheet with critical atherosclerosis multi-features (VSA), including endothelial dysfunction, monocyte recruitment, macrophages, extracellular matrix remodeling, smooth muscle cell phenotype transition, inflammatory cytokine secretion, foam cells, and calcification initiation. Notably, we also present the creation of high-throughput functional assays with VSAs and the use of these assays for evaluating therapeutics for atherosclerosis treatment. The therapeutics include conventional drugs (statin and sirolimus), candidates for treating atherosclerosis (curcumin and colchicine), and potential gene therapy (miR-146a-loaded liposomes). The high efficiency and flexibility of the scalable VSA functional assays should facilitate drug discovery and development for atherosclerosis.

Keywords: atherosclerosis, drug evaluation, 3D *in vitro* models, vascular sheet, high-throughput

Introduction

Cardiovascular diseases (CVDs) are the leading cause of death globally, primarily due to atherosclerosis caused by dyslipidemia and inflammation^{104, 105}. Atherosclerotic plaque formation in arterial walls narrows and hardens the arteries, leading to severe health issues. Thus, there is an urgent need for effective therapeutics targeting atherosclerosis.

During the development of effective therapies for atherosclerosis, *in vitro* models are commonly used to evaluate the efficacy and safety of novel therapeutics prior to initiating complicated *in vivo* and clinical studies¹⁰⁶. Compared to *in vivo* models, *in vitro* models provide human-relevant data in a cheaper, more controllable, and higher-throughput manner with improved reproducibility¹⁰⁷. *In vitro* models are generally classified into two-dimensional (2D) and three-dimensional (3D) models. While traditional *in vitro* 2D models have been widely used to assess drug safety and efficacy, these models are restricted to a 2D environment, and their cellular compositions are too simplistic to mimic atherosclerotic vessel physiology closely. In addition, most of these 2D models are not generated following atherosclerosis pathogenesis. Therefore, data generated using these models may lead to misleading predictions regarding therapeutic candidates.

Recent advances in tissue engineering, biomaterial development, and microfluidic approaches have led to extensive research on developing *in vitro* 3D culture systems to model atherosclerosis, which better recapitulates physiological architecture and pathological conditions observed *in vivo*¹⁰⁸. For example, organ-on-a-chip (OOC) models generate a dynamic, physiological environment with cell constructs that recapitulate human organ structures¹⁰⁹. Several studies, thus far, have reported atherosclerosis-related OOC systems, which either consist of an endothelial layer, a smooth muscle cell (SMC)

layer, and macrophages or only an activated endothelium and monocytes in a microfluidic device¹¹⁰. However, these current OOC platforms for atherosclerosis are still in their infancy, as they only present limited features observed in atherosclerosis and lack lipids, extracellular matrix (ECM) remodeling, calcification, and foam cells, which are the critical components of atherosclerotic plaques. Besides OOC systems, another study reported an engineered 3D spheroid pseudo-atherosclerotic plaque composed of monocytes, collagen, lipid, and macrophages¹¹¹. While this system may be the most advanced spheroid model related to atherosclerosis, it was not generated following multifactorial atherosclerosis pathogenesis and failed to faithfully resemble the layered structure of vessels. This layered structure of the vessel wall plays a significant role in atherogenesis by participating in several atherosclerotic processes, such as monocyte recruitment, stenosis development, and ECM remodeling¹¹². Thus, efforts have been made to develop tissue-engineered blood vessels (TEBVs) to model atherosclerosis and address the importance of the layered vascular structure^{113, 114}. Nevertheless, challenges, such as high cost, long maturation time, complicated fabrication processes, difficulties in scale-up production, and batch-to-batch variability, limit the use of TEBV for high-throughput therapeutic evaluation. Additionally, most TEBVs lack the outer vascular fibroblast layer, which plays a significant role in atherogenesis by participating in inflammation and extracellular matrix (ECM) remodeling^{109, 115}. Substantial evidence shows that atherogenesis occurs at the vessels' inner endothelial and outer fibroblast layers¹¹⁶. Therefore, given the limitations of current *in vitro* 2D and 3D atherosclerosis models, it is imperative to develop an advanced *in vitro* 3D atherosclerosis model that possesses a three-layer vascular structure, recapitulates critical atherosclerosis multi-features, embraces the strengths of being cost-effective,

reproducible, and scalable, and provides reliable prediction for therapeutic safety and effectiveness.

In recent years, there has been growing interest in designing high-throughput screening (HTS) assays using *in vitro* models for rapidly generating and analyzing large-scale human-relevant data, accelerating pre-clinical drug evaluation¹¹⁷. However, despite the significant progress in HTS development, most of these studies have focused on cancer research^{118, 119}, with limited studies on atherosclerosis, possibly due to its complicated pathogenesis. Furthermore, in these studies, the HTS assays were typically based on simple 2D culture systems comprising only a single type of cells, and sometimes, using non-vascular cells (HepG2 or COS-7)¹²⁰⁻¹²², possibly leading to inaccurate drug efficacy and safety predictions. Therefore, the next generation of HTS assays should use advanced 3D atherosclerosis models with multiple vascular cells to account for the critical roles of cell-cell communication and cell-ECM interaction. However, to date, no studies have yet demonstrated the development of high-throughput functional assays for evaluating potential therapeutics using 3D atherosclerosis models.

Therefore, here, we introduce an engineered *in vitro* atherosclerosis model - a 3D three-layer nanomatrix vascular sheet (VS) with critical atherosclerosis multi-features, abbreviated as VSA. Of note, we demonstrate using these VSAs to develop pioneering high-throughput functional assays beneficial for evaluating atherosclerosis therapeutics. Specifically, we first demonstrate the development of a three-layer nanomatrix VS that mimics the properly layered structure of the human vascular wall, using a state-of-the-art technology combining a layer-by-layer method, a peptide amphiphile (PA)-based nanomatrix sheet technique, and a cell-as-glue approach. Then, we present the generation

of a VSA by adding monocytes and various pro-atherosclerotic cytokines, colony-stimulating factors, and oxidized low-density lipoprotein (Ox-LDL) to the 3D three-layer nanomatrix VS (Fig. 1a) simulating atherogenesis. The critical atherosclerosis multi-features include endothelial dysfunction, monocyte recruitment, macrophage and foam cell generation, cytokine secretion, SMC phenotype transition, calcification initiation, and ECM remodeling (Fig. 1b). Notably, we create unprecedented high-throughput functional assays - foam cell and inflammation assays - composed of large-scale replicates of 3D VSAs, which enable efficient evaluation of anti-atherosclerotic therapeutics with cost-effectiveness and ease of scalability. The evaluated therapeutics include classic drugs (statin and sirolimus), drug candidates (curcumin and colchicine), and a potential gene therapy (microRNA-146a (miR-146a)-loaded liposomes (Lip-miR-146a)) (Fig. 1c). Importantly, we find that the data regarding the therapeutic effect on foam cells and inflammation generated using these VSA assays are similar to what has been reported using *in vivo* models. This groundbreaking work demonstrates a cutting-edge *in vitro* 3D atherosclerosis system that can generate high-throughput functional assays with solid potential and versatility that enable efficient evaluation of the anti-atherosclerotic effects of wide-ranging therapeutics, demonstrating considerable promise for advancing the early stage of *in vitro* drug evaluation and improving drug effect prediction before *in vivo* studies.

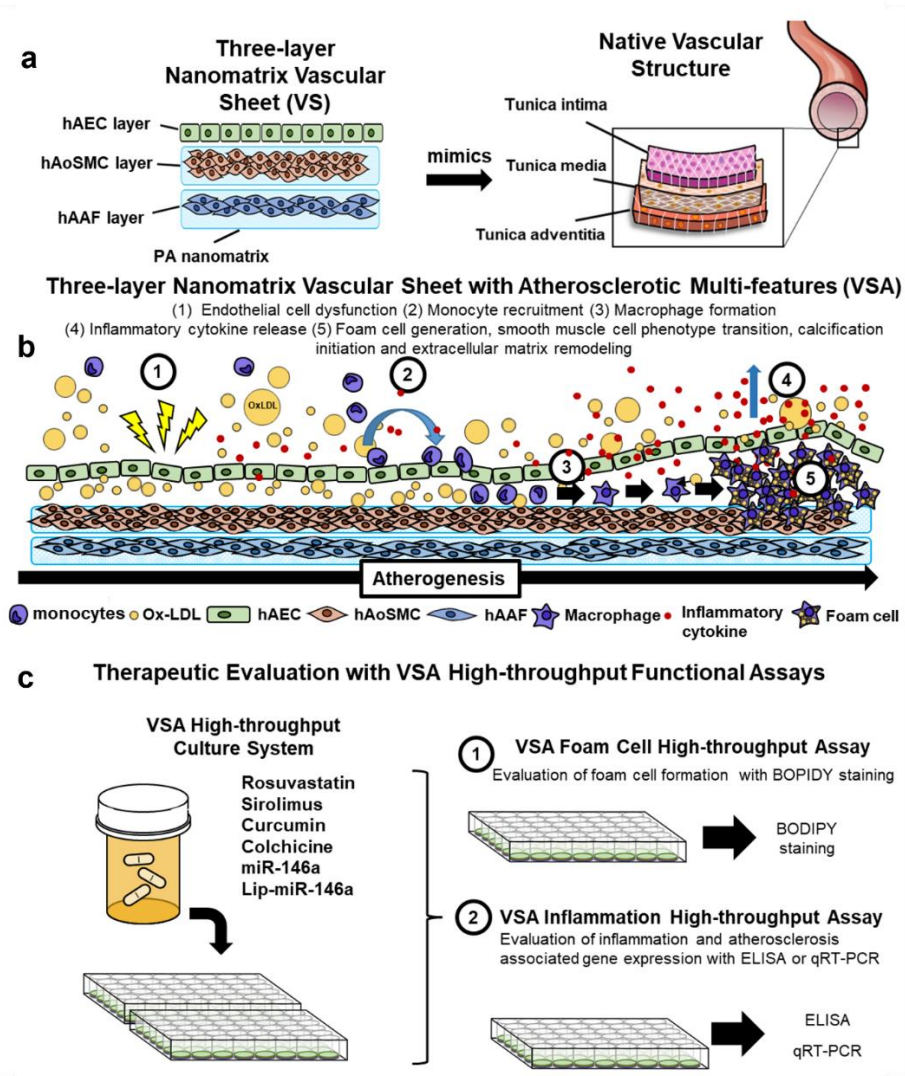


Fig.1 | Nanomatrix vascular sheet (VS), nanomatrix vascular sheet with atherosclerosis (VSA), and VSA functional assays for therapeutic evaluation. a, A schematic diagram depicts the three-layer structure of the nanomatrix vascular sheet (VS) that composes hAEC, hAoSMC, and hAAF layers, which mimics the layered structure of native vascular wall composed of tunica intima, media, and adventitia. **b,** A schematic diagram depicts a three-layer nanomatrix vascular sheet with atherosclerotic multi-features (VSA), including endothelial cell dysfunction, monocyte recruitment, macrophage formation, inflammatory cytokine release, form cell generation, SMC phenotype transition,

calcification initiation, and extracellular matrix remodeling. **c**, A schematic diagram depicts the VSA high-throughput functional assays that focus on evaluating foam cells, inflammation, and atherosclerosis-associated genes and the therapeutics evaluated using these assays in the study.

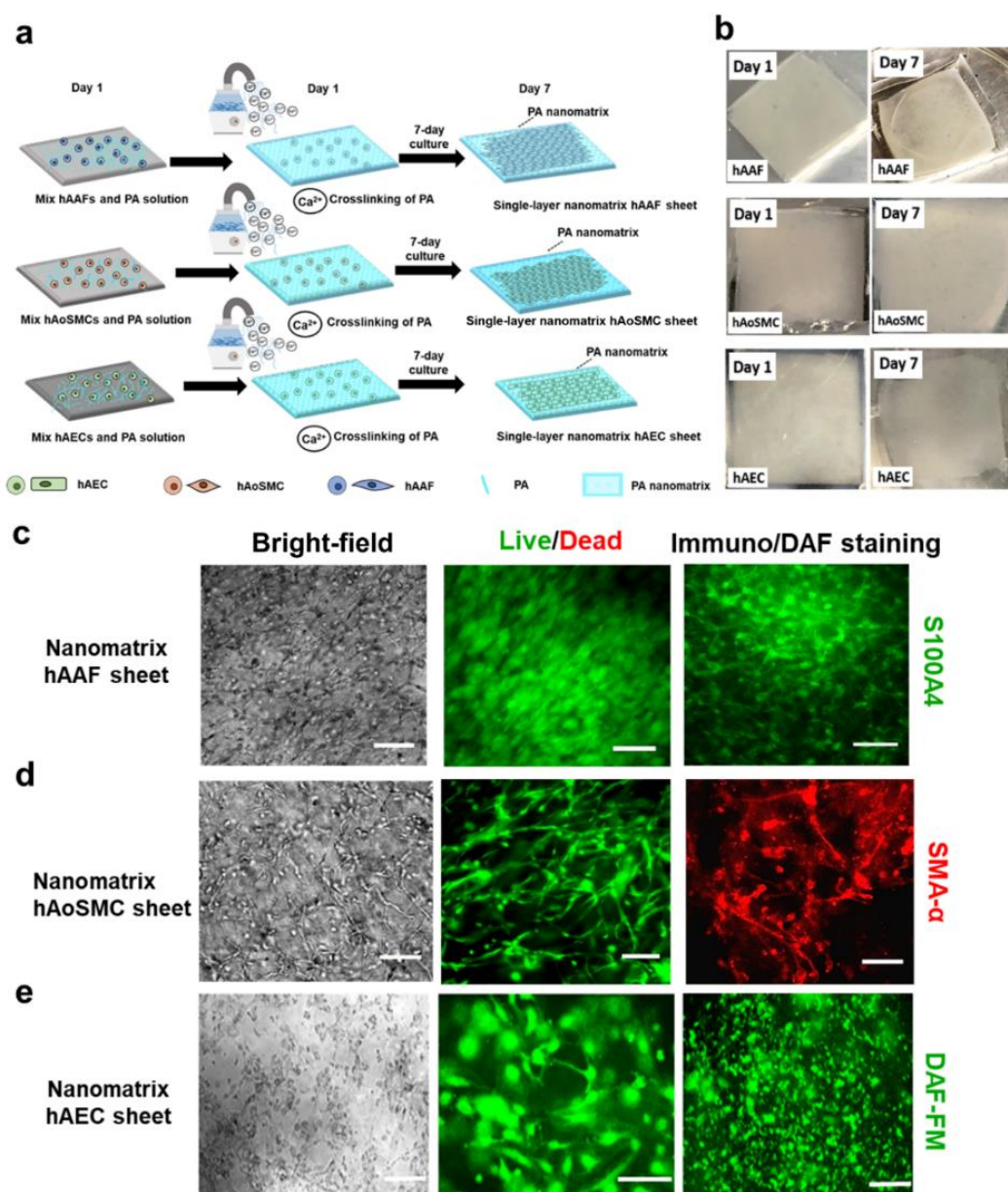


Fig.2 | Development of single-layer nanomatrix VS using nanomatrix sheet technique.

a, A Schematic diagram depicts the nanomatrix sheet technique for fabricating single-layer nanomatrix VS, including single-layer nanomatrix vascular hAAF, hAoSMC, or hAEC sheet. **b**, Representative top-down view image of single-layer nanomatrix hAAF, hAoSMC, or hAEC sheet (2 cm x 2 cm) after 1- or 7-day culture. **c**, Representative bright-field image of single-layer nanomatrix hAAF sheet and fluorescent images of single-layer nanomatrix hAAF sheet with live(green)/dead(red) staining and S100A4 immunostaining for indicating cell viability and phenotype, respectively. **d**, Representative bright-field image of single-layer nanomatrix hAoSMC sheet and the fluorescent images of single-layer nanomatrix hAoSMC sheet with live (green)/dead (red) staining and SMA- α immunostaining (red) for indicating cell viability and phenotype, respectively. **e**, Representative bright-field image of single-layer nanomatrix hAEC sheet and the fluorescent images of single-layer nanomatrix hAEC sheet with live (green)/dead (red) or DAF-FM staining (green) for indicating cell viability and endothelial function, respectively. Scale bar. 100 μ m.

Results

Development of single-layer nanomatrix VS with excellent viability and maintained phenotype, using nanomatrix sheet technique

The nanomatrix sheet technique is a new method developed in the current study for making a nanomatrix VS, which encapsulates the cells in a 3D nanomatrix composed of biocompatible ECM-mimicking PA nanofibers. Before fabricating the 3-layer nanomatrix

VS, we first explored the approach to fabricate each vascular cell layer individually, designated as a single-layer nanomatrix VS, using the PA nanomatrix sheet technique. Specifically, to make the single-layer nanomatrix VSs, primary human aortic adventitial fibroblasts (hAAFs), aortic artery smooth muscle cells (hAoSMCs), and aortic endothelial cells (hAECs) were encapsulated in the nanomatrix made by 1 or 2 wt% PA and cultured for 7 days (Fig. 2a). Interestingly, it was found that, on day 7, regardless of the cell types, the vascular cells in the 1 wt% PA nanomatrix exhibited elongated morphology with suitable cell spreading (Fig. 2c-d), in contrast to the vascular cells encapsulated in 2 wt% PA nanomatrix which remained spheroid-shaped (Supplementary Fig. 1). In addition, we showed that, for all three cell types, an integrated cell sheet could be formed as early as one day after its fabrication (Fig. 2b). Notably, after 7-day culture, these sheets became more robust and mature and showed excellent viability (Fig. 2c-e). Furthermore, the immunostaining of typical phenotype markers for hAAF (S100A4) and hAoSMC (SMA- α) demonstrated that the cells within the sheet maintained their phenotypes (Fig. 2c-d). Moreover, DAF-FM staining showed active nitric oxide secretion from hAECs (Fig. 2e), indicating the proper endothelial function of the hAEC of the VS.

Development of a double-layer nanomatrix VS combining nanomatrix sheet technique, cell-as-glue approach, and layer-by-layer assembly method

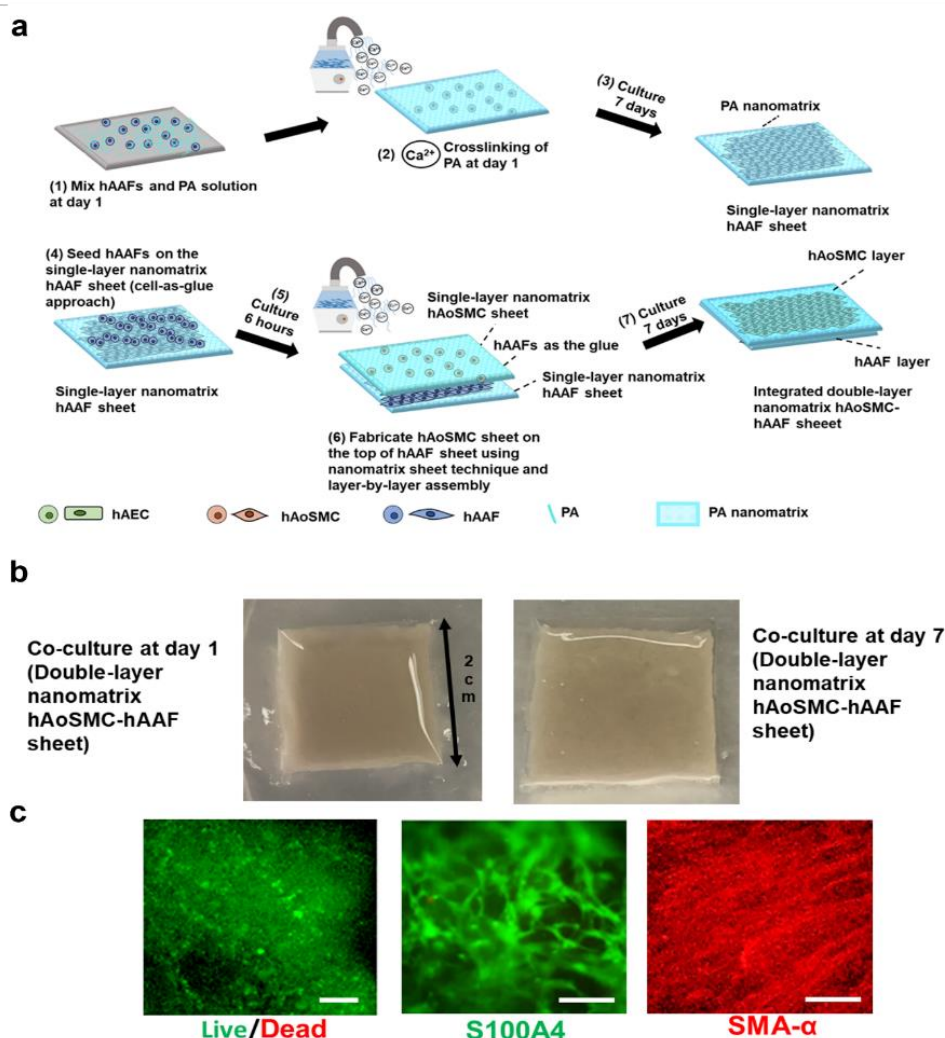
Following the successful single-layer nanomatrix VS fabrication, we explored a novel method to fabricate the double-layer nanomatrix VS- the hAoSMC-hAAF sheet. For mimicking the discrete vascular layered structure with adventitia and media, a layer-by-layer assembly method was used, where a single-layer hAAF sheet was fabricated,

followed by the fabrication and deposition of a single-layer hAoSMC sheet on the hAAF sheet (Fig. 3a). Importantly, to promote the integration of the two single-layer nanomatrix VSs into one integrated double-layer VS, a novel cell-as-glue approach was developed, taking advantage of the cell-adhesive ligands of PA. Specifically, hAAFs were used as glue and seeded on the hAAF sheet prior to sheet fabrication (Fig. 3a). We hypothesized that the hAAFs between the two single-layer nanomatrix VSs could bind the cell adhesive ligands from both sheets, thus gluing the two sheets to form an integrated double-layer VS. As expected, a firmly integrated hAoSMC-hAAF sheet was obtained after one day of co-culture, and it maintained its integrity after 7-day culture (Fig. 3b). In contrast, without hAAF seeding (Fig.3a, step 4), we found that the two single-layer nanomatrix VSs failed to integrate into one sheet, because of a detached and shrinking hAoSMC sheet formed on the hAAF sheet. Additionally, similar to cells in the single-layer nanomatrix VSs, the encapsulated hAoSMCs, and hAAFs within the hAoSMC-hAAF sheet also maintained excellent viability and their respective phenotypes (Fig. 3c).

Development of a three-layer nanomatrix VS that mimics the multilayered vascular wall structure in humans

Considering that the human arterial endothelium is a monolayer of endothelial cells (ECs), instead of using the nanomatrix sheet technique, direct seeding of hAECs on the hAoSMC-hAAF sheet was used to create the inner layer of the three-layer nanomatrix VS. However, it was noted that the direct seeding approach led to the penetration of the hAECs into the hAoSMC layer (Supplementary Fig.2), possibly due to the porous structure of the double-layer VS. Thus, hAoSMCs were seeded on the hAoSMC-hAAF double-layer VS

before hAEC seeding. The rationale behind this strategy was that hAoSMCs seeding and spreading would decrease the pore size of the double-layer VS, thereby preventing hAEC penetration (Fig. 4a). To test this strategy, a three-layer VS was fabricated using hAAFs for the bottom layer, red fluorescent protein-expressing human aortic smooth muscle cells (RFP-hAoSMCs) for the middle layer, and green fluorescent protein-expressing human aortic endothelial cells (GFP-hAECs) for the top layer. Thus, hAEC penetration could be characterized by green fluorescence in the red hAoSMC layer. Promisingly, Fig. 4b showed no penetration of GFP-hAECs when RFP-hAoSMC seeding occurred prior to GFP-hAEC seeding. More importantly, using such an approach, a well-defined three-layer nanomatrix



VS was obtained, with hAAF (tunica adventitia), RFP-hAoSMC (tunica media), and GFP-hAEC (tunica intima) layers, from bottom to top, respectively (Fig. 4b). Moreover, the top layer of the VS achieved excellent endothelialization and expressed proper endothelial phenotype, CD31 (Fig. 4c).

Fig.3 | Development of double-layer nanomatrix vascular sheet using nanomatrix sheet technique, layer-by-layer assembly and cell-as-glue approach. a, A schematic diagram illustrates the detailed procedure for developing a double-layer nanomatrix vascular sheet using the nanomatrix sheet technique, layer-by-layer assembly, and cell-as-glue approach. **b,** Representative top-down image of double-layer nanomatrix vascular sheet (hAoSMC-hAAF sheet), on day 1 and day 7 and with 1 million hAAFs /cm² as the glue, for showing double-layer nanomatrix vascular sheet formation. **c,** Representative fluorescent images of the double-layer cell sheet, hAoSMC-hAAF sheet, with live (green)/dead (red) staining and S100A4 (green) or SMA- α (red) immunostaining for showing the cell viability and phenotype in the double-layer nanomatrix vascular sheet, respectively. Scale bar, 100 μ m.

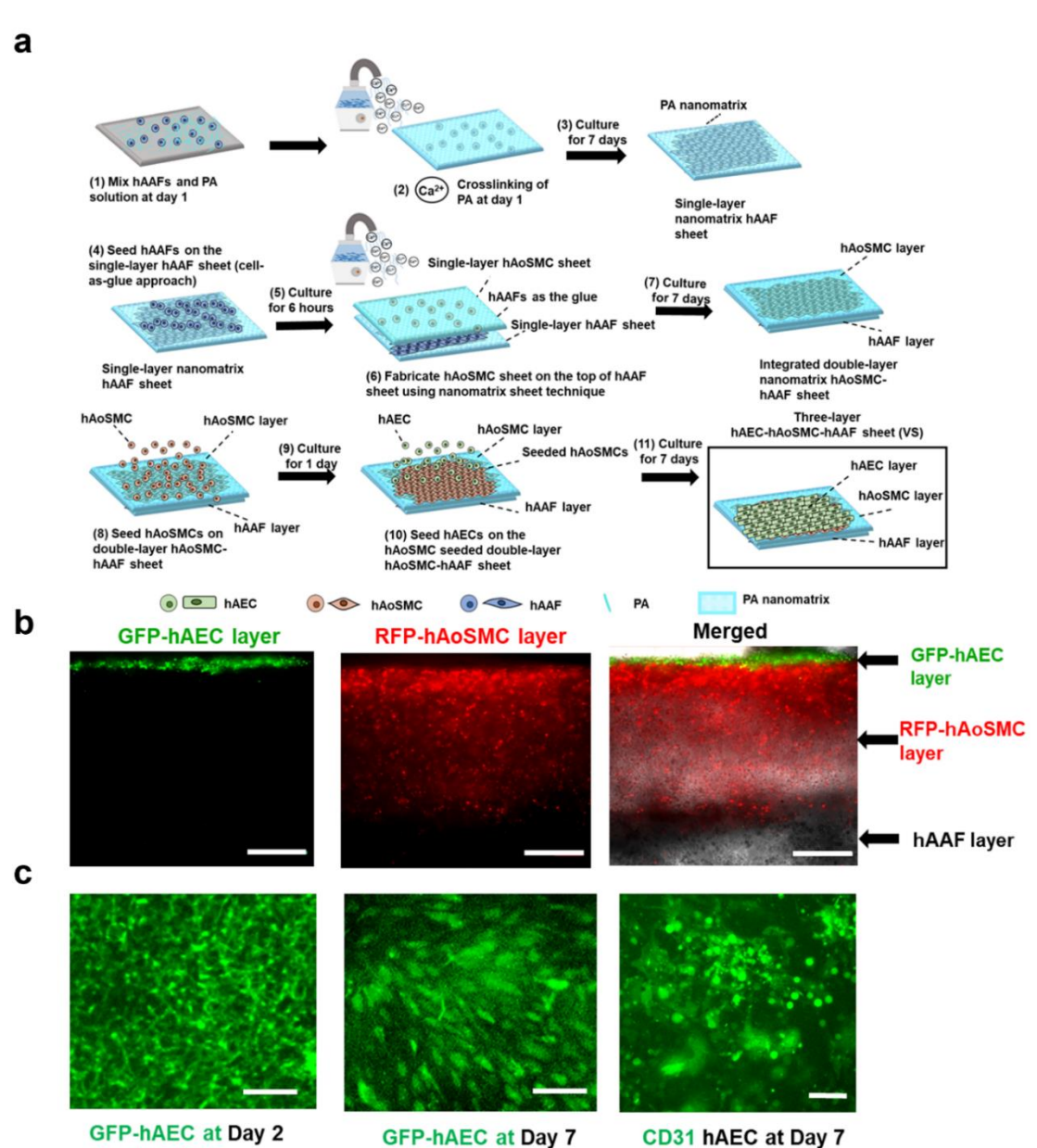


Fig.4 | Development of three-layer nanomatrix VS using nanomatrix sheet technique, layer-by-layer assembly and cell-as-glue approach. **a**, A schematic diagram illustrates the detailed procedure for fabricating a three-layer nanomatrix vascular sheet using the nanomatrix sheet technique, layer-by-layer assembly, and cell-as-glue approach. **b**, Representative fluorescent images demonstrating a cross-sectional view of the GFP-hAEC layer (green) and RFP-hAoSMC middle layer (red) of the three-layer nanomatrix vascular sheet and a representative image merged from fluorescent and optical images of the three-

layer nanomatrix vascular sheet for showing the three-layer structure of the vascular sheet. Scale bar, 200 μm . **c**, Representative fluorescent image of GFP-hAEC layer of the three-layer nanomatrix vascular sheet (GFP-hAEC-GFP-hAoSMC-hAAF sheet) on day 2 and day 7 after GFP-hAEC seeding for showing the cell morphology of the hAEC layer, and with CD31 immunostaining of hAEC layer of the three-layer nanomatrix vascular sheet (hAEC-hAoSMC-hAAF sheet) on day 7 after hAEC seeding for showing cell phenotype of the hAEC layer. Scale bar 200 μm .

Induction of endothelial dysfunction and monocyte recruitment onto the three-layer nanomatrix VS

Endothelial dysfunction and monocyte recruitment are the critical milestones of atherosclerosis initiation¹²³. To induce endothelial dysfunction in the VS, we utilized a combination of tumor necrosis factor- α (TNF- α) and Ox-LDL. Before inducing endothelial dysfunction on the VS, we explored the appropriate concentrations of TNF- α and Ox-LDL that could induce endothelial dysfunction while maintaining viability on TCPs. Compared with other conditions, 40 ng/mL TNF- α and 50 $\mu\text{g/mL}$ ox-LDL induced a high expression of the endothelial dysfunction marker intercellular adhesion molecule 1 (ICAM-1) within 24 h while maintaining relatively good viability (Supplementary Fig. 3a, b). Also, this combination resulted in significantly more recruited monocytes than the untreated group (Supplementary Fig. 4a, b). Therefore, by using this combination, successful induction of endothelial dysfunction on the VS was demonstrated by a greater expression of endothelial dysfunction markers, ICAM-1, and vascular cell adhesion protein 1 (VCAM-1), compared with the untreated controls (Fig. 5b, c). Additionally, the dysfunctional endothelial layer was observed to recruit more monocytes in great contrast to the untreated VS (Fig. 5d).

Furthermore, a cross-section view of the sheet exhibited a significant number of monocytes (blue) recruited on top of the GFP-hAEC-RFP-hAoSMC-hAAF sheet (Fig. 5e).

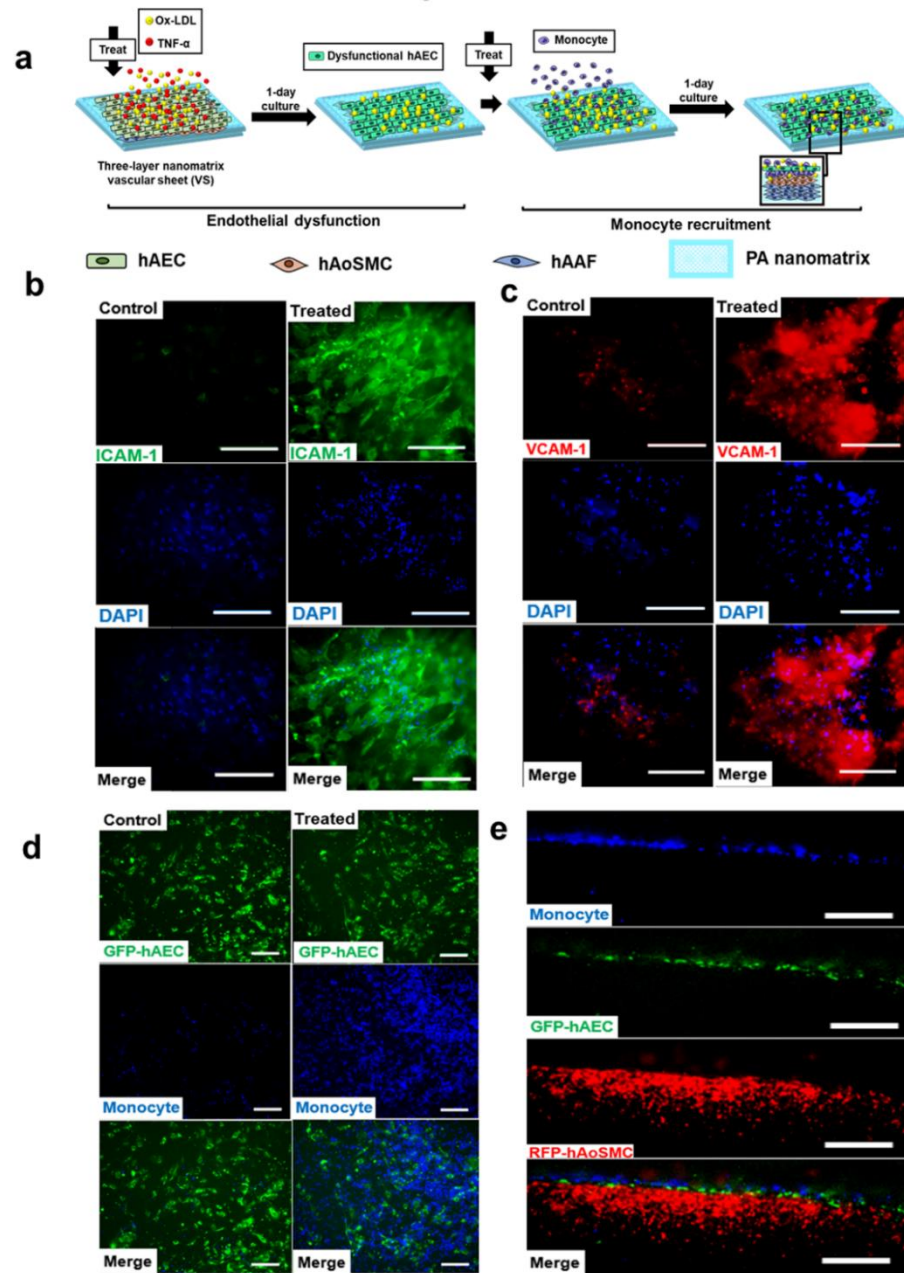


Fig.5 | Induction of endothelial dysfunction and monocyte recruitment on the three-layer nanomatrix VS. a, A schematic diagram illustrates the procedure of using Ox-LDL and TNF- α for inducing endothelial dysfunction and monocyte recruitment on the three-layer nanomatrix vascular sheet (VS). **b,** Representative fluorescent images of Ox-LDL

and TNF- α untreated (control) and treated three-layer nanomatrix vascular sheet with ICAM-1 immunostaining and DAPI staining for showing successful induction of endothelial dysfunction. Scale bar, 200 μ m. **c**, Representative fluorescent images of Ox-LDL and TNF- α untreated and treated three-layer nanomatrix vascular sheet with VCAM-1 immunostaining (red) and DAPI staining (blue) for showing successful induction of endothelial dysfunction. Scale bar, 200 μ m. **d**, Representative fluorescent images of calcein-blue stained monocytes (blue) on the GFP-hAEC layer (green) of Ox-LDL and TNF- α untreated (control) and treated three-layer nanomatrix vascular sheet for showing successful induction of monocyte recruitment. Scale bar, 400 μ m. **e**, Representative fluorescent images of the cross-section view of the GFP-hAEC layer (green) and RFP-hAoSMC layer (red) of and monocytes (blue) on the Ox-LDL and TNF- α treated three-layer nanomatrix vascular sheet for showing successful induction of monocyte recruitment. Scale bar, 400 μ m.

Induction of macrophage formation and foam cell generation in the three-layer nanomatrix VS with endothelial dysfunction and monocyte recruitment to form VSA

Following endothelial dysfunction and monocyte recruitment, monocyte differentiation into macrophages is critical for promoting inflammatory progression by secreting various pro-inflammatory cytokines¹²⁴ and taking up Ox-LDL to form foam cells¹²⁴⁻¹²⁸. Thus, we first explored the proper condition composed of pro-atherogenic cytokines and Ox-LDL for inducing macrophage differentiation and foam cell formation on TCPs. It was found that the monocytes treated with Ox-LDL, granulocyte-macrophage colony-stimulating factor (GM-CSF), macrophage colony-stimulating factor (M-CSF), and

interferon- γ (IFN- γ) transformed into foam cells with a higher amount of Ox-LDL and produced significantly more interleukin 1 β (IL-1 β) compared to the control (Supplementary Fig.4c-g). Hence, following the induction of endothelial dysfunction and monocyte recruitment on the VS, "a customized atherosclerotic medium" containing such a combination and monocytes was employed twice to induce monocytes differentiation into macrophages and the generation of foam cells, thereby forming VSA (Fig. 6a). Then, the atherosclerotic features of VSA were comprehensively evaluated at histological level (macrophage marker expression and foam cell generation), molecular level (inflammatory cytokine secretion and oxidative stress level) and genetic level (atherosclerosis-associated gene expression). Fig. 6b showed the VSA demonstrated the positive expression of cluster of differentiation 14 (CD14), a monocyte marker, and cluster of differentiation 68 (CD68), a macrophage marker, expressed by the atherosclerotic macrophages in human plaque, indicating atherosclerotic macrophage formation on the sheet. Notably, as shown in Fig. 6c-d, the boron-dipyrromethene (BODIPY) fluorescent signal of VSA was 4.54 ± 2.02 fold that of the untreated control, indicating a significant amount of foam cells and lipid accumulation induced on the sheet using our approach. Notably, aggregations of foam cells, similar to fat streaks or lipid pools, which is a critical atherosclerotic feature reported in human atherosclerotic plaque, were also observed in the VSA (Fig. 6c). In addition, critical inflammatory cytokines secreted by human atherosclerotic plaque¹²⁹⁻¹³⁴ were also produced by the VSA, including interleukin 1 α (IL-1 α) (3.60 ± 0.51 fold vs. control), IL-1 β (44.39 ± 5.32 fold vs. control), monocyte chemoattractant protein-1 (MCP-1) (1.63 ± 0.14 fold vs. control), IFN- γ (354.37 ± 23.11 fold vs. control), and interleukin 6 (IL-6) (2.07 ± 0.072 fold vs. control), and interleukin 8 (IL-8) (1.34 ± 0.076 fold vs. control),

suggesting an additional key atherosclerotic feature, inflammation, was induced in the VSA (Fig. 6f). In addition to pro-inflammatory cytokines, we also observed the secretion of IL-10, an anti-inflammatory cytokine, by the VSA. Although atherosclerosis is a chronic inflammatory disease, anti-inflammatory cytokines are also generated during inflammatory resections. One typical example is IL-10, found in human advanced atherosclerotic plaque¹³⁵. The expression of both pro-inflammatory and anti-inflammatory cytokines suggested that M1 and M2 macrophages may exist in the VSA. Meanwhile, the dynamic inflammation progression was demonstrated by the reactive oxygen species (ROS) level. It was found that ROS level increased with time during the induction process, with a 2.22 ± 0.41 fold increase from days 0 to 10 and a 1.85 ± 0.24 fold increase from days 10 to 13 (Fig. 6f).

In addition to the molecular level, the atherosclerosis-related gene expression on the VSA was also characterized and classified into five categories: 1) endothelial function, 2) SMC phenotype, 3) inflammation, 4) calcification, and 5) ECM remodeling. Compared to the control, the downregulation of platelet endothelial cell adhesion molecule-1 (PECAM-1) ($18.31 \pm 7.88\%$ vs. control) and endothelial nitric oxide synthase (eNOS) ($1.94 \pm 0.82\%$ vs. control) indicated the impaired endothelial function of the VSA (Fig. 6g). Additionally, a decreased expression of SMC contractile phenotype marker, muscle myosin heavy chain 11 (MYH11) ($11.58 \pm 10.13\%$ vs. control) but an increased expression of platelet-derived growth factor subunit B (PDGF-B) (12.95 ± 5.09 fold vs. control) was observed. SMC phenotype plays a significant role in atherosclerosis-related stenosis, and SMC phenotype transition is a hallmark of atherosclerosis¹³⁶⁻¹³⁸. Normal arterial SMCs maintain their quiescent contractile phenotype, but during atherogenesis, an abundance of

PDGF-B is generated, and the SMCs dedifferentiate into a proliferative synthetic phenotype, contributing to atherosclerosis progression¹³⁹. Thus, the decreased MYH11 and increased PDGF-B expression suggest that the SMCs in the VSA may transition from contractile to synthetic phenotypes and atherosclerosis progression in the VSA. Moreover, we observed an upregulation of transforming growth factor-beta 1 (TGF- β 1) (4.15 ± 0.88 fold vs. control), nicotinamide adenine dinucleotide phosphate oxidase 4 (NOX4) (3.05 ± 1.17 fold vs. control), and a down-regulation of cyclin-dependent kinase inhibitor 2A (CDKN2A) ($29.02 \pm 3.90\%$ vs. control). These markers are related to several crucial pathways associated with atherosclerosis. For example, the increase of TGF- β 1 was reported to lead to fibrotic matrix accumulation, thereby making the ECM susceptible to calcification¹⁴⁰. TGF- β 1 was also reported to induce NOX4 expression in SMCs, which contributes to ROS elevation¹⁴⁰, agreeing with the results shown previously in Fig.6f. As reported, CDKN2A is strongly associated with macrophage and monocyte proliferation¹⁴¹, the decreased expression of CDKN2A may suggest the increased presence of pro-inflammatory monocytes and macrophages on the VSA¹⁴¹.

We also evaluated the expressions of two genes (matrix metalloproteinases (MMP-2) and collagen type III alpha 1 (COL3A1) associated with ECM remodeling, another feature of atherosclerosis. MMP-2 is strongly related to ECM degradation leading to vulnerable plaque and rupture, while COL3A1 is associated with stenosis¹⁴². In Fig. 6h, the increased expressions of MMP-2 (1.65 ± 0.17 fold vs. control) and COL3A1 (3.81 ± 0.60 fold vs. control) indicated aggressive ECM remodeling in the VSA. Interestingly, we also noticed an increased expression of runt-related transcription factor 2 (RUNX2) (12.73 ± 3.25 fold vs. control), a typical early calcification marker, indicating calcification

may have initiated on the sheet, which was confirmed by alizarin red staining (3.14 ± 0.29 fold vs. control) (Fig.6g).

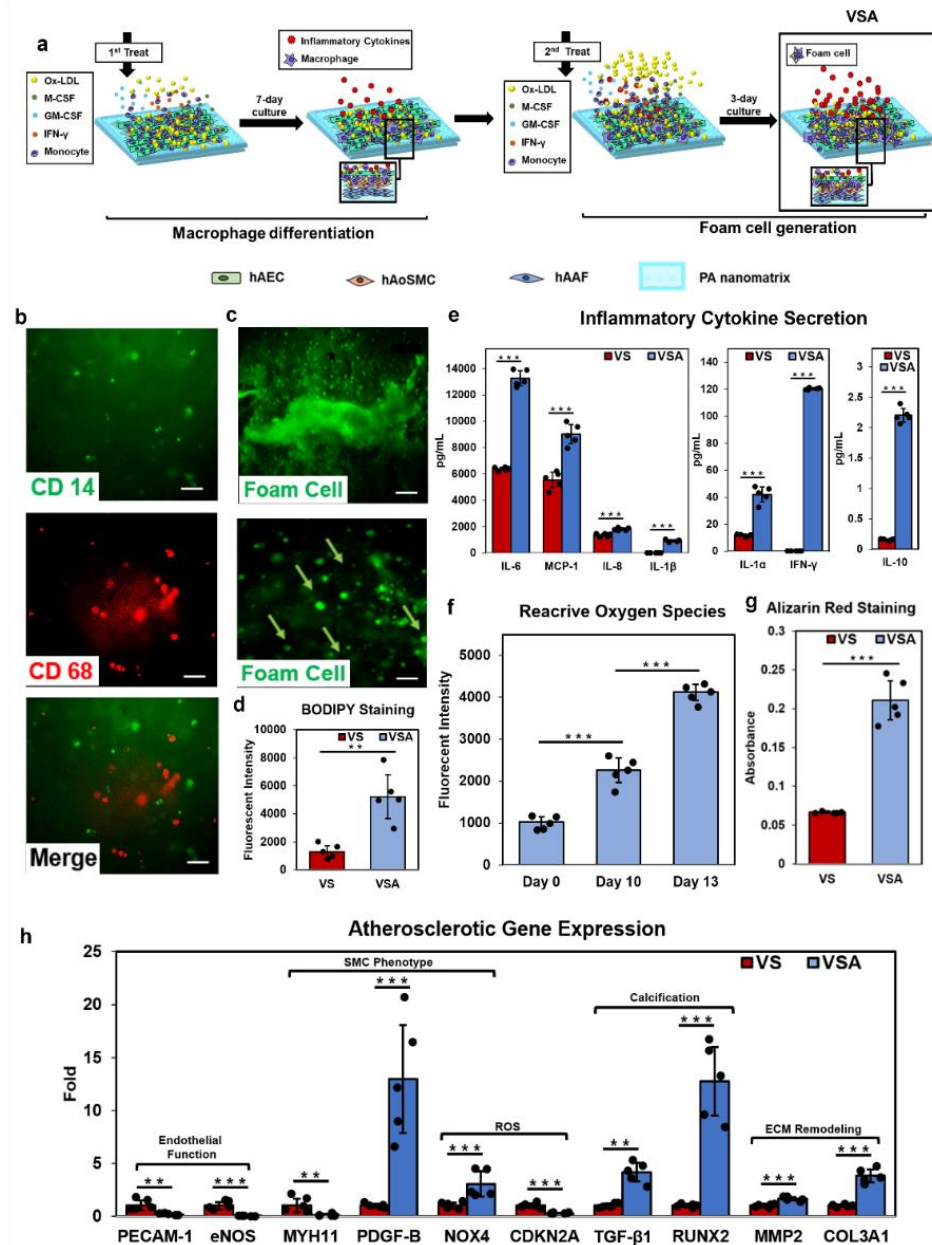


Fig.6 | Induction of macrophage formation, foam cell generation, and calcification initiation on the three-layer nanomatrix vascular sheet. a, A schematic diagram that illustrates the procedure of inducing macrophage differentiation and foam cell generation on the VS. b, Representative fluorescent images of CD14 immunostaining (green) and C68 immunostaining (red) of the VSA for showing monocyte recruitment and macrophage formation. Scale bar, 100 μ m. c, Representative fluorescent images of foam cells with

BODIPY staining (green) on the sheet for showing the foam cell, lipid pool, and foam cell aggregation. The arrows indicate the single foam cell on VSA. Scale bar, 100 μ m. d, Quantitative data of BODIPY staining of the VSA (n=5 biological replicates) and control (n=5 biological replicates) for showing the foam cell generation. Bars and error bars represent the mean \pm s.e.m. e, Inflammatory cytokine secretion by the VSA (n=5 biological replicates) compared with control (VS) (n=5 biological replicates). Bars and error bars represent the mean \pm s.e.m. f, Quantitative data of oxidative level of VSA using DCFH-DA assay (n=5 biological replicates). mean \pm s.e.m. g, Alizarin red staining of the VSA (n=5 biological replicates) and VS (n=5 biological replicates) for showing calcification initiation on the VSA. h, Atherosclerotic gene expression of the VSA (n=5 biological replicates) compared with controls (n=5 biological replicates). Bars and error bars represent the mean \pm s.e.m. The gene expression of endothelial function marker (PECAM-1, eNOS), SMC phenotype markers (MYH11, PDGF-B, NOX4), ROS production (NOX4 and CDKN2A), Calcification (RUNX2, TGF- β), ECM remodeling (MMP2, COL3A1). (*p<0.05, **p<0.01, ***p<0.001, statistical comparisons were performed by 2-sided Student's t-test between two groups and ANOVA with Tukey post hoc analysis for multiple comparisons, using SPSS 15.0 software. For the exact p-values of VSA vs. VS comparison in e, f, g, h, please refer to Supplementary Data Table. 1).

Development of VSA high-throughput functional assays for therapeutic evaluation

Taking advantage of the ease of making VSA using our approach, we pioneered several high-throughput functional assays by large-scale fabrication of VSAs in two 48-well plates containing 96 disk-shaped VSAs of around 1 cm in diameter (Fig. 7 and 8b). When used with BODIPY staining in our VSA foam cell assay, the VSA can be used for a proof-of-concept evaluation of the ability of therapeutics to prevent foam cell generation. In addition, when used with enzyme-linked immunosorbent assay (ELISA) and quantitative reverse transcription polymerase chain reaction (qRT-PCR) in our VSA inflammation assay, the VSA can be used to study the effects of therapeutics on inflammation, intraplaque angiogenesis, and ECM remodeling, crucial factors contributing to atherosclerosis progression.

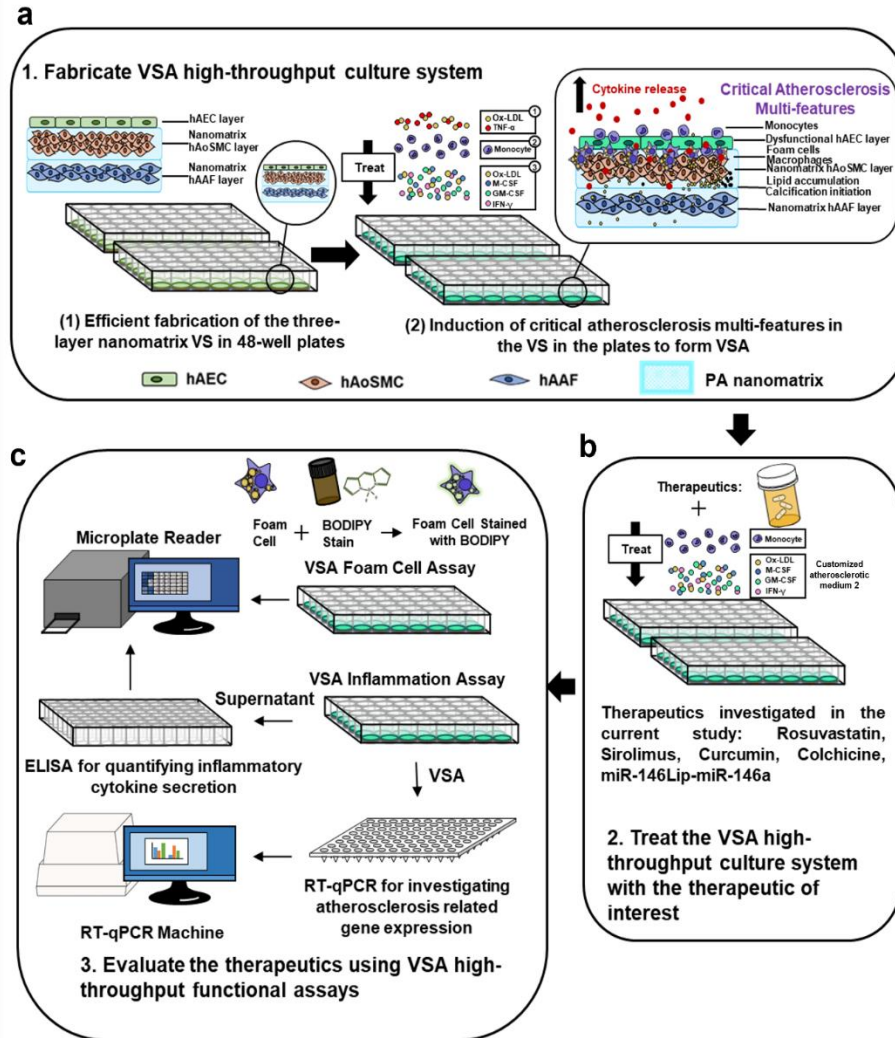


Fig.7 | The development and use of VSA high-throughput functional assays for drug evaluation. **a**, First, the VSA high-throughput culture system is fabricated using our approach by fabricating 3-layer VSs in two 48 well-plates with 96 VSs. Then the 96 VSs are treated with an atherosclerosis-inducing medium, and monocytes to form VSAs. **b**, After that, except for the VSAs used as the controls, the VSAs in both plates are treated with therapeutics of interest and cultured for 10 days with an atherosclerosis-inducing medium and monocytes. **c**, Then, one VSA plate will run a foam cell assay, and another VSA plate will run an atherosclerosis assay. All VSAs from one plate are applied with BODIPY staining, followed by quantifying the fluorescent intensity using a microplate

reader to explore the therapeutic effect on foam cell generation. All VSAs from another plate are used to explore the therapeutic effect on inflammation by studying cytokine secretion using ELISA and atherosclerosis-related gene expression using qRT-PCR. Several therapeutics are evaluated here to demonstrate the feasibility of using VSA functional assays for evaluating the therapeutic effect on atherosclerosis, including rosuvastatin, sirolimus, curcumin, colchicine, free miR-146a, and Lip-miR-146a, using the VSA functional assays.

Evaluation of the classic atherosclerotic drugs (rosuvastatin and sirolimus) using the VSA high-throughput functional assays

Rosuvastatin is a conventional orally administrated drug for preventing atherosclerosis, while sirolimus is a drug that has been used to coat coronary stents for patients with atherosclerosis^{143, 144} (Fig. 8a). Since their therapeutic effects have been widely studied (Fig. 8a), we first used the VSA assays to evaluate the effects of these two drugs. Specifically, the foam cell assay based on BODIPY-stained VSAs showed that rosuvastatin and sirolimus significantly reduced foam cell formation on the VSA (statin vs. control: $50.77 \pm 8.32\%$ vs. 100%, sirolimus vs. control: $42.73 \pm 10.62\%$ vs. 100%, Fig. 8c). Moreover, qRT-PCR revealed that statin could regulate endothelial function by upregulating the expression of PECAM-1 (146.76 ± 44.63 fold vs. control).

Furthermore, using the VSA inflammation assay evaluated with qRT-PCR, it was found that rosuvastatin may suppress intraplaque angiogenesis, as a significantly lower expression of vascular endothelial growth factor A (VEGF-A) than the control was observed. The effect of rosuvastatin on ECM remodeling was also demonstrated by

127.03±35.49 fold higher expression of COL17A1 in the rosuvastatin-treated group than in the control group and 4.46±1.75% of MMP-2 expression compared with the control group. Moreover, the IL-6 expression in the rosuvastatin-treated group was only 5.20±0.38% that of the control group (Fig. 8d), indicating the anti-inflammatory effect of statin. For sirolimus, VSA qRT-PCR revealed that it might promote inflammation resolution, as there was a significant upregulation of interleukin 10 (IL-10) (893.93±175.52 fold vs. control) but down-regulation of IL-6 (17.54±3.43% vs. control) in the sirolimus treated group compared to the control. Furthermore, suppressed angiogenesis was observed in the sirolimus-treated group with only 13.05±3.91% VEGF-A expression of the control (Fig.8d), which agrees with a previous study that showed that sirolimus could downregulate the angiogenesis by downregulating the mTOR signal pathway that involves VEGF¹⁴⁴.

Using the VSA inflammation assay evaluated with ELISA, we also investigated the regulation of several inflammatory cytokines by these two drugs. Significantly, as indicated in Fig. 7e, rosuvastatin reduced the production of crucial pro-inflammatory cytokines responsible for atherosclerosis-associated inflammation, including IL-1 α (66.78±6.52% vs. control), IL-6 (71.50±4.34% vs. control), TNF- α (39.69±5.53% vs. control), IL-8 (48.64±6.17% vs. control), and IFN- γ (44.03±3.20% vs. control). Meanwhile, statin improved the production of the anti-inflammatory cytokine IL-10; 2.10±0.50 fold of secretion in the drug-treated group was observed compared with the control (Fig. 8e). Similarly, the inflammation resolution induced by sirolimus was also detected using our VSA inflammation assay. Specifically, sirolimus reduced pro-inflammatory cytokine secretion, including IL-1 α , TNF- α , IL-8, MCP-1, and IFN- γ . Notably, the production for

MCP-1, TNF- α , and IFN- γ decreased to $22.76 \pm 2.56\%$, $40.67 \pm 6.42\%$, and $43.64 \pm 17.04\%$ of the control group, respectively. Interestingly, we also found that sirolimus reduced the expression of ECM remodeling gene COL3A1 ($22.29 \pm 3.16\%$ of control), indicating the well-known effect of sirolimus on suppressing stenosis⁴⁴. Moreover, we found that sirolimus could improve autophagy-related cytokine secretion (6.42 ± 3.59 fold for interleukin 4 (IL-4) and 1.67 ± 0.59 fold for interleukin 13 (IL-13) relative to the control) (Fig. 8e).

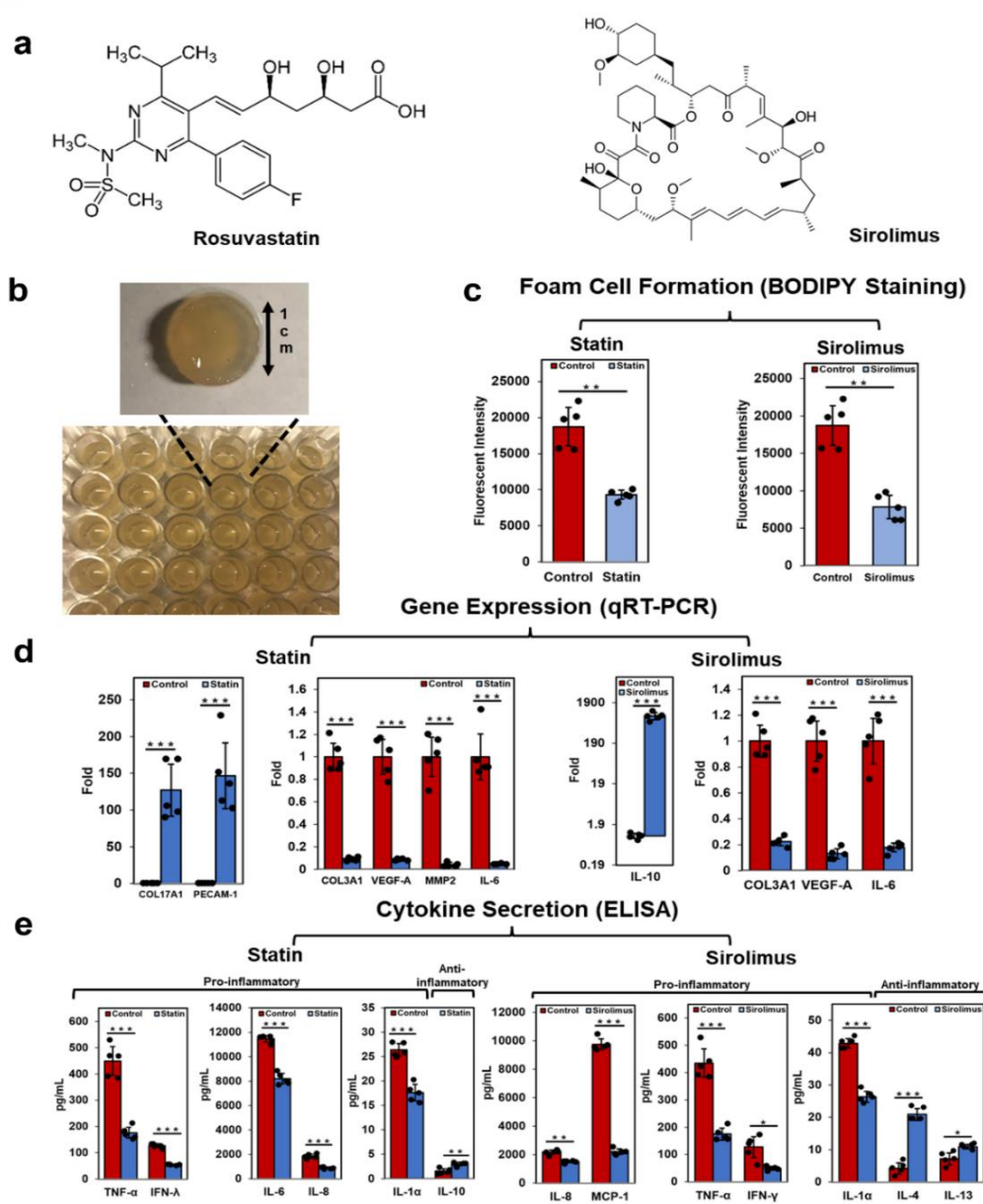


Fig.8 | Evaluation of Rosuvastatin and Sirolimus using VSA high-throughput functional assays. **a**, The chemical structure of rosuvastatin and sirolimus. **b**, Top-down view of VSA plates and single VSA. **c**, Quantitative data of BODIPY staining of VSA treated with or without statin or sirolimus for showing the effect of statin or sirolimus on foam cell generation. Bars and error bars represent the mean \pm s.e.m. (n=5 biological replicates). **d**, Quantification of atherosclerosis-related gene expression of VSAs treated with or without statin or sirolimus using qRT-PCR to show the therapeutic effect on atherosclerosis on the genetic level. Bars and error bars represent the mean \pm s.e.m. (n=5 biological replicates). **e**, Quantification of cytokine secretion of VSAs treated with or without statin and sirolimus using ELISA to show the therapeutic effect on atherosclerosis-induced inflammation on the molecular level. Bars and error bars represent the mean \pm s.e.m. (n=5 biological replicates) (* p <0.05, ** p <0.01, *** p <0.001, statistical comparisons were performed by 2-sided Student's t-test between two groups and ANOVA with Tukey post hoc analysis for multiple comparisons, using SPSS 15.0 software. For the exact p values of the comparison between VSA treated with or without statin or sirolimus in **c-e**, please refer to Supplementary Table 2).

Evaluation of curcumin and colchicine using the VSA high-throughput functional assays

Curcumin is traditionally used as a food additive and has recently been reported to have therapeutic effects, while colchicine is commonly used to treat gout and familial Mediterranean fever, a highly inflammatory condition, thereby having the potential for treating atherosclerosis due to its anti-inflammatory effects (Fig. 9a). Therefore, we used

our VSA functional assays to evaluate the potential therapeutic effects of curcumin and colchicine for atherosclerosis. Similar to statin and sirolimus, the VSA foam cell assay showed that these two drugs could also reduce foam cell generation significantly (curcumin: $31.23 \pm 5.68\%$ vs. control, colchicine: $50.86 \pm 4.57\%$ vs. control; Fig. 9a). Moreover, the results of VSA assay based on qRT-PCR revealed that curcumin participated in the regulation of genes associated with angiogenesis (VEGF-A: $38.01 \pm 5.68\%$ vs. control), ECM remodeling (MMP-2: $39.22 \pm 7.14\%$ vs. control), which agree with the finding in a recent study¹⁴⁵. Interestingly, although curcumin showed a potential anti-atherosclerotic effect, our assay demonstrated that curcumin might impair endothelial function, as downregulation of PECAM-1 expression was observed in the curcumin-treated group compared to the control (PECAM-1: $29.71 \pm 5.68\%$ vs. control) (Fig. 9c). A similar effect of curcumin on the PECAM-1 expression of activated ECs was also reported in the other study¹⁴⁶. While in contrast, we noted that colchicine might improve endothelial function by increasing PECAM-1 expression (3.35 ± 0.68 fold vs. control) (Fig. 9b). Additionally, colchicine was shown to regulate ECM remodeling, as demonstrated by decreased COL3A1 ($8.93 \pm 1.30\%$ vs. control) and MMP-2 ($6.36 \pm 1.44\%$ vs. control) expression in colchicine-treated VSAs compared to the untreated controls.

The VSA inflammation assays revealed that both drugs, curcumin, and colchicine, had anti-inflammatory properties. For example, curcumin showed an anti-inflammatory effect, as demonstrated by doubling the production of IL-10 (2.10 ± 0.29 fold vs. control) in the VSAs compared with the untreated control and reducing the production of pro-inflammatory cytokines, such as IL-1 α ($80.58 \pm 4.91\%$ vs. control), IL-8 ($40.90 \pm 5.72\%$ vs. control), and MCP-1 ($76.87 \pm 3.35\%$ vs. control). Similarly, colchicine showed a potent

anti-inflammatory effect via regulating a broad range of inflammatory cytokine secretions. It improved anti-inflammatory activity by increasing the production of IL-4 (1.39 ± 0.14 fold vs. control) while decreasing the production of cytokines, including IL-1 α ($71.31 \pm 5.84\%$), IL-8 ($42.57 \pm 1.80\%$ vs. control), MCP-1 ($26.31 \pm 1.77\%$ vs. control), TNF- α ($53.16 \pm 7.92\%$ vs. control), and IFN- γ ($61.95 \pm 7.79\%$ vs. control) (Fig. 9c). Thus, the results from the VSA functional assay indicated that curcumin and colchicine have significant anti-atherosclerosis effects and warrant further investigation.

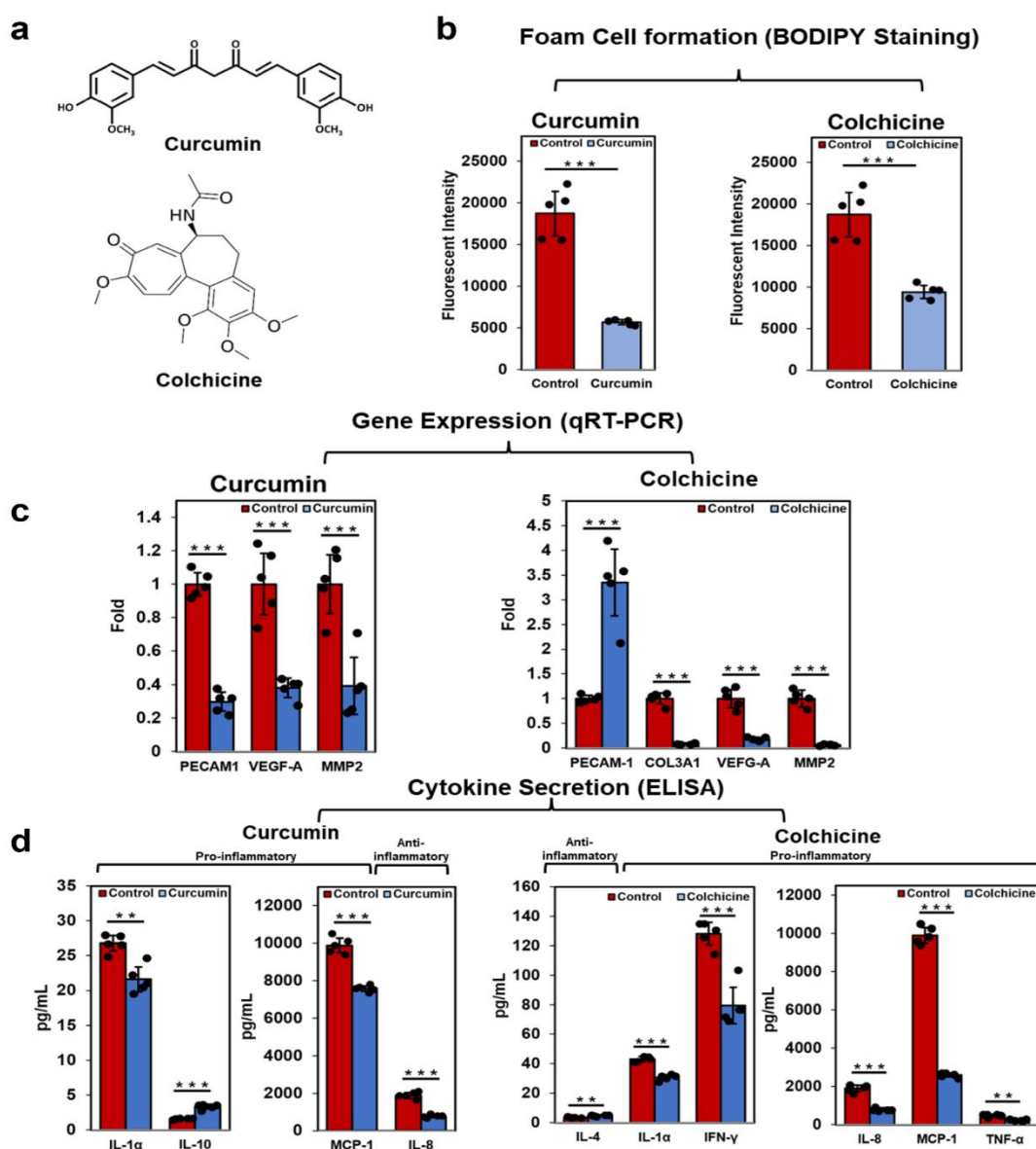


Fig.9 | Evaluation of Curcumin and Colchicine using VSA high-throughput functional assays. **a**, The chemical structure of curcumin and colchicine. **b**, Quantitative data of foam cells on the VSA treated with or without curcumin or colchicine using BODIPY staining for showing the effect of curcumin or colchicine on foam cell generation. Bars and error bars represent the mean \pm s.e.m. (n=5 biological replicates). **c**, Quantification of atherosclerosis-related gene expression of VSAs treated with or without curcumin or colchicine using qRT-PCR to show the therapeutic effect on atherosclerosis on the genetic level. Bars and error bars represent the mean \pm s.e.m. (n=5 biological replicates). **d**, Quantification of cytokine secretion of VSAs treated with or without curcumin or colchicine using ELISA to show the therapeutic effect on atherosclerosis-induced inflammation on the molecular level. Bars and error bars represent the mean \pm s.e.m. (n=5 biological replicates). (* p <0.05, ** p <0.01, *** p <0.001, statistical comparisons were performed by 2-sided Student's t-test between two groups and ANOVA with Tukey post hoc analysis for multiple comparisons, using SPSS 15.0 software. For the exact p values of the comparison between VSA treated with or without curcumin or colchicine in **b-d**, please refer to Supplementary Table 3.)

Evaluation of Lip-miR-146a using VSA high-throughput functional assays

MiR-146a has been reported to have anti-inflammatory potential, and liposomes are commonly used to improve the efficacy of microRNAs^{147, 148}. To evaluate the use of the VSA functional assay for gene-based therapeutics, Lip-miR-146a was fabricated using a conventional approach and tested for its efficacy against atherosclerosis. Therefore, to demonstrate the proof-of-concept of using the VSA functional assay for evaluating gene-

based therapeutics, Lip-miR-146a was first fabricated using an established conventional approach (Fig.10a). Fig.10b demonstrated uniform and well-shaped Lip-miR-146a obtained from using such an approach. Then, the efficacy of Lip-miR-146a on atherosclerosis was evaluated using VSA functional assays. Free miR-146a-treated VSA and untreated VSA were used as controls. Regarding inflammation resolution, at the gene level, we observed the downregulation of inflammatory genes by Lip-miR-146a (IL-1 β : $23.30 \pm 2.26\%$ vs. control; IL-6: $9.54 \pm 1.87\%$ vs. control; TNF- α : $38.14 \pm 9.05\%$ vs. control). Furthermore, at the molecular level, based on the VSA inflammation assay evaluated with ELISA, we found that Lip-miR-146a could reduce the secretion of three pro-inflammatory cytokines that were known to exacerbate atherogenesis (IL-1 β : $75.48 \pm 5.00\%$ vs. control, IFN- γ : $85.84 \pm 3.05\%$ vs. control, MCP-1: $87.04 \pm 3.10\%$ vs. control) but increase the production of anti-inflammatory cytokines (IL-10: 1.43 ± 0.10 fold vs. control, IL-13: 1.42 ± 0.04 fold vs. control). Additionally, by using our assay, we found that the efficacy of free miR-146a for inflammation resolution was compromised compared to Lip-miR-146a.

In addition to inflammation, based on the VSA assay evaluated with qRT-PCR, it is found that the lip-microRNA-146a could improve endothelial function, as demonstrated by the significant upregulation of PECAM-1 and eNOS (PECAM-1: 15.89 ± 7.42 fold vs. control; eNOS: 64.38 ± 10.87 fold vs. control). Unfortunately, due to the lipid composition of the liposomes that may interfere with the BODIPY staining, it was challenging to evaluate the effect of Lip-miR-146a using the VSA foam cell assay we developed. Thus, our future study might focus on designing a new VSA-based assay to investigate foam cell formation for liposome encapsulating therapeutics. Furthermore, to show the feasibility of using the current foam cell assay for studying microRNA efficacy, we evaluated the free

miR-146a effect using the VSA foam cell assay. Promisingly, we observed the effect of free miR-146a on foam cell generation using the VSA foam cell assay. Compared with control, foam cell generation was suppressed by the free miR-146a ($87.55 \pm 2.53\%$ vs. control) (Supplementary Fig.5).

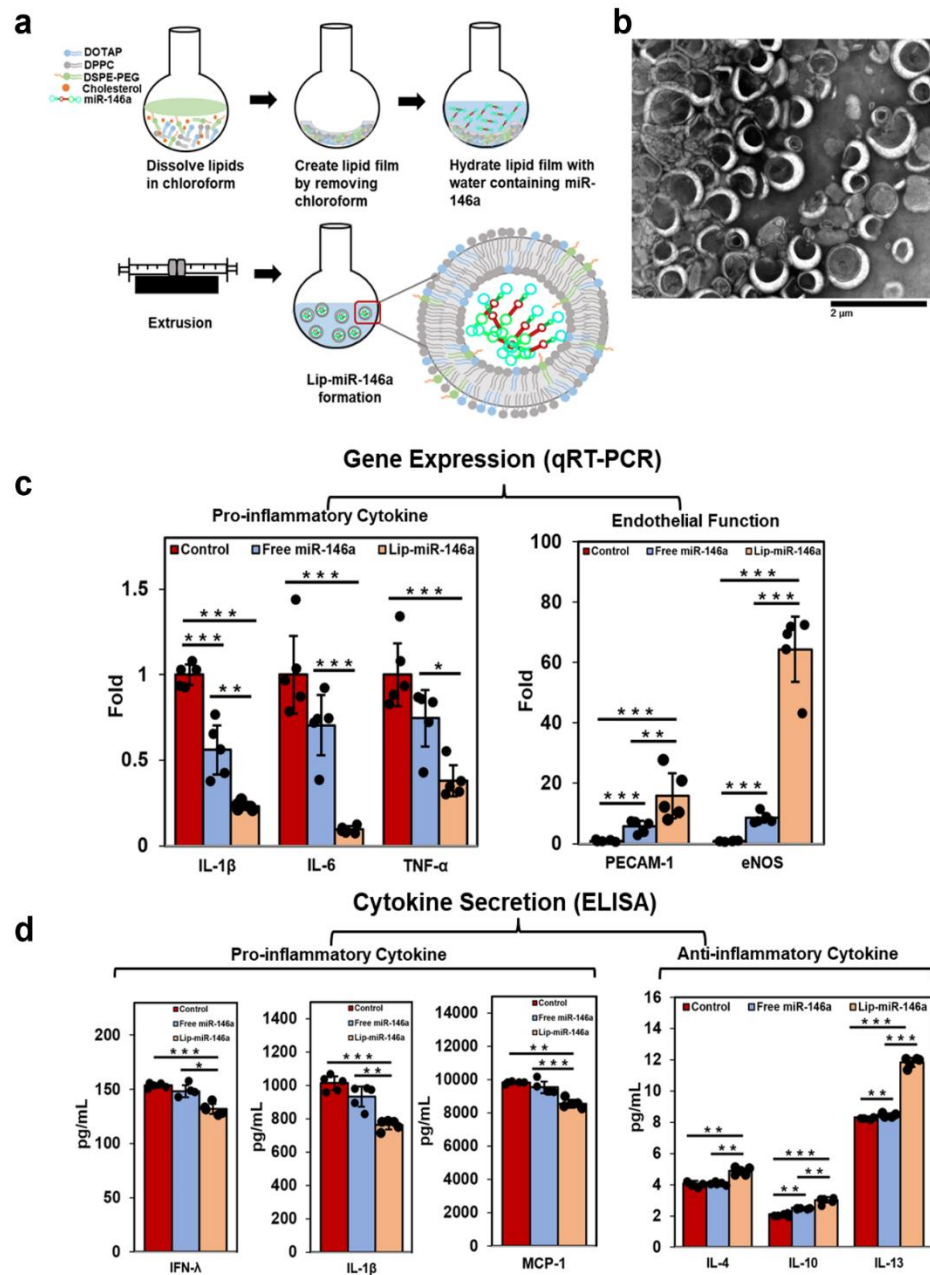


Fig.10 | Evaluation of miR146a-loaded liposomes (Lip-miR-146a) using VSA high-throughput functional assays. a, A schematic depicts the procedure for fabricating the

Lip-miR-146a. **b**, Representative images of Lip-miR-146a. **c**, Quantification of atherosclerosis-related gene expression of VSAs treated with or without free miR-146a or Lip-miR-146a using qRT-PCR to show the therapeutic effect on atherosclerosis on the genetic level. Bars and error bars represent the mean \pm s.e.m. (n=5 biological replicates). **d**, Quantification of cytokine secretion of VSAs treated with or without free miR-146a or Lip-miR-146a using ELISA to show the therapeutic effect on atherosclerosis-induced inflammation on the molecular level. Bars and error bars represent the mean \pm s.e.m. (n=5 biological replicates). (* p <0.05, ** p <0.01, *** p <0.001, statistical comparisons were performed by 2-sided Student's t-test between two groups and ANOVA with Tukey post hoc analysis for multiple comparisons, using SPSS 15.0 software. For the exact p values of the comparison among VSA treated with free miR-146a, Lip-miR-146a, and untreated VSA in **c-d**, please refer to Supplementary Table 4).

Discussion

We developed an *in vitro* atherosclerosis model, the VSA, a 3D three-layer nanomatrix VS with critical atherosclerosis multi-features. The nanomatrix atherosclerotic sheet was fabricated by first creating a three-layer nanomatrix VS using a novel approach combining a nanomatrix cell sheet technique, layer-by-layer method, and cell-as-glue approach, followed by inducing atherosclerosis in the VSs with a process that mimics *in vivo* atherogenesis.

1) The developed method for making multilayer nanomatrix VSs offers advantages over other approaches for producing cell sheets. Conventionally, 2D cell sheets are made using temperature-responsive polymers or nanoparticle-modified TCP¹⁴⁹ but these sheets

are thin and require stacking to achieve a dense multilayer structure. However, stacking poses challenges, such as shrinking and the need for additional procedures to promote adhesion. Other approaches, such as using cross-linked hydrogels, may reduce cell viability due to excess chemicals or toxic byproducts. In contrast, our approach combines the nanomatrix sheet technique and cell-as-glue approach to generate a 3D multilayered VS with a thickness of around 1 mm (Fig. 4d), similar to the total arterial wall thickness in humans, around 0.87 ± 0.23 mm¹⁵⁰. Our approach is biocompatible and enables sheet stacking without the need for cell sheet detachment or maturation. Moreover, it is versatile and can be applied to generate other types of cell sheets for different applications. The current study demonstrates three-layered nanomatrix VSs in square and disk shapes, but the fabrication of cell sheets with other shapes and sizes or more layers is feasible. In addition, our approach is not limited to atherosclerotic VSs and can be used for bone, skin, and eye applications.

2) The developed VSA demonstrates critical multi-features in atherosclerosis and can be easily scaled up for creating high-throughput functional assays. As reported, most of the previous atherosclerotic models demonstrated some features of early atherosclerosis, such as 2D models comprised of co-cultures of ECs or SMCs with monocytes and 3D spheroid models comprising foam cells, SMCs, and ECs¹⁰⁶. The most comprehensive atherosclerosis model so far was the TEBV which demonstrates endothelial activation, monocyte accumulation, foam cells, and macrophage formation and polarization¹⁰⁶. However, the VSA developed here presents not only the features observed in the TEBVs but also some features in the intermediate stage of atherosclerosis, such as calcification initiation, foam cell aggregation, lipid pools, SMC transition, and ECM remodeling. In

addition, the cytokines secreted by the VSA were reported to be produced by human atherosclerotic plaque, such as IFN- γ , IL-1 β , IL-1 α , IL-8, and IL-6 (Fig.6e), critical factors for human atherosclerosis progression, substantiated by recent transcriptional analysis studies found that the macrophages from patient plaque participated in signaling pathways associated with these cytokines^{132, 151}. It is also worth mentioning that although the current study performed functional assays for evaluating therapeutics in a 48-well format, it is feasible to create the assays in 96 and even higher-well formats. Moreover, recent clinical studies demonstrated promising therapeutic effects of drugs targeting the inhibition of IL-6¹⁵²⁻¹⁵⁴ and IL-1 β ¹⁵⁴⁻¹⁵⁶ in atherosclerosis patients; thus, the IL-6 and IL-1 β -producing VSAs possess great potential as platforms for assessing novel therapeutics for anti-IL6 or IL-1 β therapy for atherosclerosis in the future at pre-clinical stages.

3) The developed VSA high-throughput functional assays can predict the effect of therapeutic *in vivo* studies, making them a feasible, high-throughput and cost-effective way to evaluate potential drugs for treating atherosclerosis before conducting low-throughput and expensive *in vivo* studies. Specifically, the assay showed that all the therapeutics evaluated here could suppress foam cell generation, indicating their ability to reduce lesion formation, consistent with earlier findings in the literature showing their efficacy on plaque using *in vivo* atherosclerosis models¹⁵⁷⁻¹⁶². Our VSA functional assays demonstrated the suppression effects of rosuvastatin on TNF- α and IL-6, similar to what was reported in an earlier animal study regarding rosuvastatin's anti-atherosclerotic ability¹⁶⁰. Furthermore, our assay also showed that sirolimus can reduce the serum levels of MCP-1, IFN- γ , and TNF- α (Fig.8e), which is in line with previous research in the atherosclerosis mice model¹⁵⁸. Importantly, our result revealed that sirolimus could increase autophagy-related

cytokine secretion (IL-4 and IL-13) (Fig.8e), consistent with earlier findings demonstrating the autophagy-stimulating effects of sirolimus^{163, 164}. For drug candidates' potential for treating atherosclerosis, such as curcumin, our assay results correlated with the previous *in vivo* study^{165, 166}, which showed that curcumin could significantly decrease IL-8 and MCP-1 production (Fig. 8c). In addition, our assay showed that curcumin may suppress angiogenesis in the plaque by suppressing the expression of VEGF-A (Fig.9c), which agrees with a recent study that reported that with a recent study that reported the inhibitory effect of curcumin-loaded nanoparticles on intraplaque neovascularization in mice with atherosclerosis¹⁶⁷. Moreover, our assay also demonstrated the suppressive effect of curcumin on MMP-2, which was previously observed in both mouse plaque¹⁶⁷ and patients with coronary artery diseases¹⁶⁸. Additionally, our assay demonstrated that curcumin could increase the production of the anti-inflammatory cytokine - IL-10 (Fig.9d), suggesting its potential to repolarize M1 macrophages to M2 macrophages. This finding is consistent with a recent study demonstrating curcumin's ability to modulate M1 and M2 macrophages in atherosclerosis¹⁶⁹. Regarding colchicine, our assay showed that it regulated genes associated with plaque stability (e.g., MMP-2), which correlates with previous results obtained using an *in vivo* atherosclerosis model showing that colchicine may stabilize plaque¹⁷⁰. Our assay also showed the increase of IL-4 production by colchicine compared to the controls, suggesting its potential to induce M2 macrophage polarization in atherosclerosis, consistent with the recent finding that colchicine could stimulate macrophage polarization towards M2 phenotype *in vivo*¹⁷¹. Meanwhile, our VSA assays demonstrated that colchicine downregulated VEGF-A, suggesting that colchicine may inhibit angiogenesis and neovascularization in addition to its known effects of increasing

plaque stability and regulating macrophage phenotype in treating atherosclerosis. For miR-146a, using our VSA assay, we obtained similar results for miR-146a as those found in the atherosclerotic mouse model, where miR-146a downregulated gene expression of IL-1 β , IL-6, and TNF- α ¹⁷². Significantly, the improved efficacy of microRNA transfection by using liposomes was also detected by our VSA assay, demonstrating its potential to evaluate drug delivery carrier-based formulations for atherosclerosis treatment.

4) Although our current work focuses on demonstrating the proof-of-concept of using VSAs to investigate therapeutic effectiveness for atherosclerosis, this platform also enables us to study atherosclerosis pathogenesis using an efficient and cost-effective high-throughput methodology with a relatively large number of biological replicates. The VSAs provide an excellent opportunity for mechanistic research, which may be difficult to conduct using *in vivo* models. For example, by customizing the structure of VSAs, we can induce atherosclerosis on VSAs with single, double, or three-layer structures, providing unique insights into the effect of discrete layers, particularly the fibroblast layer, on atherogenesis. Additionally, our VSAs can be scaled up to develop high-throughput assays for drug safety testing, facilitating the determination of pharmacological and toxicological parameters for use in animal models later on.

Methods

Synthesis of PA and preparation of PA solution

The PA with cell adhesive ligand (RGDS) was synthesized in an Advanced Chemtech Apex 396 peptide synthesizer at a 0.30 mmol scale using standard Fmoc-chemistry, as previously described¹⁷³. As per Nature Portfolio editorial policies, this

biomaterial is available upon request to the corresponding author on condition that full compensation is provided for expenses incurred in its synthesis. A 1 or 2 wt% stock solution of PA was prepared in DI (deionized) water and adjusted to pH 7.4 through the controlled addition of sodium hydroxide (Fisher Scientific).

Cell culture

HAAFs, hAoSMCs, and hAECs were maintained in complete growth mediums (Lifeline Cell Technology). The cells used for VSA fabrication were at passage 6 or 7. U937 cells (ATCC) were maintained in suspension culture in RPMI1640 (ATCC) supplemented with 10% fetal bovine serum (FBS) (Atlanta Biologicals) and 1% penicillin-streptomycin (Gibco, US). All cells were expanded in a humified tissue culture incubator maintained at 37°C, 5% CO₂, and 20% O₂.

Fabrication of a single-layer nanomatrix VS

The hAAF (2.5 million hAAF/cm²) sheet was fabricated by encapsulating hAAFs into 1 wt% PA with vapor from a 0.1M CaCl₂ solution (Fisher Scientific) for 1 min. Then, the hAAF sheet was maintained in a hAAF complete growth medium (Lifeline cell technology) with 20% FBS and 1% penicillin-streptomycin for 7 days for cell spreading and remodeling. Likewise, the single-layer nanomatrix hAoSMC and hAEC sheets were fabricated using a similar approach and culture using hAoSMC and hAEC complete growth medium supplemented with 20% FBS, respectively. All single-layer nanomatrix VS were cultured in a humified tissue culture incubator maintained at 37°C, 5% CO₂, and 20% O₂.

Fabrication of a double-layer nanomatrix VS

The double-layered hAAF-hAoSMC sheet was fabricated by seeding hAAFs (1 million/cm²) on the hAAF sheet and culturing for 6 hours, followed by fabrication of the hAoSMC sheet above the hAAF-seeded hAAF sheet using a similar method as the single-layer hAoSMC sheet. Finally, the hAAF-hAoSMC sheet was cultured for 7 days using complete hAoSMC and hAAF medium (1:1) supplemented with 20% FBS for cell spreading and remodeling. All double-layer nanomatrix VS were cultured in a humidified tissue culture incubator maintained at 37°C, 5% CO₂, and 20% O₂.

Fabrication of a three-layer nanomatrix VS

Following the hAAF-hAoSMC sheet fabrication, hAoSMCs (0.1 million hAoSMC/cm²) were first seeded and cultured for one day. Then, hAECs were seeded (1 million/cm²) on the hAoSMC-seeded hAoSMC-hAAF sheet and cultured for complete hAoSMC, hAAF and hAEC medium (1:1:1) were supplemented with 20% FBS for another 7 days for cell spreading, remodeling, and confluent endothelialization. All three-layer nanomatrix VS were cultured in a humidified tissue culture incubator maintained at 37°C, 5% CO₂, and 20% O₂.

Induction of the VSA from the three-layer nanomatrix VS

Endothelial dysfunction was induced using a Dulbecco's modified Eagle's medium (DMEM) (Corning) containing TNF- α (40 ng/mL) (Sino biological,) and Ox-LDL (50 μ g/mL) (Athens Research & Technology), and 0.5% FBS (Atlanta Biologicals) and 1% penicillin-streptomycin (Gibco, US) for 1 day. The monocyte adhesion were induced via

the addition of a DMEM medium containing U937 monocytes (ATCC) (1 million/mL), 0.5% FBS and 1% penicillin-streptomycin for one day, and the macrophage formation were induced by adding "customized atherosclerotic medium 1", comprising a DMEM medium containing Ox-LDL (50 μ g/mL), recombinant human (rh) M-CSF (100 ng/mL) (R&D Systems), rh GM-CSF (25 ng/mL) (R&D Systems), rh IFN- γ (100 ng/mL) (R&D Systems), and 0.5% FBS as well as U937 monocytes (0.1 million/mL) followed by culturing the sheet for 7 days. Fresh medium was added into the VSA after 3-day culture. Then, foam cell formation was achieved by adding the "customized atherosclerotic medium 2" with higher Ox-LDL concentration comprising a DMEM medium containing Ox-LDL (150 μ g/mL), rhM-CSF (100 ng/mL), rhGM-CSF (25 ng/mL), rhIFN- γ (100 ng/mL), 0.5% FBS and U937 monocytes (0.1 million/mL), followed by culturing the sheet for 3 days. All culture for induction were cultured in a humidified tissue culture incubator maintained at 37°C, 5% CO₂, and 20% O₂.

Live/Dead staining

First, the live (green) and dead (red) reagent (Invitrogen) were thawed at room temperature and mixed to create the 2X working solution. Next, the medium for the VSs was replaced with PBS, and an equal volume of 2X working solution was added. Then, the VSs were stained with live/dead staining solution and incubated in the dark for 15 min, followed by imaging at ex/em 488nm/515nm (live) and 570 nm/602 nm (dead) using a fluorescent microscope.

DAF-FM diacetate staining

Briefly, a 5 mM DAF-FM stock solution (Invitrogen) was prepared by dissolving in dimethyl sulfoxide (DMSO), and a 5 μ M working solution in PBS was prepared. After removal of the supernatant, the working solution was added, and the VSs were incubated for 1 h at 37°C in the dark. Then the probe was replaced with PBS, and the VSs were incubated for another 30 min before they were imaged using the fluorescent microscope or quantified at ex/em 485 nm/528 nm using a microplate reader.

Immunostaining

Conventional immunostaining techniques were performed following standard protocols. Specifically, samples were incubated with 4% formaldehyde for 10 min, then treated with PBS containing 0.25% Triton X-100 for 10 min followed by PBS with 0.1% Tween 20, 1% BSA, and 22.52 mg/mL glycine for 30 min. Primary antibodies (Abcam), diluted 100 times in PBS with 0.1% Tween 20 and 1% BSA, were added to the samples (VSs or VSAs) and incubated overnight at 4°C. After the removal of primary antibody, secondary antibodies (Abcam), diluted 100 times in 1 % BSA, were added and incubated for 1 h in the dark before they were imaged immediately using a fluorescent microscope. For each step, samples were washed 3 times with PBS. Detailed information for primary and secondary antibodies is provided in reporting summary.

DCFH-DA staining for ROS activity

5 mM 2',7'-Dichlorodihydrofluorescein diacetate (DCFH-DA) stock solution (Invitrogen) was prepared by dissolving in DMSO and stored at -20°C. Before the experiment, a 5 μ M working solution was prepared by adding stock solution to PBS. VSAs

(n=5 biological replicates) were gently washed with PBS, then DCFH-DA was added. Next, samples were incubated in the dark for 1 h, and then quantified immediately at ex/em 485 nm/528 nm.

Monocyte adhesion

First, U937 cells were cultured with Calcein Blue, AM (Invitrogen) in the dark for 30 min and then washed with PBS to remove the excess Calcein Blue, AM. Then the stained U937 cells were added to a sheet, incubated for 30 min, washed to remove the unattached U937 cells, immediately imaged, and quantified at ex/em 322nm/435nm.

Alizarin Red S (ARS) staining

Alizarin Red S staining kit (Sciencell) was used to evaluate calcification following protocol. Briefly, after washing with PBS, the VSAs (n=5 biological replicates) were fixed with 4% formaldehyde. Then, the VSAs were washed with DI water. ARS was added after the complete removal of the water, and the VSAs were incubated for 30 min at room temperature with gentle shaking. After that, the ARS was removed, and the VSAs were washed, followed by incubation with 10% acetic acid for 30 minutes, sealing, and heating at 85°C for 10 min. After centrifugation of the fully-cooled samples for 15 min at 20,000 g, the supernatant was neutralized with 10% ammonium hydroxide, and the absorbance at 405 nm was measured by a microplate reader.

Preparation of therapeutics for high-throughput therapeutic evaluation

(1) Preparation of free miR-146a, Lip-miR-146a: Hsa-miR-146a-5p *mirVana*® miRNA (Thermo Fisher) mimic stock solution (50 μ M) was prepared by dissolving 5 nm of miR-146a in 100 μ L of RNase-free water. Then, Lip-miR-146a stock solution (1.38 μ M) was prepared. Briefly, to prepare the stock solution (25 μ M liposome), 1, 2-dioleoyl-sn-glycero-3-phosphocholine (DPPC), 1,2-dioleoyl-3-trimethylammonium-propane (DOTAP), 1,2-distearoyl-sn-glycero-3-phosphoethanolamine-N-[carboxy(polyethylene glycol)-2000] (DSPE-PEG), and cholesterol ovine wool (CHOL) (Avanti Polar Lipids) were dissolved in chloroform (1 mL) with the molar ratio of 55:15:3:27. Then, overnight dehydration under vacuum, 2h-encapsulation by rehydration with RNase free water containing miR-146a (1.5 μ M), and extrusion through 0.4 μ m (10 passages) and 0.2 μ m (30 passages) pore polycarbonate membrane filters in an extruder set (Avestin) were performed sequentially. To measure encapsulation efficiency (EE), the supernatant was collected after 10-min centrifugation (16,000 rpm), and the encapsulated miR-146a was extracted by digesting liposomes in ethanol with repeated free-thaw cycles. The miR-146a amount was analyzed using Qubit microRNA assay (Molecular Probes) and BioTek Synergy H1 plate reader at 500 nm excitation and 528 nm emission. EE was calculated by (encapsulated miR-146a)/(total miR-146a), and determined to be around 69%. The 600 nM miR-146a that was free or encapsulated in liposomes was prepared by dilution from the stock solution into the atherosclerotic medium.

(2) Preparation of rosuvastatin, sirolimus, curcumin, and colchicine stock solution: Rosuvastatin (Thermo Fisher) and sirolimus (Thermo Fisher) stock solutions (1 mM and 25 mM, respectively) were prepared by dissolving the drugs in DMSO and stored in the dark at -30°C. Curcumin (Thermo Fisher)

and colchicine (Thermo Fisher) stock solutions (200 mM and 100 mM, respectively) were prepared by dissolving the drugs in ethanol.

VSA foam cell assay for therapeutic evaluation

(1) Fabrication of VSA high throughput culture systems: our large-scale VSA high throughput culture system was achieved by fabricating individual VSAs in each well of 48-well tissue culture plate, following the same method described in the previous section.

(2) Treatment of VSAs with drugs, free miR-146a, or Lip-miR-146a: on day 0, Rosuvastatin (10 μ M), sirolimus (10 nM), curcumin (200 μ M), colchicine (100 nM), free miR-146a (600 nM), and Lip-miR-146a (600 nM) were applied to the VSAs (n=5 biological replicates for each therapeutic) by dilution of the stock solution into the "customized atherosclerotic medium 1 "containing monocytes. Then, the VSAs were co-cultured with the drugs, free miR-146a, and Lip-miR-146a for 10 days prior to BODIPY staining. Fresh customized atherosclerotic medium 2 with monocytes were added to the co-culture system on day 3 and day 7, respectively.

(3) BODIPY staining: On day 10, 10 mM BODIPY stock solution (Invitrogen) was prepared by dissolving in DMSO and stored at -20°C. Before the experiment, 100 times diluted working solution was prepared from stock solution using PBS. Then the VSA, after treated with the drugs, free miR-146a, and Lip-miR146a for 10 days were gently washed with PBS, then BODIPY was added, incubated in the dark for 30 min, imaged immediately using a microscope, and quantified at ex/em 485 nm/520 nm.

VSA inflammation assay for therapeutic evaluation

(1) Fabrication of VSA high throughput culture systems: the culture systems were fabricated using the same approach shown in the VSA foam cell assay part. (2) Treatment of VSAs with therapeutics, including rosuvastatin (10 μ M), sirolimus (10 nM), curcumin (200 μ M), colchicine (100 nM), free miR-146a (600 nM), and Lip-miR146a (600 nM) were applied to the VSAs (n=5 biological replicates for each therapeutic) by dilution of stock solution into the "customized atherosclerotic medium 2" on day 0. Then, the VSAs were co-cultured with the drugs, free miR-146a, and Lip-miR-146a for 10 days prior to RNA extraction or ELISA. Fresh customized atherosclerotic medium 2 were added to the co-culture system on day 3 and day 7, respectively. (3) RNA extraction and real-time qRT-PCR: On day 10, before phase separation, EDTA (Ethylenediaminetetraacetic acid) was added to bind the calcium and help disintegrate the nanomatrix VSAs. For phase separation, TRIzolTM reagent (Invitrogen) was added to the samples (≥ 9 times of the sample volume) and incubated for 5 min. Then chloroform was added, mixed by shaking, and centrifuged (11,600g, 15 min, 4°C) to obtain phase separation. The upper transparent aqueous phase was collected and purified using the Direct-zolTM RNA Miniprep Plus kit following the protocol (Zymo Research). RNA was suspended in nuclease-free water, and an ND-1000 UV spectrophotometer (Nanodrop) was used to quantify the concentration and purity of RNA for each sample. Complementary DNA was then synthesized using 50 ng of RNA, which was reverse transcribed in a 2720 Thermo Cycler (Applied Biosystems) using a Verso cDNA Synthesis Kit (Thermo Fisher) according to the manufacturer's protocol. Samples were prepared in a 96-well PCR plate using the TaqMan Master Mix protocol. Each sample consisted of 2 μ L of cDNA solution, 10 μ L of 2x master mix, 7 μ L

of RNA-free water, and 1 μ L of gene primer from a TaqMan Gene Expression Assay kit (Applied Biosystems). The PCR plate was run in a LightCycler 480 (Roche Life Science) for the following cycles: pre-incubation at 50 °C for 2 minutes and 95 °C for 10 min; amplification for 45 cycles, at 95 °C for 15 seconds, and 60 °C for 1 minute during each cycle; melting at 95°C for 5 seconds and 65 °C for 1 minute, and cooling at 40°C for 30 seconds. (4) ELISA: On day 10, the supernatant from each sample was collected for ELISA. An ELISA-based quantitative array platform (RayBiotech) was used to measure the major inflammatory cytokine secretion. Briefly, supernatant from the VSAs was collected for ELISA quantification. After blocking, the supernatant was added and incubated overnight at 4°C, followed by a wash step. Next, the detection antibody cocktail (that targets all the cytokines above) was added and incubated for 2 h at room temperature, followed by a wash step. Finally, cy3 equivalent dye-conjugated streptavidin was added and incubated for 1 h in the dark at room temperature. After a thorough wash and dry, the signals were measured and analyzed via a laser scanner (Molecular Devices).

Statistical analysis

Results for all experimental groups were expressed as mean \pm standard deviation. Statistical comparisons were performed by 2-sided Student's t-test between two groups and ANOVA with Tukey post hoc analysis for multiple comparisons, using SPSS 15.0 software. A value of $p \leq 0.05$ was considered statistically significant.

References

1. Allen, R.M. et al. LDL delivery of microbial small RNAs drives atherosclerosis through macrophage TLR8. *Nat. Cell Biol* 24, 1701-1713 (2022).
2. Libby, P. The changing landscape of atherosclerosis. *Nature* 592, 524-533 (2021).
3. Chen, J. et al. Recent Progress in in vitro Models for Atherosclerosis Studies. *Front. Cardiovasc. Med* 8, 790529 (2021).
4. Geraili, A. et al. Controlling Differentiation of Stem Cells for Developing Personalized Organ-on-Chip Platforms. *Adv. Healthc. Mater.* 7, 1700426 (2018).
5. Yang, J., Zhang, Y.S., Yue, K. & Khademhosseini, A. Cell-laden hydrogels for osteochondral and cartilage tissue engineering. *Acta Biomater.* 57, 1-25 (2017).
6. Rogal, J., Zbinden, A., Schenke-Layland, K. & Loskill, P. Stem-cell based organ-on-a-chip models for diabetes research. *Adv. Drug Deliv. Rev.* 140, 101-128 (2019).
7. Poussin, C. et al. 3D human microvessel-on-a-chip model for studying monocyte-to-endothelium adhesion under flow – application in systems toxicology. *ALTEX* 37, 47-63 (2020).
8. Mallone, A., Stenger, C., Von Eckardstein, A., Hoerstrup, S.P. & Weber, B. Biofabricating atherosclerotic plaques: In vitro engineering of a three-dimensional human fibroatheroma model. *Biomaterials* 150, 49-59 (2018).
9. Douglas, G. & Channon, K.M. The pathogenesis of atherosclerosis. *Medicine* 42, 480-484 (2014).
10. Lee, J.H. et al. Emulating Early Atherosclerosis in a Vascular Microphysiological System Using Branched Tissue-Engineered Blood Vessels. *Adv. Biosyst.* 5, 2000428 (2021).
11. Chen, Z. et al. Real-time observation of leukocyte–endothelium interactions in tissue-engineered blood vessel. *Lab Chip* 18, 2047-2054 (2018).
12. Tillie, R.J.H.A., van Kuijk, K. & Sluimer, J.C. Fibroblasts in atherosclerosis: heterogeneous and plastic participants. *Curr. Opin. Lipidol.* 31 (2020).
13. Milutinović, A., Šuput, D. & Zorc-Pleskovič, R. Pathogenesis of atherosclerosis in the tunica intima, media, and adventitia of coronary arteries: An updated review. *Bosn J Basic Med Sci* 20, 21-30 (2020).

14. Zeng, W., Guo, L., Xu, S., Chen, J. & Zhou, J. High-throughput screening technology in industrial biotechnology. *Trends Biotechnol* 38, 888-906 (2020).
15. Castro, F. et al. Advances on colorectal cancer 3D models: The needed translational technology for nanomedicine screening. *Advanced Drug Delivery Reviews* 175, 113824 (2021).
16. Tuveson, D. & Clevers, H. Cancer modeling meets human organoid technology. *Science* 364, 952-955 (2019).
17. Yang, Y. et al. Identification of novel human high-density lipoprotein receptor up-regulators using a cell-based high-throughput screening assay. *SLAS Discov.* 12, 211-219 (2007).
18. Xu, Y. et al. Suberanilohydroxamic acid as a pharmacological Kruppel-Like Factor 2 activator that represses vascular inflammation and atherosclerosis. *J. Am. Heart Assoc.* 6, e007134 (2017).
19. Wang, X. et al. A small-molecule inhibitor of PCSK9 transcription ameliorates atherosclerosis through the modulation of FoxO1/3 and HNF1 α . *EBioMedicine* 52, 102650 (2020).
20. Xu, S. et al. Endothelial Dysfunction in Atherosclerotic Cardiovascular Diseases and Beyond: From Mechanism to Pharmacotherapies. *Pharmacol. Rev.* 73, 924 (2021).
21. Tousoulis, D., Oikonomou, E., Economou, E.K., Crea, F. & Kaski, J.C. Inflammatory cytokines in atherosclerosis: current therapeutic approaches. *Eur. Heart J.* 37, 1723-1732 (2016).
22. Maguire, E.M., Pearce, S.W.A. & Xiao, Q. Foam cell formation: A new target for fighting atherosclerosis and cardiovascular disease. *Vascul. Pharmacol.* 112, 54-71 (2019).
23. Yu, X.-H., Fu, Y.-C., Zhang, D.-W., Yin, K. & Tang, C.-K. Foam cells in atherosclerosis. *Clinica. Chimica. Acta* 424, 245-252 (2013).
24. Chistiakov, D.A., Melnichenko, A.A., Myasoedova, V.A., Grechko, A.V. & Orekhov, A.N. Mechanisms of foam cell formation in atherosclerosis. *J. Mol. Med.* 95, 1153-1165 (2017).
25. Fatkhullina, A.R., Peshkova, I.O. & Koltsova, E.K. The role of cytokines in the development of atherosclerosis. *Biochemistry* 81, 1358-1370 (2016).
26. Georgakis, M.K. et al. Monocyte-chemoattractant protein-1 levels in human atherosclerotic lesions associate with plaque vulnerability. *Arterioscler. Thromb. Vasc. Biol.* 41, 2038-2048 (2021).

27. Rus, H.G., Vlaicu, R. & Niculescu, F. Interleukin-6 and interleukin-8 protein and gene expression in human arterial atherosclerotic wall. *Atherosclerosis* 127, 263-271 (1996).
28. Jiang, X. et al. Inflammasome-Driven Interleukin-1 α and Interleukin-1 β Production in Atherosclerotic Plaques Relates to Hyperlipidemia and Plaque Complexity. *JACC: Basic to Translational Science* 4, 304-317 (2019).
29. Fernandez, D.M. et al. Single-cell immune landscape of human atherosclerotic plaques. *Nat. Med.* 25, 1576-1588 (2019).
30. Frostegård, J. et al. Cytokine expression in advanced human atherosclerotic plaques: dominance of pro-inflammatory (Th1) and macrophage-stimulating cytokines. *Atherosclerosis* 145, 33-43 (1999).
31. Nelken, N.A., Coughlin, S.R., Gordon, D. & Wilcox, J.N. Monocyte chemoattractant protein-1 in human atheromatous plaques. *J. Clin. Investig.* 88, 1121-1127 (1991).
32. Mallat, Z. et al. Expression of Interleukin-10 in Advanced Human Atherosclerotic Plaques. *Arterioscler. Thromb. Vasc. Biol.* 19, 611-616 (1999).
33. Liu, M. & Gomez, D. Smooth Muscle Cell Phenotypic Diversity. *Arterioscler. Thromb. Vasc. Biol.* 39, 1715-1723 (2019).
34. Negishi, K. et al. An Myh11 single lysine deletion causes aortic dissection by reducing aortic structural integrity and contractility. *Sci. Rep.* 12, 8844 (2022).
35. Goikuria, H. et al. in *Cells*, Vol. 7 (2018).
36. He, C. et al. PDGFR β signalling regulates local inflammation and synergizes with hypercholesterolaemia to promote atherosclerosis. *Nat. Commun* 6, 7770 (2015).
37. Toma, I. & McCaffrey, T.A. Transforming growth factor- β and atherosclerosis: interwoven atherogenic and atheroprotective aspects. *Cell Tissue Res* 347, 155-175 (2012).
38. Kuo, C.-L. et al. Cdkn2a is an atherosclerosis modifier locus that regulates monocyte/macrophage proliferation. *Arterioscler. Thromb. Vasc. Biol.* 31, 2483-2492 (2011).
39. Motz, K. et al. Interferon- γ treatment of human laryngotracheal stenosis-derived fibroblasts. *JAMA Otolaryngology–Head & Neck Surgery* 143, 1134-1140 (2017).
40. Davies, J.T. et al. Current and Emerging Uses of Statins in Clinical Therapeutics: A Review. *Lipid Insights* 9, LPI.S37450 (2016).

41. Liu, Y., Yang, F., Zou, S. & Qu, L. in *Front Pharmacol*, Vol. 9 1520 (2018).
42. Li, Y., Tian, L., Sun, D. & Yin, D. Retracted: Curcumin ameliorates atherosclerosis through upregulation of miR-126. *J. Cell. Physiol.* 234, 21049-21059 (2019).
43. S. Karimian, M., Pirro, M., P. Johnston, T., Majeed, M. & Sahebkar, A. Curcumin and Endothelial Function: Evidence and Mechanisms of Protective Effects. *Curr. Pharm. Des.* 23, 2462-2473 (2017).
44. Fredman, G. & Tabas, I. Boosting Inflammation Resolution in Atherosclerosis: The Next Frontier for Therapy. *Am. J. Pathol.* 187, 1211-1221 (2017).
45. Boca, S. et al. Nanoscale delivery systems for microRNAs in cancer therapy. *Cell. Mol. Life Sci.* 77, 1059-1086 (2020).
46. Imashiro, C. & Shimizu, T. Fundamental technologies and recent advances of cell-sheet-based tissue engineering. *Int. J. Mol. Sci.* 22, 425 (2021).
47. Holzapfel, G.A., Sommer, G., Gasser, C.T. & Regitnig, P. Determination of layer-specific mechanical properties of human coronary arteries with nonatherosclerotic intimal thickening and related constitutive modeling. *Am J Physiol Heart Circ Physiol* 289, H2048-2058 (2005).
48. Depuydt, M.A.C. et al. Microanatomy of the Human Atherosclerotic Plaque by Single-Cell Transcriptomics. *Circ. Res.* 127, 1437-1455 (2020).
49. Fernández-Ruiz, I. Promising anti-IL-6 therapy for atherosclerosis. *Nat. Rev. Cardiol* 18, 544-544 (2021).
50. Ridker, P.M. et al. IL-6 inhibition with ziltivekimab in patients at high atherosclerotic risk (RESCUE): a double-blind, randomised, placebo-controlled, phase 2 trial. *The Lancet* 397, 2060-2069 (2021).
51. Engelen, S.E., Robinson, A.J.B., Zurke, Y.-X. & Monaco, C. Therapeutic strategies targeting inflammation and immunity in atherosclerosis: how to proceed? *Nat. Rev. Cardiol* 19, 522-542 (2022).
52. Ridker, P.M. et al. Anti-inflammatory therapy with canakinumab for atherosclerotic disease. *N. Engl. J. Med.* 377, 1119-1131 (2017).
53. Fernández-Ruiz, I. Anti-IL-1 β therapy lowers leukocyte supply and uptake in atherosclerosis. *Nat. Rev. Cardiol* 19, 5-5 (2022).
54. Li, Y. et al. CD47-and Integrin $\alpha 4/\beta 1$ -Comodified-Macrophage-Membrane-Coated Nanoparticles Enable Delivery of Colchicine to Atherosclerotic Plaque. *Adv. Healthc. Mater.* 11, 2101788 (2022).

55. Zhao, L. et al. Low-dose oral sirolimus reduces atherogenesis, vascular inflammation and modulates plaque composition in mice lacking the LDL receptor. *Br. J. Pharmacol* 156, 774-785 (2009).
56. Yu, P. et al. Rosuvastatin Reduces Aortic Sinus and Coronary Artery Atherosclerosis in SR-B1 (Scavenger Receptor Class B Type 1)/ApoE (Apolipoprotein E) Double Knockout Mice Independently of Plasma Cholesterol Lowering. *Arterioscler. Thromb. Vasc. Biol.* 38, 26-39 (2018).
57. Suh, J.S. et al. Rosuvastatin Prevents the Exacerbation of Atherosclerosis in Ligature-Induced Periodontal Disease Mouse Model. *Sci. Rep.* 10, 6383 (2020).
58. Gao, S. et al. Curcumin ameliorates atherosclerosis in apolipoprotein E deficient asthmatic mice by regulating the balance of Th2/Treg cells. *Phytomedicine* 52, 129-135 (2019).
59. Zhang, S., Zou, J., Li, P., Zheng, X. & Feng, D. Curcumin protects against atherosclerosis in apolipoprotein E-knockout mice by inhibiting toll-like receptor 4 expression. *J. Agric. Food Chem.* 66, 449-456 (2018).
60. Song, Y. et al. Platelet membrane-coated nanoparticle-mediated targeting delivery of Rapamycin blocks atherosclerotic plaque development and stabilizes plaque in apolipoprotein E-deficient (ApoE^{-/-}) mice. *Nanomedicine: Nanotechnology, Biology and Medicine* 15, 13-24 (2019).
61. Ma, J. et al. Expression of miRNA-155 in carotid atherosclerotic plaques of apolipoprotein E knockout (ApoE^{-/-}) mice and the interventional effect of rapamycin. *Int. Immunopharmacol* 46, 70-74 (2017).
62. Jain, S.K., Rains, J., Croad, J., Larson, B. & Jones, K. Curcumin supplementation lowers TNF- α , IL-6, IL-8, and MCP-1 secretion in high glucose-treated cultured monocytes and blood levels of TNF- α , IL-6, MCP-1, glucose, and glycosylated hemoglobin in diabetic rats. *Antioxid. Redox Signal.* 11, 241-249 (2009).
63. Zhao, J.-F. et al. Molecular mechanism of curcumin on the suppression of cholesterol accumulation in macrophage foam cells and atherosclerosis. *Mol Nutr Food Res.* 56, 691-701 (2012).
64. Meng, N. et al. A novel curcumin-loaded nanoparticle restricts atherosclerosis development and promotes plaques stability in apolipoprotein E deficient mice. *J. Biomater. Appl.* 33, 946-954 (2019).
65. Mogharrabi, M. et al. The effects of nanomicelle of curcumin on the matrix metalloproteinase (MMP-2, 9) activity and expression in patients with coronary artery disease (CAD): A randomized controlled clinical trial. *ARYA Atheroscler* 16, 136-145 (2020).

66. Momtazi-Borojeni, A.A., Abdollahi, E., Nikfar, B., Chaichian, S. & Ekhlas-Hundrieser, M. Curcumin as a potential modulator of M1 and M2 macrophages: new insights in atherosclerosis therapy. *Heart Fail. Rev.* 24, 399-409 (2019).
67. Cecconi, A. et al. Effects of colchicine on atherosclerotic plaque stabilization: a multimodality imaging study in an animal model. *J. Cardiovasc. Transl. Res.* 14, 150-160 (2021).
68. Wang, L. et al. Colchicine-containing nanoparticles attenuates acute myocardial infarction injury by inhibiting inflammation. *Cardiovasc. Drugs Ther.* 36, 1075-1089 (2022).
69. Chu, T. et al. miR-146a contributes to atherosclerotic plaque stability by regulating the expression of TRAF6 and IRAK-1. *Mol. Biol. Rep.*, 1-12 (2022).
70. Chen, J. et al. Angiogenic and Osteogenic Synergy of Human Mesenchymal Stem Cells and Human Umbilical Vein Endothelial Cells Cocultured on a Nanomatrix. *Sci. Rep.* 8, 15749 (2018).

CONCLUSIONS

In response to the current challenges and limitation of commercial BMS and DES, we have developed a prohealing nanomatrix stent coating. To evaluate the effect of this coating with the existence of major vascular cells including endothelial cells, smooth muscle cells, monocytes, macrophage, and foam cells, an *in vitro* vascular double layer model was used. *In vitro* results indicated that, compared with commercial BMS and DES, the prohealing nanomatrix coated stent could 1) improve endothelialization and endothelial functions, 2) regulate smooth muscle cell (SMC) phenotype to reduce SMC proliferation and migration, 3) suppress inflammation through a multifactorial manner, and 4) reduce foam cell formation, extracellular matrix remodeling, and calcification. This revealed the therapeutic effect of prohealing nanomatrix coated stent on vascular recovery. Then, a rabbit balloon injured iliac artery model was used to conduct the *in vivo* study. Consistently, *in vivo* results demonstrated that compared with commercial BMS and DES, this prohealing nanomatrix coated stent enhanced re-endothelialization with negligible restenosis, inflammation, or thrombosis.

Due to the weaknesses of current *in vitro* and *in vivo* models for the therapeutics and devices evaluation, an advanced three-layered vascular sheet with atherosclerotic features (VSA) was developed. This VSA contains fibroblast, smooth muscle, and endothelial layer, with endothelial dysfunction, monocyte recruitment, macrophages, extracellular matrix remodeling, smooth muscle cell phenotype transition, inflammatory

cytokine secretion, foam cells, and calcification initiation. The response of classical therapeutics for CVD treatment (rosuvastatin and sirolimus) in VSA is consistent with previous reports in animal models and clinical studies. And other drug candidates and gene therapies (curcumin, colchicine, and liposome encapsulated miR-146a) were also evaluated in VSA, which showed potential treatment for atherosclerosis. Therefore, this VSA is a efficient and effective in vitro model for future CVD drug and device evaluation.

FUTURE STUDIES

It was found that the restenosis under atherosclerotic conditions in stented arteries is more aggressive than healthy stented arteries in animal model. Thus, despite the promising results of our *in vivo* results in rabbit model, it is necessary to optimize the current coating design to suppress this aggressive restenosis under diseased conditions. In the future study, the popular restenosis-inhibiting agent, everolimus, was chosen to combine with prohealing nanomatrix stent coating. Current preliminary results indicated that the NO released from nanomatrix could promote endothelialization and complement the side effect of everolimus on endothelium and the combination of everolimus and prohealing nanomatrix could have more suppression on SMC proliferation. Therefore, the prohealing nanomatrix stent coating is updated to dual-action stent coating, which contains liposome encapsulated everolimus and the prohealing nanomatrix. The VSA and a high fat diet rabbit model will be utilized to investigate the effect of dual-action stent under atherosclerotic conditions.

LIST OF REFERENCES

1. Serruys, P.W., Kutryk, M.J.B. & Ong, A.T.L. Coronary-Artery Stents. *New England Journal of Medicine* 354, 483-495 (2006).
2. Shuchman, M. Debating the Risks of Drug-Eluting Stents. *New England Journal of Medicine* 356, 325-328 (2007).
3. Denardo, S.J., Carpinone, P.L., Vock, D.M., Batich, C.D. & Pepine, C.J. Changes to Polymer Surface of Drug-Eluting Stents During Balloon Expansion. *JAMA* 307, 2148-2150 (2012).
4. Babapulle, M.N., Joseph, L., Bélisle, P., Brophy, J.M. & Eisenberg, M.J. A hierarchical Bayesian meta-analysis of randomised clinical trials of drug-eluting stents. *The Lancet* 364, 583-591 (2004).
5. Inoue, T. et al. Vascular Inflammation and Repair. *JACC: Cardiovascular Interventions* 4, 1057-1066 (2011).
6. Finn, A.V. et al. Pathological Correlates of Late Drug-Eluting Stent Thrombosis. *Circulation* 115, 2435-2441 (2007).
7. Joner, M. et al. Pathology of Drug-Eluting Stents in Humans. *Journal of the American College of Cardiology* 48, 193-202 (2006).
8. Finn, A.V. et al. Vascular Responses to Drug Eluting Stents. *Arteriosclerosis, Thrombosis, and Vascular Biology* 27, 1500-1510 (2007).
9. Briguori, C. et al. In-stent restenosis in small coronary arteries. *Journal of the American College of Cardiology* 40, 403-409 (2002).
10. Acharya, G. & Park, K. Mechanisms of controlled drug release from drug-eluting stents. *Advanced Drug Delivery Reviews* 58, 387-401 (2006).
11. Kuramitsu, S. et al. Risk Factors and Long-Term Clinical Outcomes of Second-Generation Drug-Eluting Stent Thrombosis. *Circulation: Cardiovascular Interventions* 12, e007822 (2019).
12. Schwartz, R.S. et al. Drug-Eluting Stents in Preclinical Studies. *Circulation: Cardiovascular Interventions* 1, 143-153 (2008)

13. Nakazawa, G. et al. Evaluation of Polymer-Based Comparator Drug-Eluting Stents Using a Rabbit Model of Iliac Artery Atherosclerosis. *Circulation: Cardiovascular Interventions* 4, 38-46 (2011).
14. Nakazawa, G. et al. Drug-eluting stent safety: findings from preclinical studies. *Expert Review of Cardiovascular Therapy* 6, 1379-1391 (2008).
15. Heldman, A.W. et al. Paclitaxel Stent Coating Inhibits Neointimal Hyperplasia at 4 Weeks in a Porcine Model of Coronary Restenosis. *Circulation* 103, 2289-2295 (2001).
16. Suzuki, T. et al. Stent-Based Delivery of Sirolimus Reduces Neointimal Formation in a Porcine Coronary Model. *Circulation* 104, 1188-1193 (2001).
17. Coronary Drug-Eluting Stents-Nonclinical and Clinical Studies: FDA Guidance for Industry. 2008.
18. Virmani, R., Kolodgie, F.D., Farb, A. & Lafont, A. Drug eluting stents: are human and animal studies comparable? *Heart* 89, 133 (2003).
19. Park, S.-J., Kang, S.-J., Virmani, R., Nakano, M. & Ueda, Y. In-Stent Neoatherosclerosis. *Journal of the American College of Cardiology* 59, 2051-2057 (2012).
20. Arbustini, E., Favalli, V. & Narula, J. Functionally Incomplete Re-Endothelialization of Stents and Neoatherosclerosis*. *JACC: Cardiovascular Interventions* 10, 2388-2391 (2017).
21. Li, M., Qian, M., Kyler, K. & Xu, J. Endothelial-Vascular Smooth Muscle Cells Interactions in Atherosclerosis. *Front Cardiovasc Med* 5, 151 (2018).
22. Joner, M. et al. Endothelial Cell Recovery Between Comparator Polymer-Based Drug-Eluting Stents. *Journal of the American College of Cardiology* 52, 333-342 (2008).
23. Otsuka, F. et al. The importance of the endothelium in atherothrombosis and coronary stenting. *Nature Reviews Cardiology* 9, 439-453 (2012).
24. Cai, H. & Harrison, D.G. Endothelial Dysfunction in Cardiovascular Diseases: The Role of Oxidant Stress. *Circulation Research* 87, 840-844 (2000).
25. Jun, H.W., Yuwono, V., Paramonov, S.E. & Hartgerink, J.D. Enzyme-Mediated Degradation of Peptide-Amphiphile Nanofiber Networks. *Advanced Materials* 17, 2612-2617 (2005).
26. Jun, H.-W. et al. Abstract 10174: Native Endothelium Mimicking Self-Assembled Nanomatrix for Drug-Eluting Stents. *Circulation* 122, A10174-A10174 (2010).

27. Andukuri, A. et al. A hybrid biomimetic nanomatrix composed of electrospun polycaprolactone and bioactive peptide amphiphiles for cardiovascular implants. *Acta Biomaterialia* 7, 225-233 (2011).
28. Andukuri, A. et al. Evaluation of the effect of expansion and shear stress on a self-assembled endothelium mimicking nanomatrix coating for drug eluting stents in vitro and in vivo. *Biofabrication* 6, 035019 (2014).
29. Andukuri, A., Minor, W.P., Kushwaha, M., Anderson, J.M. & Jun, H.-W. Effect of endothelium mimicking self-assembled nanomatrices on cell adhesion and spreading of human endothelial cells and smooth muscle cells. *Nanomedicine: Nanotechnology, Biology and Medicine* 6, 289-297 (2010).
30. Andukuri, A. et al. Enhanced Human Endothelial Progenitor Cell Adhesion and Differentiation by a Bioinspired Multifunctional Nanomatrix. *Tissue Engineering Part C: Methods* 19, 375-385 (2012).
31. Alexander, G.C. et al. Nanomatrix Coated Stent Enhances Endothelialization but Reduces Platelet, Smooth Muscle Cell, and Monocyte Adhesion under Physiologic Conditions. *ACS Biomaterials Science & Engineering* 4, 107-115 (2018).
32. Alexander, G.C. et al. Novel Multifunctional Nanomatrix Reduces Inflammation in Dynamic Conditions in Vitro and Dilates Arteries ex Vivo. *ACS Applied Materials & Interfaces* 8, 5178-5187 (2016).
33. Ban, K. et al. Cell Therapy with Embryonic Stem Cell-Derived Cardiomyocytes Encapsulated in Injectable Nanomatrix Gel Enhances Cell Engraftment and Promotes Cardiac Repair. *ACS Nano* 8, 10815-10825 (2014).
34. Lee, S.-J. et al. Enhanced Therapeutic and Long-Term Dynamic Vascularization Effects of Human Pluripotent Stem Cell-Derived Endothelial Cells Encapsulated in a Nanomatrix Gel. *Circulation* 136, 1939-1954 (2017).
35. Brott Brigitta, C. & Chatterjee, A. Drug-Eluting Balloon Therapy for In-Stent Restenosis of Drug-Eluting Stents. *JACC: Cardiovascular Interventions* 11, 979-980 (2018).
36. Chen, J. et al. Recent advances in nanomaterials for therapy and diagnosis for atherosclerosis. *Advanced Drug Delivery Reviews* 170, 142-199 (2021).
37. Kushwaha, M. et al. A nitric oxide releasing, self assembled peptide amphiphile matrix that mimics native endothelium for coating implantable cardiovascular devices. *Biomaterials* 31, 1502-1508 (2010).


38. Mehilli, J. et al. Randomized Trial of Paclitaxel- Versus Sirolimus-Eluting Stents for Treatment of Coronary Restenosis in Sirolimus-Eluting Stents. *Journal of the American College of Cardiology* 55, 2710-2716 (2010).

APPENDIX A

IACUC APPROVAL



MEMORANDUM

DATE: 14-Dec-2020
TO: Jun, Ho-Wook
FROM: 
 Robert A. Kesterson, Ph.D., Chair
 Institutional Animal Care and Use Committee (IACUC)
SUBJECT: NOTICE OF APPROVAL

The following application was approved by the University of Alabama at Birmingham Institutional Animal Care and Use Committee (IACUC) on 14-Dec-2020.

Protocol PI: Jun, Ho-Wook
Title: Prohealing Multifunctional Endothelium Nanomatrix Coated Stent
Sponsor: National Heart, Lung, and Blood Institute/NIH/DHHS
Animal Project Number (APN): IACUC-10223

This institution has an Animal Welfare Assurance on file with the Office of Laboratory Animal Welfare (OLAW), is registered as a Research Facility with the USDA, and is accredited by the Association for Assessment and Accreditation of Laboratory Animal Care International (AAALAC).

This protocol is due for full review by 16-Sep-2022.

Institutional Animal Care and Use Committee (IACUC)

403 Community Health on 19th | 933 19th Street South

Mailing Address:

CH19 403 | 1720 2nd Ave South | Birmingham AL 35294-2041

phone: 205.934.7692 | fax: 205.934.1188

www.uab.edu/iacuc | iacuc@uab.edu

APPENDIX B



NON-GLP NON-CLINICAL STUDY PROTOCOL

Study Title:

Study to Evaluate Endothelial Healing Following Nanomatrix Coated Stents in a Rabbit Iliac Artery Balloon Injury Model at 4 and 28 Days Post Implant.

T3 Labs Study Code: DY01B

1.0 STUDY OVERVIEW AND PERSONNEL

T3 Labs Study Code	DY01B
Sponsor Study Code	N/A
Study Title	Study to Evaluate Endothelial Healing Following Nanomatrix Coated Stents in a Rabbit Iliac Artery Balloon Injury Model at 4 and 28 days post implant.
Estimated Start Date	November, 2017
Study Duration/Time points	4 and 28 days
Test Article	PAYK-NO Nanomatrix coated stents
Control Article	<ol style="list-style-type: none"> 1. Promus Premier everolimus-eluting stent (Boston scientific) 2. Rebel bare metal stent (Boston Scientific)
Test System	New Zealand White Rabbit
Sponsor	University of Alabama 806 Shelby Building, 1825 University Blvd Birmingham, AL 35294
Sponsor Contact	Brigitta C. Brott, MD Professor of Medicine and Biomedical Engineering Director, Interventional Cardiology Fellowship Program University of Alabama at Birmingham FOT 907, Interventional Cardiology 1720 2 nd Avenue South Birmingham, AL 35294 E-mail: bbrott@uabmc.edu Phone: 205-934-7898

Test Facility Name Address, Phone, and Fax	T3 Labs (Translational Testing and Training Laboratories) 380B Northyards Blvd Atlanta, GA 30313 Phone: 404-894-5227 Fax: 404-894-5270
Principal Investigator	Name: Irena Brants E-mail: irena.brants@t3labs.org Phone: 678-576-2957
Program Manager	N/A
Test Facility Management (GLP only)	N/A
Test Facility QAU	Name: Kenneth Zielmanski E-mail: kenneth.zielmanski@t3labs.org Phone: 404-894-5277
Contributing Scientist(s)	<p>Attending Veterinarian Name: Ashley Strong, DVM E-mail: Ashley.strong@t3labs.org Phone: 404-309-0614</p> <p>Interventionalist: Name: Antwawn Bryant E-mail: Antwawn.bryant@t3labs.org Phone: 404-894-5227</p> <p>Study Pathologist: Name: Peter Anderson</p>

	E-mail: panderson@uabmc.edu
Contract Test Sites (Histopath, Bloodwork, Microbiology, PK, Analytical Services etc.)	Name of Histopathology Test Site Name: Pathology Core Research Laboratory / Department of Pathology University of Alabama at Birmingham Contact: Dezhi (Annie) Wang, MD, HTL, QIHC (ASCP), Lab Manager Address: LHRB B37 / 1919 7 th Avenue South Birmingham, AL 35294 Phone: 205-934-4415

2.0 STUDY REVIEWS AND APPROVALS

PRINCIPAL INVESTIGATOR:

I will abide by all T3 Labs policies and procedures as well as other applicable laws, policies, and regulations governing the use of animals regulated for teaching and research. I will use the provisions in the Guide for the Care and Use of Laboratory Animals as a guideline.

I will oversee all experiments involving live animals. Furthermore, I will ensure that all listed personnel are qualified or will be trained in proper procedures, including animal handling, anesthesia, surgery, post-procedural management and euthanasia. Also I will ensure that individuals not listed in this protocol will not have responsibility in experiments involving animals.

I certify that non-T3 Labs individuals listed as participants in this study are authorized to conduct procedures involving animals under this protocol and have received training in the physiology, handling, and care of this species; aseptic surgical methods and techniques (as necessary); the concept, availability, and use of research or testing methods that limit the use of animals or minimize distress; the proper use of anesthetics, analgesics, and tranquilizers (as necessary); procedures for reporting animal welfare concerns.

I certify that I have reviewed the pertinent scientific literature and the sources and/or databases as noted in this document, and have found no valid alternative to any procedures described herein which may cause more than momentary pain or distress, whether it is relieved or not.

I certify that I have determined that the research proposed herein is not un-necessarily duplicative of previously reported research.

I certify that the protocol, including details related to animal care and use (e.g. study design, model selection, proposed surgical techniques and necessary measures to

alleviate pain and distress), was reviewed by T3 Labs attending veterinarian or veterinarian designee **prior** to submission for IACUC approval.

T3 Labs Study Code: DY01B

Sponsor Study Code: N/A

The undersigned certify that this protocol completely and accurately describes study objectives, methods, schedule, roles and responsibilities, and provides justification for model selection, number of animals needed and measures planned to alleviate pain and distress to the best of their knowledge.

Name and Role	Signature	Date
Irena Brants Principal Investigator	<i>Irena Brants</i>	11-28-17
Brigitta C. Brott, MD Sponsor	<i>Brigitta C. Brott, MD</i>	11/27/2017
Kenneth Zielmanski Sucha Khanna Quality Assurance Unit (Review only)	<i>Sucha Khanna</i>	11-28-17
John Calvert, PhD IACUC Chair/Representative	<i>John Calvert</i>	11-28-17
Ashley Strong, DVM Attending Veterinarian or Delegate	<i>Ashley Strong</i>	11/28/17

TABLE OF CONTENTS

1.0 STUDY OVERVIEW AND PERSONNEL	134
2.0 STUDY REVIEWS AND APPROVALS	136
3.0 STUDY COMPLIANCE	141
4.0 LAY SUMMARY	142
5.0 STUDY OBJECTIVES	142
6.0 TEST AND/OR CONTROL ARTICLES	142
6.1 TEST ARTICLE	142
6.2 CONTROL ARTICLE	143
6.3 RESERVE SAMPLES	143
6.4 TEST ARTICLE CHARACTERIZATION	143
6.5 TEST AND CONTROL ARTICLE ACCOUNTABILITY	144
6.6 ACCESSORIES, EQUIPMENT AND SURGICAL SUPPLIES	144
7.0 DESCRIPTION OF THE TEST SYSTEM	144
7.1 SOURCE AND EXPERIMENTAL HISTORY	145
7.2 JUSTIFICATION FOR SPECIES SELECTION	145
7.3 JUSTIFICATION FOR THE USE OF ANIMALS	145
7.4 JUSTIFICATION FOR THE NUMBER OF ANIMALS	145
8.0 ANIMAL WELFARE	146
8.1 PAIN/DISTRESS CLASSIFICATION (PLACE “N/A” FOR ALL NON-APPLICABLE FIELDS)	146
8.2 ENDPOINTS AND MINIMIZATION OF PAIN AND DISTRESS	146
9.0 MANDATORY ASSURANCE STATEMENTS	147
9.1 ALTERNATIVES	147
9.2 DUPLICATIVE RESEARCH	148
9.3 BLOOD SAMPLE COLLECTION VOLUMES AND FREQUENCY:	148
9.4 HAZARDOUS MATERIAL	148
10.0 STUDY DESIGN	149
10.1 PRE-STUDY ACTIVITIES	150
10.2 ANIMAL CARE	151

	139
10.3 HUSBANDRY EXEMPTIONS	152
11.0 METHODS	153
11.1 IN-LIFE METHODS	153
11.2 RANDOMIZATION	153
11.3 CONTROL OF BIAS	153
11.4 EXCLUSION CRITERIA	154
11.5 FASTING	154
11.6 MEDICATIONS	154
<i>11.6.1 Pre-Operative Medications</i>	<i>154</i>
<i>11.6.2 Intra-Operative Medications</i>	<i>154</i>
<i>11.6.3 Post-Operative Medications</i>	<i>155</i>
<i>11.6.4 Euthanasia Agents</i>	<i>155</i>
<i>11.6.5 Emergency or Supportive Medications</i>	<i>156</i>
<i>11.6.6 Contra-indicated Medications</i>	<i>156</i>
11.7 ANIMAL PREPARATION FOR SURGERY	156
11.8 INTRA-OPERATIVE ANIMAL MONITORING	156
11.9 DIGITAL PHOTOGRAPHY	157
11.10 INTRA-OPERATIVE PROCEDURES	157
11.11 PROCEDURE CLOSE	158
11.12 ANIMAL RECOVERY	158
11.13 FOLLOW UP PROCEDURE	158
11.14 POST-OPERATIVE CARE	158
11.15 UNANTICIPATED EVENTS AND ACTIONS	158
11.16 CLINICAL PATHOLOGY	159
11.17 DISPOSITION OF ANIMALS / METHOD OF EUTHANASIA	159
<i>11.17.1 Scheduled Euthanasia Timepoint(s)</i>	<i>159</i>
<i>11.17.2 Early Death/Unscheduled Euthanasia/Moribund Animals</i>	<i>159</i>
11.18 PATHOLOGY AND HISTOLOGY FOR SCHEDULED EUTHANASIA	159
<i>11.18.1 Gross Necropsy</i>	<i>159</i>
<i>11.18.2 SEM</i>	<i>160</i>
<i>11.18.3 Histology</i>	<i>160</i>
<i>11.18.4 OCT</i>	<i>160</i>
12.0 SHIPPING INFORMATION	161

	140
13.0 STATISTICAL ANALYSIS	161
14.0 REPORTS AND RECORDS	161
14.1 REPORTS	161
14.2 STUDY MATERIAL DISPOSITION	161
<i>14.2.1 Non-GLP Study Material Retention</i>	<i>161</i>
15.0 DEVIATIONS	161
16.0 AMENDMENTS	162

3.0 STUDY COMPLIANCE

<input checked="" type="checkbox"/>	This Non-GLP study will be conducted in accordance with the requirements of the Animal Welfare Act and amendments. Compliance will be accomplished by conforming to the standards in the Guide for the Care and the Use of Laboratory Animals, ILAR, National Academy Press, latest edition. Planned protocol changes will be documented via a protocol amendment which will include a description of the change(s), rationale for the change(s) and will be signed, at a minimum, by Principal Investigator, Sponsor and/or IACUC.
<input type="checkbox"/>	This study will comply with the guidelines for nonclinical laboratory studies as described in the Code of Federal Regulations, 21 Part 58, and with any applicable amendments. (GLP compliant)

The Test Facility is accredited by the Association for the Assessment and Accreditation of Laboratory Animal Care, International (AAALAC) and registered with the United States Department of Agriculture to conduct research in laboratory animals.

T3 Labs Institutional Animal Care and Use Committee (IACUC) oversees the specific use of animals by formally reviewing study protocols/amendments and granting approval prior to initiation of work as per T3 Labs SOP GA046. Planned protocol changes will be documented via a protocol amendment by the Principal Investigator. Amendments will include a description of the change(s), rationale for the change(s) and will be signed, at a minimum, by the following: IACUC (if related to animal care), Sponsor, Principal Investigator, QAU and Testing Facility Management. If a non-GLP approved protocol has undergone more than four (4) IACUC amendments or substantive changes that alter the original objectives of the protocol, the IACUC may require the Principal Investigator to submit a new protocol in order to clarify the requested changes. The new protocol would incorporate all changes into one clean document. In such event, original protocol will be made inactive and a new protocol generated (same study code may remain if preferable).

IACUC approved protocols are in effect for three (3) years but Principal Investigator must comply with annual protocol renewal process. Protocol will be terminated at the end of third annual review period.

Deviations will be documented in a timely manner, communicated to and approved by the Principal Investigator and included in the Final Report with any effect on study integrity evaluated by the Principal Investigator.

4.0 LAY SUMMARY

Coronary or peripheral stent implants help hold open an artery so that blood can flow through the blocked or clogged artery. The stent-a small, lattice-shaped wire mesh tube, props open the artery and remains permanently in place. Stents are often coated with drugs that slowly release a drug to block cell proliferation in a diseased artery. This prevents fibrosis that, together with clots (thrombi), could otherwise block the stented artery, a process called restenosis.

The purpose of this study will be to assess efficacy of the nanomatrix coated stents in a rabbit iliac artery injury model. Most critical measures for success will include evaluation of re-endothelialization (regrowth of endothelial tissue following damage), restenosis, inflammation and thrombosis at short and intermediate time points. Findings will be compared to commercially available drug eluting stents and a bare metal stent at two time points: 4 and 28 days post implant.

5.0 STUDY OBJECTIVES

Primary objective of the study will be to evaluate efficacy of the prohealing multifunctional endothelium nanomatrix coated stent on enhanced endothelial healing in a rabbit iliac artery balloon injury model. Prohealing ability (degree of endothelialization) will be evaluated at short term and intermediate time points by variety of methods: SEM, immunochemistry, morphometry, OCT, and histology to assess endothelial cell coverage and underlying neointima formation, thrombosis, inflammation, and cytotoxicity.

6.0 TEST AND/OR CONTROL ARTICLES

6.1 Test Article

Name	PAYK-NO Nanomatrix coated stents
Description	Self assembled nanomatrix coated onto commercially available stents
Lot number	To be documented in study records
Supplier	Sponsor
Storage Requirements	Ambient
Handling	Aseptic / Per IFU

If the items specified above are Expired or NOT Pharmaceutical grade, provide a Justification below (Refer to POL 073, <i>Guidance on Use of Expired Medical Materials</i>):
N/A

6.2 Control Article

Name	1. Promus Premier 2. Rebel bare metal stent
Description	1. Promus PREMIER™ Everolimus-eluting platinum chromium coronary stent

GA025-1 Rev 05	Protocol Template	Effective Date: 06/06/17	Page 10 of 29
	<p>system, the company's next-generation durable polymer drug-eluting stent (DES).</p> <p>2. The REBEL stent system consists of a bare metal stent and a delivery catheter. The stent is made from a platinum chromium alloy and is used to treat coronary artery disease. The stent is the same design as the Promus Premier stent, but without the drug component.</p>		
Lot number	To be documented in study records		
Supplier	Abbott Vascular		
Storage Requirements	Ambient		
Handling	Aseptic / Per IFU		
If the items specified above are Expired or NOT Pharmaceutical grade, provide a Justification below (Refer to POL 073, <i>Guidance on Use of Expired Medical Materials</i>):			
N/A			

6.3 Reserve Samples
Not applicable for this non-GLP study.

6.4 Test Article Characterization
Not applicable

6.5 Test and Control Article Accountability

While at T3 Labs, Test and Control article accountability will be maintained as per T3 Labs's SOP,

GA007, *Procedure for Test and Control Article Handling; Receipt, Storage and Distribution, Including Shipping Off-Site*. Disposition of all unused test and/or control articles will be as indicated in the study records.

6.6 Accessories, Equipment and Surgical Supplies

The following accessory items may be used:

- Appropriate size vascular introducers (5F) or equivalent
- Appropriate size guide catheters (5F MP) or equivalent
- Emerge PTCA balloon catheter (3.0x15mm)
- Luge guidewire, (0.014") or equivalent
- Indeflator
- BD Medical spinal needles for vascular access
- OCT catheters
- OCT imaging system

List represents equipment and accessories that may be needed. It is not a requirement to utilize every line item. All equipment and accessory items used including product name, description and expiration/calibration due dates will be documented in the study records.

7.0 DESCRIPTION OF THE TEST SYSTEM

This study will be conducted using the animal model outlined below:

Species	Rabbit
Strain	New Zealand White
Age	Appropriate for body weight
Weight¹	2.8 – 5.0kg
Gender	Male and Female

¹ Animals outside of this weight range may still be considered acceptable for enrollment in the study by the Principal Investigator and/or Sponsor if deemed appropriate. If acceptable, weight exceptions will not be considered a deviation.

Number	18 + 4 back-ups for total of 22 rabbits
---------------	---

7.1 Source and Experimental History

The animals will be purchased from a single T3 Labs approved vendor. The animals will be healthy with no history of prior use.

7.2 Justification for species selection

Rabbits have been selected based on the extensive knowledge regarding cardiovascular implants, especially stents. The iliac arteries of New Zealand White rabbits are appropriately sized target vessels for the evaluation of cardiovascular devices and vascular procedures. These vessels approximate the size of human coronary arteries and they produce responses similar to the restenosis lesions that develop after angioplasty in humans. The use of rabbit iliac artery model is strongly recommended for preclinical evaluation of new drug-eluting stents. In addition, the size of rabbit iliac arteries allows for use of human adult sized catheters and devices and allows for the direct transfer of the technology to human trials.

7.3 Justification for the Use of Animals

Are <i>in-vitro</i> options available? (Y/N)	N
Are live systemic interactions needed? (Y/N)	Y
Is this study being performed to satisfy the Food and Drug Administration (FDA) requirements? (Y/N)	N
List FDA guidance or other document(s) if marked Y above	N/A
Written justification for the use of animals: In the judgment of the investigators who have extensive experience and current knowledge in the science of interventional cardiology, determination of the effects of stent implantation in the rabbit iliac artery cannot be predicted or modeled by cell culture systems, computer algorithms, or any other known entity aside from a large mammal. Research into treatment of restenosis using animal model will increase the ability to minimize need for invasive and potentially dangerous procedures in humans. Restenosis and the evaluation of local tissue response to stents is a complex clinical problem. In order to understand this process, it is critical that a whole animal is utilized to duplicate the human state as closely as possible <i>in vivo</i> . The effects of conditions <i>in vivo</i> in an intact vessel preclude exclusive use of non-animal models.	

7.4 Justification for the Number of Animals

The number of animals is the minimum number required for statistical verification. Based on power analysis twelve stents total will be needed for each stent type: n=4 of each will be analyzed at 4 days and n=8 of each will be analyzed at 28 days post implant for

total of 36 implant sites or 18 rabbits. 4 back-up rabbits may be enrolled in case of early mortality. Each rabbit will receive two stents, one in each hind leg. This is a reasonable but not excessive number of animals to evaluate prohealing between two different DES (Nanomatrix and Boston Scientific Promus Premier) and a bare metal stent at two time points: 4 days (6 rabbits) and 28 days (12 rabbits).

8.0 ANIMAL WELFARE

8.1 Pain/Distress Classification (place “n/a” for all non-applicable fields)

Class B: Animals bred, conditioned, or held for use in teaching, testing, experiments, research, or surgery but not yet needed for such purposes.			
Year 1: n/a	Year 2: n/a	Year 3: n/a	Total: n/a
Class C: Non-Painful/Non-Stressful: The experimental design involves procedures that cause NO pain or momentary, slight pain, discomfort or distress.			
Year 1: n/a	Year 2: n/a	Year 3: n/a	Total: n/a
Class D: Painful/Stressful WITH Analgesia/Anesthesia/Tranquilizers: The experimental design involves procedures that may involve short-term pain, discomfort or distress which will be treated with appropriate anesthetics/analgesics.			
Year 1: 22	Year 2: 0	Year 3: 0	Total: 22
Class E: Painful/Stressful WITHOUT Pain or Stress Relieving Measures: The experimental design involves procedures that involve pain, discomfort or distress (greater than that attending routine injection) which cannot / will not be alleviated through the administration of appropriate anesthetic, analgesic or tranquilizer drugs.			
Year 1: n/a	Year 2: n/a	Year 3: n/a	Total: n/a
Scientific justification for Class E Procedures: N/A			

8.2 Endpoints and Minimization of Pain and Distress

The Guide states that there are certain studies that require special consideration for humane endpoints (tumor models, infectious diseases, vaccine modeling, pain modeling, trauma, production of monoclonal antibodies, assessment of toxicologic effects, organ or system failure, and models of cardiovascular shock). For studies involving these situations, T3 Labs **SOP AR015, Procedures for Moribund or Dead Animals and Determination of Clinical Endpoints** will be followed unless otherwise described below.

Endpoints will follow T3 Labs SOP AR015 (Y/N)	Y
---	---

Anesthetics, analgesics or tranquilizers will be used to alleviate pain and/or distress. The agent(s), dose, route, frequency, and duration of administration are as per T3 Labs SOP AR006 , <i>Use of Sedatives, Analgesics, and Anesthetics</i> . (Y/N)	Y
Provide justification for endpoints not following T3 Labs SOP AR015 and/or other methods used to alleviate pain and/or distress: N/A	

9.0 MANDATORY ASSURANCE STATEMENTS

9.1 Alternatives

Alternatives may include: Replacement – non-animal alternatives such as *in vitro* systems; Refinements – non-painful alternative or less painful alternative procedures or the use of phylogenetically lower animal species; or Reduction in the animal numbers.

Type of Search Conducted (ex: Online, periodical, etc.)	Source (PubMed, Agricola, Nerac)	Keywords	Years Covered	Results
Online	Pubmed	Rabbit iliac percutaneous angioplasty	1982 - present	54
Online	Agricola	Rabbit iliac percutaneous angioplasty	2011-2015	2
Online	Pubmed	Rabbit Iliac reendothelialization	1998 – 2016	24
Online	Agricola	Rabbit Iliac reendothelialization	2015 – 2016	2

A search of the PubMed database conducted on August 14th using keywords “rabbit iliac percutaneous angioplasty” resulted in 54 citations dating from 1982 - 2016, none of which discussed a suitable alternative in terms of replacement with a less sentient or in vitro model, reduction of animal numbers, or refinement of procedures to make them less painful or distressful. Search using keywords “rabbit iliac reendothelialization” resulted in 24 citations dating from 1998 – 2016 but none discussed a suitable alternative

in terms of replacement with a less sentient or in vitro model, reduction of animal numbers, or refinement of procedures to make them less painful or distressful.

A search of the Agricola database conducted on August 14th using keywords “rabbit iliac percutaneous angioplasty” and “rabbit iliac re-endothelialization” resulted in 2 citations each dating from 2011 – 2016 but none discussed a suitable alternative in terms of replacement with a less sentient or in vitro model, reduction of animal numbers, or refinement of procedures to make them less painful or distressful.

9.2 Duplicative Research

The Principal Investigator is also required to provide written assurance that the proposed study is not unnecessarily duplicative of previous work.

Is this duplicative research? (Y/N)	N
Provide justification if duplicative research: N/A	

9.3 Blood Sample Collection Volumes and Frequency:

Sample collection volumes adhere to guidelines provided in T3 Labs SOP AR058 , <i>Specimen Collection and Labeling for Laboratory Tests</i> . (Y/N or N/A)	Y
If not, provide justification and the precautionary measures to be taken: N/A	

9.4 Hazardous Material

Will any hazardous agents be used in this study? Y/N (If Y, please add details below or indicate N/A)	N
Chemical(s)	N/A
Safety Data Sheet (SDS) on file at T3 Labs as required by 29CFR1910.1450(h)(2)(iii) (Y/N)	N
Physical hazard - combustible liquid, compressed gas, flammable, etc. (Y/N)	N
Health hazard – carcinogen, corrosive, toxic, irritant, sensitizer, etc. (Y/N)	N
Biological agent(s)	N/A
Bio-safety level	N/A

Laser(s) (Eye protection required)	N/A
Cell line(s)	N/A
Radioisotope(s)	N/A

10.0 STUDY DESIGN

Following appropriate acclimation, and aspirin pretreatment, study animals will be sedated to undergo iliac artery balloon injury procedure via left or right carotid access and using standard catheterization techniques: Boston Scientific Emerge balloon catheter will be inflated and deflated three times for 30 seconds with 30 second reflow after each inflation to ensure balloon injury. Following denudation of the target segment, Test or Control stent will be deployed over the guide wire into the iliac artery in attempt to deploy the stent over the injured area of the vessel. Stents will be deployed slightly oversized with a stent to artery ratio of 1.1:1. Stents will be implanted in a randomized fashion in eighteen (18) rabbit iliac vessels using standard interventional procedures. Each animal will receive one stent per iliac vessel for a total of two stents per animal. Each animal will receive two stents of the same type (2 PAYK-NO, 2 Rebel, or 2 Promus Premier). A total of 6 animals (n=2 rabbits per stent type for total of 12 implant sites) will be needed for the short time point (4 days) and a total of 12 animals or 4 rabbits per stent type will be needed for the one month time point. Four (4) backup animals may be enrolled as needed to replace early casualties due to surgical complications during the stent implant procedure.

There will be 2 arms to this study and the implant matrix below will be used as a primary guide:

Table 1: Stent Implant and Evaluation Matrix

	Animal Number	Stent Type		Time Point	Evaluation Method
		Left Iliac	Right Iliac		
Arm 1	1	Control - BMS	Control - BMS	4 days	SEM / Histology
	2	Control - DES	Control - DES	4 days	SEM / Histology
	3	Test	Test	4 days	SEM / Histology
	4	Control - BMS	Control - BMS	4 days	SEM / Histology
	5	Control - DES	Control - DES	4 days	SEM / Histology
	6	Test	Test	4 days	SEM / Histology
Arm 2	7	Control - BMS	Control - BMS	28 days	SEM / Histology
	8	Control - DES	Control - DES	28 days	SEM / Histology
	9	Test	Test	28 days	SEM / Histology
	10	Control - BMS	Control - BMS	28 days	Histology
	11	Control - DES	Control - DES	28 days	Histology
	12	Test	Test	28 days	Histology
	13	Control - BMS	Control - BMS	28 days	Histology
	14	Control - DES	Control - DES	28 days	Histology
	15	Test	Test	28 days	Histology
	16	Control - BMS	Control - BMS	28 days	OCT
	17	Control - DES	Control - DES	28 days	OCT
	18	Test	Test	28 days	OCT

Animals will be fully recovered and released for routine care until scheduled follow-up and termination procedure. Implanted animals will receive oral antiplatelet therapy for the duration of the study and at scheduled termination (4 days +/-1 day for Arm 1 and 28 days +/- 2 days for Arm 2), animals will be sedated as for the initial procedure and will undergo follow-up angiography via carotid artery (opposite from the vessel accessed during the initial procedure). In addition, 3 animals enrolled in Arm 2 will undergo OCT (Optical Coherence Tomography) procedure prior to euthanasia. At necropsy, iliac arteries will be rinsed with cold saline followed by perfusion fixed with formalin. Post perfusion, iliac treatment sites will be identified and carefully excised to include unstented areas (~ 2-3cm) proximal and distal to the stented segment. Adjacent muscle and downstream iliac artery segments will also be harvested to evaluate for possible systemic inflammation and toxicity. Harvested specimens will be immersion fixed in 10% NBF for a minimum of 24 hours prior to off-site shipping for further processing and analysis.

10.1 Pre-Study Activities

The following prestudy activities: premedication and daily animal observations may be performed prior to the availability of a signed final protocol while animals are held

under T3 Labs holding protocol. These activities will be documented in the study records if they are performed prior to the protocol being signed by the Principal Investigator.

10.2 Animal Care

Animal Identification	Animals will be identified per T3 Labs SOP AR001 , <i>Research Animal Identification</i> .
Housing and Environmental Controls	Animals will be housed in cages or pens that meet or exceed the weight/space specifications outlined in the Animal Welfare Act Regulations. Pens or cages will be identified as per T3 Labs SOPs AR019 <i>Routine Care For Rabbits</i> . The T3 Labs housing facilities will provide appropriate ambient lighting and ambient temperature. Animal rooms, pens and cage cleaning will be performed according to T3 Labs SOPs. Animals will be housed at T3 Labs for the duration of the study.
Food	<p>The animals will be fed as specified in T3 Labs' SOP AR019 <i>Routine Care for Rabbits</i>. All animals will be fed once daily. Animals will be fed an amount appropriate for their weight and activity (typically approximately 200 grams daily).</p> <p>T3 Labs performs periodic feed analysis according to SOP AR036, <i>Animal Feed Storage and Testing</i>. No contaminants are known to be present in the</p>
	<p>feed at levels that would affect the outcome or integrity of the study. Therefore, no additional feed analysis will be performed during this study unless required by PI and/or Sponsor.</p>
Water	<p>Rabbits are provided water ad libitum a fresh, clean water bottle or lixit valve.</p> <p>If water bottles are low, they can be refilled and/or replaced as needed. During cage changes, the water bottle should be replaced with clean sanitized bottles of fresh water and ensured it does not leak. T3 Labs performs periodic water testing according to SOP AR038, <i>Monitoring and Documenting Water Quality Provided to Animals</i>. No contaminants are known to be present in the water at levels that would affect the outcome or integrity of the study. Therefore, no additional water analysis will be performed during this study unless required by PI and/or Sponsor.</p>

Acclimation and Quarantine Period	Animals will be acclimated for a minimum of 3 days per T3 Labs SOP AR045 <i>Quarantine, Acclimation and Enrollment</i> .
Animal Observations	Animals will be observed at least once daily per T3 Labs SOP AR011 <i>Assessment and Documentation of Animal Welfare</i> and SOP AR009 <i>Animal Medical Record System</i> .
Feed Intake	Amount of feed administered will be documented once daily.

10.3 Husbandry Exemptions

The Guide states that single housing of social species should be the exception. Social housing will be considered by T3 Labs as the default method of housing unless otherwise justified based on social incompatibility resulting from inappropriate behavior, veterinary concerns regarding animal well-being, exemptions allowed by T3 Labs **Policy 75**, or scientific necessity approved by the IACUC. Diet, environmental enrichment is considered standard per T3 Labs **SOPs AR011, AR018, AR019, AR020, AR034, AR036, AR043, AR048, AR061** unless otherwise justified below:

Is any exemption requested? (Y/N) If Y, please provide Duration and Justification below.	N
Requested exemption from social housing (<i>Check if needed post operatively</i>)	<input type="checkbox"/>
Requested exemption from environmental enrichment devices	<input type="checkbox"/>
Requested exemption from exercise	<input type="checkbox"/>
Requested exemption from normal diet and/or water provisions	<input type="checkbox"/>
Requested exemption from standard caging	<input type="checkbox"/>
Requested exemption for restraint:	<input type="checkbox"/>

Duration and Description of Exemption(s):	N/A
Justification for Exemption(s):	N/A

11.0 METHODS

11.1 In-life Methods

Upon enrollment into the study, several in-life activities will be performed. **Table 1** summarizes the various activities during the course of the study.

Table 2: In-Life Methods

Activity	Frequency			
	Arrival	Day 0	Termination	Daily
SOAP	x	x	x	
Body Weight	x	x	x	
Balloon Injury		x		
Stent Implant		x		
Observations				x
Angiography		x	x	
OCT			X (n=3 rabbits from Arm 2 only)	

11.2 Randomization

Animals will be randomized to receive Control or Test stents per methods described in T3 Labs **GA006**, *Proper Practices of Randomization*.

11.3 Control of Bias

The Interventionalist cannot be blinded during the implant procedure as it will be easy to visually tell apart the Test article from the Control stents. The study Pathologist will be masked to the implant matrix at the time of the assessments and will only be unmasked for reporting purposes after the assessments have been performed.

11.4 Exclusion Criteria

No additional exclusion criteria apply. If an animal is excluded due to health reasons, the animal may be transferred off the study to the internal housing protocol (naïve pool) or euthanized, as determined by the Principal Investigator in consultation with the Veterinarian.

11.5 Fasting

N/A

11.6 Medications

Medications or doses not specified below may be administered as deemed necessary by the Veterinarian or surgeon. Dosages for pre-operative, anesthetic or analgesic drugs may be calculated using the most recent body weight obtained prior to the day of procedure.

11.6.1 Pre-Operative Medications

Indication	Name	Dose	Route	Frequency	Applicable Procedure
Antiplatelet	Aspirin	40mg	PO	Q-3 days, SID	Pre-Initial
Sedation	Ketamine	35mg/kg	IM	To effect	Pre-Initial and Pre-Terminal Follow-up
	Xylazine	5mg/kg	IM	To effect	
Anesthesia	Isoflurane	0.5-5%	Inhalant via nose cone or induction box	As needed	Pre-Initial and Pre-Terminal Follow-up
Analgesia	Buprenorphine	0.02 – 0.03 mg/kg	SQ or IM	Once	Pre-Initial

11.6.2 Intra-Operative Medications

Indication	Name	Dose	Route	Frequency	Applicable Procedure
Anesthesia	Isoflurane	0.5-5%	Inhalant via nose cone	Maintenance	Initial and Terminal Follow-up
	Propofol	1 – 2 mg/kg	Slow IV bolus to effect	As needed to aid anesthesia	Initial and Terminal Follow-up
Maintenance IV fluids	LRS or Saline	2.5 – 5ml/kg/hr	IV	For maintenance	Initial
Anti-spasm	Nitroglycerine	200ug-1mg	Intra iliac artery	As needed	Initial Procedure
Antibiotic	Baytril	10mg/kg	IM or SQ	Once prior to cutdown	Initial
Anticoagulation	Heparin	150U/kg followed by maintenance dose of 50U/kg as needed	IV	To achieve and maintain ACT at or above 250sec	Initial and Terminal
Immed Post-op Analgesia	Buprenorphine	0.02 – 0.03 mg/kg	SQ or IM	Once	Initial

11.6.3 Post-Operative Medications

Indication	Name	Dose	Route	Frequency	Applicable Procedure
Antibiotic	Baytril	10mg/kg	IM or SQ	SID on Days 1-3	Initial
Analgesia	Buprenorphine	0.03 – 0.04mg/kg	SQ or IM	BID on Days 1- 2	Initial
Antiplatelet	Aspirin	40mg	PO	SID until termination	Initial

11.6.4 Euthanasia Agents

Indication	Name	Dose	Route	Frequency	Applicable Procedure
Anticoagulation	Heparin	150U/kg	IV	Once	Terminal
Euthanasia	Euthasol	100mg/kg	IV	To effect	Terminal

11.6.5 Emergency or Supportive Medications

Emergency or supportive medications may be administered at the discretion of the Surgeon or Veterinarian excluding administration of any identified contra-indicated medications in

Section 11.6.6.

11.6.6 Contra-indicated Medications

Any nonsteroidal anti-inflammatory drugs (NSAID). Aspirin is required as antiplatelet agent.

11.7 Animal Preparation for Surgery

Following proper acclimation, animals will be sedated per Section 11.6.1. followed by maintenance inhalant isoflurane via face mask or nose cone. An IV catheter will be placed in a peripheral ear vein for administration of medications and maintenance IV fluids during the procedure. The neck area will be clipped and shaved before placement in the dorsal recumbency. ECG leads will be placed for monitoring during the procedure. Surgical area will be scrubbed and surgical cutdown will be performed and short vascular sheath will be placed in the left or right carotid artery. At this time animal will be heparinized to achieve activated clotting time above 250 seconds.

11.8 Intra-operative Animal Monitoring

Animals will be monitored during the balloon injury and stent deployment procedure according to T3 labs **SOP AR009** *Animal Medical Record System*. Animal will be monitored to determine the depth of anesthesia using palpebral reflexes in combination with physiological status, specifically heart rate, respiration rate, and body temperature. Percent inhalant anesthetic administered will be recorded on the procedure record periodically throughout the procedure.

Table 3: Intra-Op Animal Monitoring

Parameter	Frequency	Method
Temperature, Pulse, Respiration	Approximately every 30 mins	
ACT	Once post heparin and then at the discretion of the operator.	Arterial blood

11.9 Digital Photography

Representative photographs and/or video of observations and procedure may be taken.

11.10 Intra-Operative Procedures

Procedure will start once ACT has reached 250 seconds.

Balloon Injury Procedure:

Using fluoroscopy visualization, a guiding catheter will be placed in the carotid artery and advanced over the aortic arch into the abdominal aorta. A coronary guidewire will then be placed in the iliac artery followed by a PTCA balloon catheter. The balloon will be inflated to 2 atm and deflated through the iliac artery three times for 30 seconds with 30 second reflow after each inflation to insure balloon injury. Angiography of the iliac arteries will be done before and after balloon injury procedure and mean vessel diameter of the target vessel segment determined. Stent will be deployed to the denuded area prior to repeating the steps in the contralateral iliac artery of the same animal.

Stent Implant Procedure:

Following balloon injury steps, a stent mounted on a delivery balloon will be advanced over the guidewire into one of the iliac arteries. A single stent will be deployed as slightly oversized, with a stent to artery ratio of 1.1:1.0 using fluoroscopy for visualization and standard catheterization techniques for deployment. A single stent will be implanted per iliac artery (denuded area) based on the implant matrix detailed in **Table 1, Stent Implant and Evaluation Matrix** and post-implant angiography of the stented iliac artery performed. Contralateral iliac artery of each rabbit will also receive a stent for a total of two stents per animal.

Any indication of impaired flow through the target vessel segment following balloon injury or stent implant will be documented in the study records. Nitroglycerin may be injected directly into the treated vessel to prevent or treat a vessel spasm.

11.11 Procedure Close

After removal of all devices, the carotid artery used for access will be ligated and access site surgically repaired – repeat angiography prior to termination will utilize the other carotid artery for access. To minimize post-operative bleeding risks, heparin will be withheld towards the end of procedure.

11.12 Animal Recovery

Following closure of the access sites, animal will be recovered and returned for routine care for assigned observation time. In addition to post-op antibiotics and pain medication, all study animals will receive daily dose of oral antiplatelet Aspirin until scheduled termination including the day of follow-up angiography and euthanasia.

11.13 Follow Up Procedure

At termination, rabbits will be anesthetized and will undergo catheterization as for the stent implant procedure, except that aseptic technique will not be needed. Iliac angiography will be performed with each vessel displayed in a projection angle as close as possible to the angle used for the stent implant.

Selected animals assigned to Arm 2 will undergo optical coherence tomography (OCT) examination of the treated iliac arteries prior to termination. The OCT image wire will be advanced to the stented artery segment and OCT imaging will be conducted by proximal balloon inflation and saline flushing to establish local exsanguination during imaging.

Heparin 150 U/kg will be injected intravenously prior to termination.

All animals will be terminated per Section 11.6.4 while still under deep anesthesia with inhalant isoflurane.

11.14 Post-Operative Care

Animals will be observed and cared for daily until scheduled termination. Healing of carotid vascular access sites will be monitored and examined daily until completely healed.

11.15 Unanticipated Events and Actions

Any signs of bleeding, swelling, discharge of any type or infection at the vascular access sites will be appropriately documented and communicated to the veterinarian and Principal Investigator per T3 Labs **SOP GA044**, *Study Director Notifications*.

11.16 Clinical Pathology

N/A

11.17 Disposition of Animals / Method of Euthanasia

11.17.1 Scheduled Euthanasia Timepoint(s)

Scheduled euthanasia will be performed at the completion of the follow-up restudy procedures at 4+/- 1 day (n=6 rabbits) and 28+/- 2 days (12 rabbits) post balloon injury and stent implant procedure.

11.17.2 Early Death/Unscheduled Euthanasia/Moribund Animals

All early death or unscheduled terminations will be necropsied as soon as possible by qualified personnel in order to determine the cause of death. At minimum, thoracic and abdominal organs will be exposed and examined for abnormalities:

Abnormal findings will be documented in the necropsy records. Samples of abnormal tissues maybe collected and sent for histology processing and microscopic evaluation. Tissue samples collected will be fixed in 10% buffered formalin for future gross assessment and histopathological analyses if deemed necessary

Stented iliac artery segments will be harvested and processed for analysis at the discretion of the PI and Sponsor. Stented segments from deceased animals may or may not be perfusion fixed. Even though perfusion fixation may not be feasible, reviewing the histology might give an idea of whether there was a device failure.

11.18 Pathology and Histology for Scheduled Euthanasia

11.18.1 Gross Necropsy

Following confirmation of euthanasia, animal will be immediately transported for gross necropsy and tissue harvest procedure. Stented iliac arteries will be perfusion-rinsed with 0.9% saline solution and perfusion fixed *in situ* with 10% neutral buffered formalin (NBF). Aorta will be cannulated and infused with ~250-300ml of saline at around 60mmHg pressure or by placing perfusion solution approximately 100cm above the work table. Once blood is flushed out, perfusion will be switched to 10% NBF. Stented vessel segments will be removed such that ~2-3cm of unstented vessel proximal and distal from the stent is collected. The proximal end of the vessel will be labeled with suture or equivalent. Harvested vessel segments will be placed into prelabeled appropriately sized plastic test tube with a screw top lid

(completely filled with formalin) and stored on their side to prevent distortion of the specimen. Following fixation, specimens will be transferred to University of Alabama for SEM, histomorphometry or immunohistochemistry analysis.

Digital photographs will be taken with a labelled ruler in the field. The label will at a minimum contain study code, animal number and date. All findings (normal and abnormal) will be documented in the necropsy records.

11.18.2 SEM

Upon receipt at histology test site, stented segments will be longitudinally dissected and distributed for SEM observation, histomorphometry and immunohistochemical staining according to **Table 1**, *Stent Implant and Evaluation Matrix*.

En face SEM will be performed at 15x, 50x, 200x, and 600x magnifications to evaluate degree of endothelialization. The SEM images will be digitally assembled for a complete view of the entire luminal stent surface. Endothelial cell coverage on the struts will be traced using morphometry software. The stent endothelialization score will be defined as the extent of the circumference of the arterial lumen covered by endothelial cells and scored from 1 to 3 (1= \leq 25%; 2=25-75%; 3= \geq 75%). Stented segments will also be evaluated by light microscopy and analyzed with the morphometry software. Each stent section will be analyzed for strut opposition, fibrin deposition, granuloma reactions, mineralization, and hemorrhage.

11.18.3 Histology

In order to assess thrombus formation, inflammation, and neointima formation, stents will be dehydrated and embedded in methylmethacrylate resin. Neointimal thickness will be measured using computerguided morphometric measurements. The presence of fibrin and the amount of fibrin will be graded on a scale of 0 to 3. Inflammation will be scored on a scale from 0 to 5. In addition to stented arteries, adjacent muscles, and iliac artery samples downstream of the implant site will also be evaluated to identify possible systemic inflammation and toxicity.

11.18.4 OCT

OCT analysis will be conducted offline by investigators blinded to the stent type. Analysis of stent cross sections will be performed at a maximum of 1mm intervals or frame by frame if irregularities are observed. Stent struts will be counted and classified as 1) embedded or contained within the vessel wall; 2) apposed and covered if the tissue is seen

above the strut; 3) apposed and uncovered if no tissue is detected, and 4) malapposed or incomplete stent apposition.

12.0 SHIPPING INFORMATION

All tissues harvested will be shipped to Sponsor after minimum of three (3) day formalin fixation.

Shipments will be directed to the address listed in Section 1.0, Histology Test Site.

13.0 STATISTICAL ANALYSIS

Where applicable, statistical analysis will be performed by Sponsor.

14.0 REPORTS AND RECORDS

14.1 Reports

Formal final report will not be required. Any data and images obtained during the study will be provided to the Sponsor at the end of procedures. Principal Investigator will also provide a summary of animal enrollment, test and control article distribution, and overview of animal health and medications received during the study.

14.2 Study Material Disposition

14.2.1 Non-GLP Study Material Retention

At the time of Study closure (when IACUC approval becomes inactive), or within 2 months from the necropsy of the last study animal, any remaining study materials to include study binders, digital images or any remaining wet tissues will be transferred to Sponsor per T3 Labs SOP AR060. Per USDA/PHS regulations, T3 Labs will retain original protocol, amendments and digital scans of animal records for three years prior to disposition according to T3 Labs **SOP QA012, Record Retention**.

15.0 DEVIATIONS

Any deviations to the protocol needed during the course of the study will be documented as per T3 Labs

SOP GA016, Deviation System. All deviations will be communicated to and approved by the Study Director (GLP) or Principal Investigator (non-GLP) and impact on to the study outcome will be assessed.

For GLP studies, all protocol deviations will be included in the Final Report.

16.0 AMENDMENTS

Any amendments to the protocol initiated during the course of the study will be documented as per T3

Labs **SOP GA025**, *Protocol, Amendment and Report Development* and approved by the Study Director

(GLP) or Principal Investigator (non-GLP). All amendments will be included in the Final Report, if written.

References

1. Serruys, P.W., Kutryk, M.J.B. & Ong, A.T.L. Coronary-Artery Stents. *New England Journal of Medicine* **354**, 483-495 (2006).
2. Shuchman, M. Debating the Risks of Drug-Eluting Stents. *New England Journal of Medicine* **356**, 325-328 (2007).
3. Denardo, S.J., Carpinone, P.L., Vock, D.M., Batich, C.D. & Pepine, C.J. Changes to Polymer Surface of Drug-Eluting Stents During Balloon Expansion. *JAMA* **307**, 2148-2150 (2012).
4. Babapulle, M.N., Joseph, L., Bélisle, P., Brophy, J.M. & Eisenberg, M.J. A hierarchical Bayesian meta-analysis of randomised clinical trials of drug-eluting stents. *The Lancet* **364**, 583-591 (2004).
5. Inoue, T. et al. Vascular Inflammation and Repair. *JACC: Cardiovascular Interventions* **4**, 1057-1066 (2011).
6. Finn, A.V. et al. Pathological Correlates of Late Drug-Eluting Stent Thrombosis. *Circulation* **115**, 2435-2441 (2007).
7. Joner, M. et al. Pathology of Drug-Eluting Stents in Humans. *Journal of the American College of Cardiology* **48**, 193-202 (2006).
8. Finn, A.V. et al. Vascular Responses to Drug Eluting Stents. *Arteriosclerosis, Thrombosis, and Vascular Biology* **27**, 1500-1510 (2007).
9. Briguori, C. et al. In-stent restenosis in small coronary arteries. *Journal of the American College of Cardiology* **40**, 403-409 (2002).
10. Acharya, G. & Park, K. Mechanisms of controlled drug release from drug-eluting stents. *Advanced Drug Delivery Reviews* **58**, 387-401 (2006).
11. Kuramitsu, S. et al. Risk Factors and Long-Term Clinical Outcomes of Second-Generation Drug-Eluting Stent Thrombosis. *Circulation: Cardiovascular Interventions* **12**, e007822 (2019).
12. Schwartz, R.S. et al. Drug-Eluting Stents in Preclinical Studies. *Circulation: Cardiovascular Interventions* **1**, 143-153 (2008).
13. Nakazawa, G. et al. Evaluation of Polymer-Based Comparator Drug-Eluting Stents Using a Rabbit Model of Iliac Artery Atherosclerosis. *Circulation: Cardiovascular Interventions* **4**, 38-46 (2011).

14. Nakazawa, G. et al. Drug-eluting stent safety: findings from preclinical studies. *Expert Review of Cardiovascular Therapy* **6**, 1379-1391 (2008).
15. Heldman, A.W. et al. Paclitaxel Stent Coating Inhibits Neointimal Hyperplasia at 4 Weeks in a Porcine Model of Coronary Restenosis. *Circulation* **103**, 2289-2295 (2001).
16. Suzuki, T. et al. Stent-Based Delivery of Sirolimus Reduces Neointimal Formation in a Porcine Coronary Model. *Circulation* **104**, 1188-1193 (2001).
17. Coronary Drug-Eluting Stents-Nonclinical and Clinical Studies: FDA Guidance for Industry. 2008.
18. Virmani, R., Kolodgie, F.D., Farb, A. & Lafont, A. Drug eluting stents: are human and animal studies comparable? *Heart* **89**, 133 (2003).
19. Park, S.-J., Kang, S.-J., Virmani, R., Nakano, M. & Ueda, Y. In-Stent Neointimal Hyperplasia. *Journal of the American College of Cardiology* **59**, 2051-2057 (2012).
20. Arbustini, E., Favalli, V. & Narula, J. Functionally Incomplete Re-Endothelialization of Stents and Neointimal Hyperplasia*. *JACC: Cardiovascular Interventions* **10**, 2388-2391 (2017).
21. Li, M., Qian, M., Kyler, K. & Xu, J. Endothelial-Vascular Smooth Muscle Cells Interactions in Atherosclerosis. *Front Cardiovasc Med* **5**, 151 (2018).
22. Joner, M. et al. Endothelial Cell Recovery Between Comparator Polymer-Based Drug-Eluting Stents. *Journal of the American College of Cardiology* **52**, 333-342 (2008).
23. Otsuka, F. et al. The importance of the endothelium in atherothrombosis and coronary stenting. *Nature Reviews Cardiology* **9**, 439-453 (2012).
24. Cai, H. & Harrison, D.G. Endothelial Dysfunction in Cardiovascular Diseases: The Role of Oxidant Stress. *Circulation Research* **87**, 840-844 (2000).
25. Jun, H.W., Yuwono, V., Paramonov, S.E. & Hartgerink, J.D. Enzyme-Mediated Degradation of Peptide-Amphiphile Nanofiber Networks. *Advanced Materials* **17**, 2612-2617 (2005).
26. Jun, H.-W. et al. Abstract 10174: Native Endothelium Mimicking Self-Assembled Nanomatrix for Drug-Eluting Stents. *Circulation* **122**, A10174-A10174 (2010).

27. Andukuri, A. et al. A hybrid biomimetic nanomatrix composed of electrospun polycaprolactone and bioactive peptide amphiphiles for cardiovascular implants. *Acta Biomaterialia* **7**, 225-233 (2011).
28. Andukuri, A. et al. Evaluation of the effect of expansion and shear stress on a self-assembled endothelium mimicking nanomatrix coating for drug eluting stents in vitro and in vivo. *Biofabrication* **6**, 035019 (2014).
29. Andukuri, A., Minor, W.P., Kushwaha, M., Anderson, J.M. & Jun, H.-W. Effect of endothelium mimicking self-assembled nanomatrices on cell adhesion and spreading of human endothelial cells and smooth muscle cells. *Nanomedicine: Nanotechnology, Biology and Medicine* **6**, 289-297 (2010).
30. Andukuri, A. et al. Enhanced Human Endothelial Progenitor Cell Adhesion and Differentiation by a Bioinspired Multifunctional Nanomatrix. *Tissue Engineering Part C: Methods* **19**, 375-385 (2012).
31. Alexander, G.C. et al. Nanomatrix Coated Stent Enhances Endothelialization but Reduces Platelet, Smooth Muscle Cell, and Monocyte Adhesion under Physiologic Conditions. *ACS Biomaterials Science & Engineering* **4**, 107-115 (2018).
32. Alexander, G.C. et al. Novel Multifunctional Nanomatrix Reduces Inflammation in Dynamic Conditions in Vitro and Dilates Arteries ex Vivo. *ACS Applied Materials & Interfaces* **8**, 5178-5187 (2016).
33. Ban, K. et al. Cell Therapy with Embryonic Stem Cell-Derived Cardiomyocytes Encapsulated in Injectable Nanomatrix Gel Enhances Cell Engraftment and Promotes Cardiac Repair. *ACS Nano* **8**, 10815-10825 (2014).
34. Lee, S.-J. et al. Enhanced Therapeutic and Long-Term Dynamic Vascularization Effects of Human Pluripotent Stem Cell-Derived Endothelial Cells Encapsulated in a Nanomatrix Gel. *Circulation* **136**, 1939-1954 (2017).
35. Brott Brigitta, C. & Chatterjee, A. Drug-Eluting Balloon Therapy for In-Stent Restenosis of Drug-Eluting Stents. *JACC: Cardiovascular Interventions* **11**, 979-980 (2018).
36. Chen, J. et al. Recent advances in nanomaterials for therapy and diagnosis for atherosclerosis. *Advanced Drug Delivery Reviews* **170**, 142-199 (2021).
37. Kushwaha, M. et al. A nitric oxide releasing, self assembled peptide amphiphile matrix that mimics native endothelium for coating implantable cardiovascular devices. *Biomaterials* **31**, 1502-1508 (2010).

38. Mehilli, J. et al. Randomized Trial of Paclitaxel- Versus Sirolimus-Eluting Stents for Treatment of Coronary Restenosis in Sirolimus-Eluting Stents. *Journal of the American College of Cardiology* **55**, 2710-2716 (2010).
39. Sigwart, U., Puel, J., Mirkovitch, V., Joffre, F. & Kappenberger, L. Intravascular Stents to Prevent Occlusion and Re-Stenosis after Transluminal Angioplasty. *New England Journal of Medicine* **316**, 701-706 (1987).
40. Rajendran, P. et al. The vascular endothelium and human diseases. *Int J Biol Sci* **9**, 1057-1069 (2013).
41. Gimbrone, M.A. Vascular endothelium: An integrator of pathophysiologic stimuli in atherosclerosis. *The American Journal of Cardiology* **75**, 67B-70B (1995).
42. Weintraub, W.S. The Pathophysiology and Burden of Restenosis. *The American Journal of Cardiology* **100**, S3-S9 (2007).
43. Bennett, M.R. IN-STENT STENOSIS: PATHOLOGY AND IMPLICATIONS FOR THE DEVELOPMENT OF DRUG ELUTING STENTS. *Heart* **89**, 218 (2003).
44. Hamasaki, S. & Tei, C. Effect of coronary endothelial function on outcomes in patients undergoing percutaneous coronary intervention. *Journal of Cardiology* **57**, 231-238 (2011).
45. Gori, T. Endothelial Function: A Short Guide for the Interventional Cardiologist. *International Journal of Molecular Sciences* **19** (2018).
46. Camenzind, E. A meta-analysis of first generation drug eluting stent programs. Program and abstracts from the World Congress of Cardiology 2006. *Program and abstracts from the World Congress of Cardiology 2006, Barcelona, 2-5 September 2006* (2006).
47. Nakamura, D. et al. Failure Mechanisms and Neoatherosclerosis Patterns in Very Late Drug-Eluting and Bare-Metal Stent Thrombosis. *Circulation: Cardiovascular Interventions* **9**, e003785 (2016).
48. Fuentes, L. et al. IVUS Findings in Late and Very Late Stent Thrombosis. A Comparison Between Bare-metal and Drug-eluting Stents. *Revista Española de Cardiología (English Edition)* **71**, 335-343 (2018).
49. Kereiakes Dean, J. et al. Stent Thrombosis in Drug-Eluting or Bare-Metal Stents in Patients Receiving Dual Antiplatelet Therapy. *JACC: Cardiovascular Interventions* **8**, 1552-1562 (2015).

50. Alraies, M.C., Darmoch, F., Tummala, R. & Waksman, R. Diagnosis and management challenges of in-stent restenosis in coronary arteries. *World J Cardiol* **9**, 640-651 (2017).
51. Kuramitsu, S., Shirai, S. & Ando, K. Mechanism of in-stent restenosis after second-generation drug-eluting stents (DES): is it different from bare-metal stents and first-generation DES? *J Thorac Dis* **7**, E599-602 (2015).
52. Ahanchi, S.S., Tsihlis, N.D. & Kibbe, M.R. The role of nitric oxide in the pathophysiology of intimal hyperplasia. *Journal of Vascular Surgery* **45**, A64-A73 (2007).
53. Wise, S.G., Waterhouse, A., Michael, P. & Ng, M.K.C. Extracellular Matrix Molecules Facilitating Vascular Biointegration. *Journal of Functional Biomaterials* **3**, 569-587 (2012).
54. van Hinsbergh, V.W.M. Endothelium—role in regulation of coagulation and inflammation. *Seminars in Immunopathology* **34**, 93-106 (2012).
55. Kuo, P.C. & Schroeder, R.A. The emerging multifaceted roles of nitric oxide. *Ann Surg* **221**, 220-235 (1995).
56. Kapadia, M.R. et al. Nitric oxide and nanotechnology: A novel approach to inhibit neointimal hyperplasia. *Journal of Vascular Surgery* **47**, 173-182 (2008).
57. Andukuri, A. et al. Evaluation of the effect of expansion and shear stress on a self-assembled endothelium mimicking nanomatrix coating for drug eluting stents in vitro and in vivo. *Biofabrication* **6**, 035019 (2014).
58. Li, M., Qian, M., Kyler, K. & Xu, J. Endothelial–Vascular Smooth Muscle Cells Interactions in Atherosclerosis. *Frontiers in Cardiovascular Medicine* **5** (2018).
59. Fan, L.-j. & Karino, T. Effect of serum concentration on adhesion of monocytic THP-1 cells onto cultured EC monolayer and EC-SMC co-culture. *Journal of Zhejiang University SCIENCE B* **9**, 623-629 (2008).
60. Jia, L.-X. et al. ER stress dependent microparticles derived from smooth muscle cells promote endothelial dysfunction during thoracic aortic aneurysm and dissection. *Clinical Science* **131**, 1287-1299 (2017).
61. Anderson, J.M. et al. Osteogenic differentiation of human mesenchymal stem cells synergistically enhanced by biomimetic peptide amphiphiles combined with conditioned medium. *Acta Biomaterialia* **7**, 675-682 (2011).
62. Gimbrone, M.A. & García-Cardena, G. Vascular endothelium, hemodynamics, and the pathobiology of atherosclerosis. *Cardiovascular Pathology* **22**, 9-15 (2013).

63. Lawson, C. & Wolf, S. ICAM-1 signaling in endothelial cells. *Pharmacological Reports* **61**, 22-32 (2009).
64. Woodfin, A., Voisin, M.-B. & Nourshargh, S. PECAM-1: A Multi-Functional Molecule in Inflammation and Vascular Biology. *Arteriosclerosis, Thrombosis, and Vascular Biology* **27**, 2514-2523 (2007).
65. Laszik, Z.G., Zhou, X.J., Ferrell, G.L., Silva, F.G. & Esmon, C.T. Down-Regulation of Endothelial Expression of Endothelial Cell Protein C Receptor and Thrombomodulin in Coronary Atherosclerosis. *The American Journal of Pathology* **159**, 797-802 (2001).
66. Chistiakov, D.A., Orekhov, A.N. & Bobryshev, Y.V. Vascular smooth muscle cell in atherosclerosis. *Acta Physiologica* **214**, 33-50 (2015).
67. Liu, R., Leslie, K.L. & Martin, K.A. Epigenetic regulation of smooth muscle cell plasticity. *Biochimica et Biophysica Acta (BBA) - Gene Regulatory Mechanisms* **1849**, 448-453 (2015).
68. Yurdagul, A., Jr., Finney, A.C., Woolard, Matthew D. & Orr, A.W. The arterial microenvironment: the where and why of atherosclerosis. *Biochemical Journal* **473**, 1281-1295 (2016).
69. Wang, G., Jacquet, L., Karamariti, E. & Xu, Q. Origin and differentiation of vascular smooth muscle cells. *The Journal of Physiology* **593**, 3013-3030 (2015).
70. Durgin, B.G. & Straub, A.C. Redox control of vascular smooth muscle cell function and plasticity. *Laboratory Investigation* **98**, 1254-1262 (2018).
71. Frismantiene, A., Philippova, M., Erne, P. & Resink, T.J. Smooth muscle cell-driven vascular diseases and molecular mechanisms of VSMC plasticity. *Cellular Signalling* **52**, 48-64 (2018).
72. Liu, M. & Gomez, D. Smooth Muscle Cell Phenotypic Diversity. *Arteriosclerosis, Thrombosis, and Vascular Biology* **39**, 1715-1723 (2019).
73. Shi, X. et al. A novel role of VEPH1 in regulating AoSMC phenotypic switching. *Journal of Cellular Physiology* **235**, 9336-9346 (2020).
74. Boersema, M. et al. Local Medial Microenvironment Directs Phenotypic Modulation of Smooth Muscle Cells After Experimental Renal Transplantation. *American Journal of Transplantation* **12**, 1429-1440 (2012).
75. Mammoto, A., Hendee, K., Muyleart, M. & Mammoto, T. Endothelial Twist1-PDGFB signaling mediates hypoxia-induced proliferation and migration of α SMA-positive cells. *Scientific Reports* **10**, 7563 (2020).

76. Zhang, Y. et al. Expression of platelet-derived growth factor in the vascular walls of patients with lower extremity arterial occlusive disease. *Exp Ther Med* **9**, 1223-1228 (2015).
77. Alexander, M.R., Murgai, M., Moehle, C.W. & Owens, G.K. Interleukin-1 β modulates smooth muscle cell phenotype to a distinct inflammatory state relative to PDGF-DD via NF- κ B-dependent mechanisms. *Physiological Genomics* **44**, 417-429 (2012).
78. Negishi, K. et al. An Myh11 single lysine deletion causes aortic dissection by reducing aortic structural integrity and contractility. *Scientific Reports* **12**, 8844 (2022).
79. Liu, R. et al. Ten-Eleven Translocation-2 (TET2) Is a Master Regulator of Smooth Muscle Cell Plasticity. *Circulation* **128**, 2047-2057 (2013).
80. Goikuria, H. et al. Characterization of Carotid Smooth Muscle Cells during Phenotypic Transition. *Cells* **7** (2018).
81. Zhao, X.N., Li, Y.N. & Wang, Y.T. in *Genet Mol Res*, Vol. 15 (2016).
82. Tse, K., Tse, H., Sidney, J., Sette, A. & Ley, K. T cells in atherosclerosis. *International Immunology* **25**, 615-622 (2013).
83. Maiuri, M.C. et al. Macrophage Autophagy in Atherosclerosis. *Mediators of Inflammation* **2013**, 584715 (2013).
84. Chen, F., Haigh, S., Barman, S. & Fulton, D. From form to function: the role of Nox4 in the cardiovascular system. *Frontiers in Physiology* **3** (2012).
85. Zhang, M. et al. Increased plasma BMP-2 levels are associated with atherosclerosis burden and coronary calcification in type 2 diabetic patients. *Cardiovascular Diabetology* **14**, 64 (2015).
86. Durham, A.L., Speer, M.Y., Scatena, M., Giachelli, C.M. & Shanahan, C.M. Role of smooth muscle cells in vascular calcification: implications in atherosclerosis and arterial stiffness. *Cardiovascular Research* **114**, 590-600 (2018).
87. Sun, Y. et al. Smooth Muscle Cell-Specific Runx2 Deficiency Inhibits Vascular Calcification. *Circulation Research* **111**, 543-552 (2012).
88. Grootaert, M.O.J. et al. Vascular smooth muscle cell death, autophagy and senescence in atherosclerosis. *Cardiovascular Research* **114**, 622-634 (2018).

89. Lim, W.-W. et al. Interleukin-11 is important for vascular smooth muscle phenotypic switching and aortic inflammation, fibrosis and remodeling in mouse models. *Scientific Reports* **10**, 17853 (2020).
90. Kini Annapoorna, S. et al. Intracoronary Imaging, Cholesterol Efflux, and Transcriptomes After Intensive Statin Treatment. *Journal of the American College of Cardiology* **69**, 628-640 (2017).
91. Bundy, R.E., Marczin, N., Birks, E.F., Chester, A.H. & Yacoub, M.H. Transplant atherosclerosis: Role of phenotypic modulation of vascular smooth muscle by nitric oxide. *General Pharmacology: The Vascular System* **34**, 73-84 (2000).
92. Saran, U., Foti, M. & Dufour, J.-F. Cellular and molecular effects of the mTOR inhibitor everolimus. *Clinical Science* **129**, 895-914 (2015).
93. Buccheri, D., Piraino, D., Andolina, G. & Cortese, B. Understanding and managing in-stent restenosis: a review of clinical data, from pathogenesis to treatment. *J Thorac Dis* **8**, E1150-e1162 (2016).
94. Cambien, B.a., Pomeranz, M., Millet, M.-A., Rossi, B. & Schmid-Alliana, A. Signal transduction involved in MCP-1-mediated monocytic transendothelial migration. *Blood* **97**, 359-366 (2001).
95. Gao, S. et al. Curcumin induces M2 macrophage polarization by secretion IL-4 and/or IL-13. *Journal of Molecular and Cellular Cardiology* **85**, 131-139 (2015).
96. Mantovani, A., Sica, A. & Locati, M. Macrophage Polarization Comes of Age. *Immunity* **23**, 344-346 (2005).
97. Shi, X. et al. Calcification in Atherosclerotic Plaque Vulnerability: Friend or Foe? *Frontiers in Physiology* **11** (2020).
98. Halwani, D.O., Anderson, P.G., Brott, B.C., Anayiotos, A.S. & Lemons, J.E. The role of vascular calcification in inducing fatigue and fracture of coronary stents. *Journal of Biomedical Materials Research Part B: Applied Biomaterials* **100B**, 292-304 (2012).
99. McDonald Robert, A. et al. Reducing In-Stent Restenosis. *Journal of the American College of Cardiology* **65**, 2314-2327 (2015).
100. Palomino-Morales, R., Torres, C., Perales, S., Linares, A. & Alejandre, M.J. Inhibition of extracellular matrix production and remodeling by doxycycline in smooth muscle cells. *Journal of Pharmacological Sciences* **132**, 218-223 (2016).
101. Kuzuya, M. & Iguchi, A. Role of Matrix Metalloproteinases in Vascular Remodeling. *Journal of Atherosclerosis and Thrombosis* **10**, 275-282 (2003).

102. Freitas-Rodríguez, S., Folgueras, A.R. & López-Otín, C. The role of matrix metalloproteinases in aging: Tissue remodeling and beyond. *Biochimica et Biophysica Acta (BBA) - Molecular Cell Research* **1864**, 2015-2025 (2017).
103. Olejarz, W., Łacheta, D. & Kubiak-Tomaszewska, G. Matrix Metalloproteinases as Biomarkers of Atherosclerotic Plaque Instability. *International Journal of Molecular Sciences* **21** (2020).
104. Allen, R.M. et al. LDL delivery of microbial small RNAs drives atherosclerosis through macrophage TLR8. *Nat. Cell Biol* **24**, 1701-1713 (2022).
105. Libby, P. The changing landscape of atherosclerosis. *Nature* **592**, 524-533 (2021).
106. Chen, J. et al. Recent Progress in in vitro Models for Atherosclerosis Studies. *Front. Cardiovasc. Med* **8**, 790529 (2021).
107. Geraili, A. et al. Controlling Differentiation of Stem Cells for Developing Personalized Organ-on-Chip Platforms. *Adv. Healthc. Mater.* **7**, 1700426 (2018).
108. Yang, J., Zhang, Y.S., Yue, K. & Khademhosseini, A. Cell-laden hydrogels for osteochondral and cartilage tissue engineering. *Acta Biomater.* **57**, 1-25 (2017).
109. Rogal, J., Zbinden, A., Schenke-Layland, K. & Loskill, P. Stem-cell based organ-on-a-chip models for diabetes research. *Adv. Drug Deliv. Rev.* **140**, 101-128 (2019).
110. Poussin, C. et al. 3D human microvessel-on-a-chip model for studying monocyte-to-endothelium adhesion under flow – application in systems toxicology. *ALTEX* **37**, 47-63 (2020).
111. Mallone, A., Stenger, C., Von Eckardstein, A., Hoerstrup, S.P. & Weber, B. Biofabricating atherosclerotic plaques: In vitro engineering of a three-dimensional human fibroatheroma model. *Biomaterials* **150**, 49-59 (2018).
112. Douglas, G. & Channon, K.M. The pathogenesis of atherosclerosis. *Medicine* **42**, 480-484 (2014).
113. Lee, J.H. et al. Emulating Early Atherosclerosis in a Vascular Microphysiological System Using Branched Tissue-Engineered Blood Vessels. *Adv. Biosyst.* **5**, 2000428 (2021).
114. Chen, Z. et al. Real-time observation of leukocyte–endothelium interactions in tissue-engineered blood vessel. *Lab Chip* **18**, 2047-2054 (2018).
115. Tillie, R.J.H.A., van Kuijk, K. & Sluimer, J.C. Fibroblasts in atherosclerosis: heterogeneous and plastic participants. *Curr. Opin. Lipidol.* **31** (2020).

116. Milutinović, A., Šuput, D. & Zorc-Pleskovič, R. Pathogenesis of atherosclerosis in the tunica intima, media, and adventitia of coronary arteries: An updated review. *Bosn J Basic Med Sci* **20**, 21-30 (2020).
117. Zeng, W., Guo, L., Xu, S., Chen, J. & Zhou, J. High-throughput screening technology in industrial biotechnology. *Trends Biotechnol* **38**, 888-906 (2020).
118. Castro, F. et al. Advances on colorectal cancer 3D models: The needed translational technology for nanomedicine screening. *Advanced Drug Delivery Reviews* **175**, 113824 (2021).
119. Tuveson, D. & Clevers, H. Cancer modeling meets human organoid technology. *Science* **364**, 952-955 (2019).
120. Yang, Y. et al. Identification of novel human high-density lipoprotein receptor up-regulators using a cell-based high-throughput screening assay. *SLAS Discov.* **12**, 211-219 (2007).
121. Xu, Y. et al. Suberanilohydroxamic acid as a pharmacological Kruppel-Like Factor 2 activator that represses vascular inflammation and atherosclerosis. *J. Am. Heart Assoc.* **6**, e007134 (2017).
122. Wang, X. et al. A small-molecule inhibitor of PCSK9 transcription ameliorates atherosclerosis through the modulation of FoxO1/3 and HNF1 α . *EBioMedicine* **52**, 102650 (2020).
123. Xu, S. et al. Endothelial Dysfunction in Atherosclerotic Cardiovascular Diseases and Beyond: From Mechanism to Pharmacotherapies. *Pharmacol. Rev.* **73**, 924 (2021).
124. Tousoulis, D., Oikonomou, E., Economou, E.K., Crea, F. & Kaski, J.C. Inflammatory cytokines in atherosclerosis: current therapeutic approaches. *Eur. Heart J.* **37**, 1723-1732 (2016).
125. Maguire, E.M., Pearce, S.W.A. & Xiao, Q. Foam cell formation: A new target for fighting atherosclerosis and cardiovascular disease. *Vascul. Pharmacol.* **112**, 54-71 (2019).
126. Yu, X.-H., Fu, Y.-C., Zhang, D.-W., Yin, K. & Tang, C.-K. Foam cells in atherosclerosis. *Clinica. Chimica. Acta* **424**, 245-252 (2013).
127. Chistiakov, D.A., Melnichenko, A.A., Myasoedova, V.A., Grechko, A.V. & Orekhov, A.N. Mechanisms of foam cell formation in atherosclerosis. *J. Mol. Med.* **95**, 1153-1165 (2017).
128. Fatkhullina, A.R., Peshkova, I.O. & Koltsova, E.K. The role of cytokines in the development of atherosclerosis. *Biochemistry* **81**, 1358-1370 (2016).

129. Georgakis, M.K. et al. Monocyte-chemoattractant protein-1 levels in human atherosclerotic lesions associate with plaque vulnerability. *Arterioscler. Thromb. Vasc. Biol.* **41**, 2038-2048 (2021).
130. Rus, H.G., Vlaicu, R. & Niculescu, F. Interleukin-6 and interleukin-8 protein and gene expression in human arterial atherosclerotic wall. *Atherosclerosis* **127**, 263-271 (1996).
131. Jiang, X. et al. Inflammasome-Driven Interleukin-1 α and Interleukin-1 β Production in Atherosclerotic Plaques Relates to Hyperlipidemia and Plaque Complexity. *JACC: Basic to Translational Science* **4**, 304-317 (2019).
132. Fernandez, D.M. et al. Single-cell immune landscape of human atherosclerotic plaques. *Nat. Med.* **25**, 1576-1588 (2019).
133. Frostegård, J. et al. Cytokine expression in advanced human atherosclerotic plaques: dominance of pro-inflammatory (Th1) and macrophage-stimulating cytokines. *Atherosclerosis* **145**, 33-43 (1999).
134. Nelken, N.A., Coughlin, S.R., Gordon, D. & Wilcox, J.N. Monocyte chemoattractant protein-1 in human atheromatous plaques. *J. Clin. Investig.* **88**, 1121-1127 (1991).
135. Mallat, Z. et al. Expression of Interleukin-10 in Advanced Human Atherosclerotic Plaques. *Arterioscler. Thromb. Vasc. Biol.* **19**, 611-616 (1999).
136. Liu, M. & Gomez, D. Smooth Muscle Cell Phenotypic Diversity. *Arterioscler. Thromb. Vasc. Biol.* **39**, 1715-1723 (2019).
137. Negishi, K. et al. An Myh11 single lysine deletion causes aortic dissection by reducing aortic structural integrity and contractility. *Sci. Rep.* **12**, 8844 (2022).
138. Goikuria, H. et al. in *Cells*, Vol. 7 (2018).
139. He, C. et al. PDGFR β signalling regulates local inflammation and synergizes with hypercholesterolaemia to promote atherosclerosis. *Nat. Commun* **6**, 7770 (2015).
140. Toma, I. & McCaffrey, T.A. Transforming growth factor- β and atherosclerosis: interwoven atherogenic and atheroprotective aspects. *Cell Tissue Res* **347**, 155-175 (2012).
141. Kuo, C.-L. et al. Cdkn2a is an atherosclerosis modifier locus that regulates monocyte/macrophage proliferation. *Arterioscler. Thromb. Vasc. Biol.* **31**, 2483-2492 (2011).
142. Motz, K. et al. Interferon- γ treatment of human laryngotracheal stenosis-derived fibroblasts. *JAMA Otolaryngology–Head & Neck Surgery* **143**, 1134-1140 (2017).

143. Davies, J.T. et al. Current and Emerging Uses of Statins in Clinical Therapeutics: A Review. *Lipid Insights* **9**, LPI.S37450 (2016).
144. Liu, Y., Yang, F., Zou, S. & Qu, L. in *Front Pharmacol*, Vol. 9 1520 (2018).
145. Li, Y., Tian, L., Sun, D. & Yin, D. Retracted: Curcumin ameliorates atherosclerosis through upregulation of miR-126. *J. Cell. Physiol.* **234**, 21049-21059 (2019).
146. S. Karimian, M., Pirro, M., P. Johnston, T., Majeed, M. & Sahebkar, A. Curcumin and Endothelial Function: Evidence and Mechanisms of Protective Effects. *Curr. Pharm. Des.* **23**, 2462-2473 (2017).
147. Fredman, G. & Tabas, I. Boosting Inflammation Resolution in Atherosclerosis: The Next Frontier for Therapy. *Am. J. Pathol.* **187**, 1211-1221 (2017).
148. Boca, S. et al. Nanoscale delivery systems for microRNAs in cancer therapy. *Cell. Mol. Life Sci.* **77**, 1059-1086 (2020).
149. Imashiro, C. & Shimizu, T. Fundamental technologies and recent advances of cell-sheet-based tissue engineering. *Int. J. Mol. Sci.* **22**, 425 (2021).
150. Holzapfel, G.A., Sommer, G., Gasser, C.T. & Regitnig, P. Determination of layer-specific mechanical properties of human coronary arteries with nonatherosclerotic intimal thickening and related constitutive modeling. *Am J Physiol Heart Circ Physiol* **289**, H2048-2058 (2005).
151. Depuydt, M.A.C. et al. Microanatomy of the Human Atherosclerotic Plaque by Single-Cell Transcriptomics. *Circ. Res.* **127**, 1437-1455 (2020).
152. Fernández-Ruiz, I. Promising anti-IL-6 therapy for atherosclerosis. *Nat. Rev. Cardiol* **18**, 544-544 (2021).
153. Ridker, P.M. et al. IL-6 inhibition with ziltivekimab in patients at high atherosclerotic risk (RESCUE): a double-blind, randomised, placebo-controlled, phase 2 trial. *The Lancet* **397**, 2060-2069 (2021).
154. Engelen, S.E., Robinson, A.J.B., Zurke, Y.-X. & Monaco, C. Therapeutic strategies targeting inflammation and immunity in atherosclerosis: how to proceed? *Nat. Rev. Cardiol* **19**, 522-542 (2022).
155. Ridker, P.M. et al. Antiinflammatory therapy with canakinumab for atherosclerotic disease. *N. Engl. J. Med.* **377**, 1119-1131 (2017).
156. Fernández-Ruiz, I. Anti-IL-1 β therapy lowers leukocyte supply and uptake in atherosclerosis. *Nat. Rev. Cardiol* **19**, 5-5 (2022).

157. Li, Y. et al. CD47-and Integrin $\alpha 4/\beta 1$ -Comodified-Macrophage-Membrane-Coated Nanoparticles Enable Delivery of Colchicine to Atherosclerotic Plaque. *Adv. Healthc. Mater.* **11**, 2101788 (2022).
158. Zhao, L. et al. Low-dose oral sirolimus reduces atherogenesis, vascular inflammation and modulates plaque composition in mice lacking the LDL receptor. *Br. J. Pharmacol* **156**, 774-785 (2009).
159. Yu, P. et al. Rosuvastatin Reduces Aortic Sinus and Coronary Artery Atherosclerosis in SR-B1 (Scavenger Receptor Class B Type 1)/ApoE (Apolipoprotein E) Double Knockout Mice Independently of Plasma Cholesterol Lowering. *Arterioscler. Thromb. Vasc. Biol.* **38**, 26-39 (2018).
160. Suh, J.S. et al. Rosuvastatin Prevents the Exacerbation of Atherosclerosis in Ligature-Induced Periodontal Disease Mouse Model. *Sci. Rep.* **10**, 6383 (2020).
161. Gao, S. et al. Curcumin ameliorates atherosclerosis in apolipoprotein E deficient asthmatic mice by regulating the balance of Th2/Treg cells. *Phytomedicine* **52**, 129-135 (2019).
162. Zhang, S., Zou, J., Li, P., Zheng, X. & Feng, D. Curcumin protects against atherosclerosis in apolipoprotein E-knockout mice by inhibiting toll-like receptor 4 expression. *J. Agric. Food Chem.* **66**, 449-456 (2018).
163. Song, Y. et al. Platelet membrane-coated nanoparticle-mediated targeting delivery of Rapamycin blocks atherosclerotic plaque development and stabilizes plaque in apolipoprotein E-deficient (ApoE^{-/-}) mice. *Nanomedicine: Nanotechnology, Biology and Medicine* **15**, 13-24 (2019).
164. Ma, J. et al. Expression of miRNA-155 in carotid atherosclerotic plaques of apolipoprotein E knockout (ApoE^{-/-}) mice and the interventional effect of rapamycin. *Int. Immunopharmacol* **46**, 70-74 (2017).
165. Jain, S.K., Rains, J., Croad, J., Larson, B. & Jones, K. Curcumin supplementation lowers TNF- α , IL-6, IL-8, and MCP-1 secretion in high glucose-treated cultured monocytes and blood levels of TNF- α , IL-6, MCP-1, glucose, and glycosylated hemoglobin in diabetic rats. *Antioxid. Redox Signal.* **11**, 241-249 (2009).
166. Zhao, J.-F. et al. Molecular mechanism of curcumin on the suppression of cholesterol accumulation in macrophage foam cells and atherosclerosis. *Mol Nutr Food Res.* **56**, 691-701 (2012).
167. Meng, N. et al. A novel curcumin-loaded nanoparticle restricts atherosclerosis development and promotes plaques stability in apolipoprotein E deficient mice. *J. Biomater. Appl.* **33**, 946-954 (2019).

168. Mogharrabi, M. et al. The effects of nanomicelle of curcumin on the matrix metalloproteinase (MMP-2, 9) activity and expression in patients with coronary artery disease (CAD): A randomized controlled clinical trial. *ARYA Atheroscler* **16**, 136-145 (2020).
169. Momtazi-Borojeni, A.A., Abdollahi, E., Nikfar, B., Chaichian, S. & Ekhlas-Hundrieser, M. Curcumin as a potential modulator of M1 and M2 macrophages: new insights in atherosclerosis therapy. *Heart Fail. Rev.* **24**, 399-409 (2019).
170. Cecconi, A. et al. Effects of colchicine on atherosclerotic plaque stabilization: a multimodality imaging study in an animal model. *J. Cardiovasc. Transl. Res.* **14**, 150-160 (2021).
171. Wang, L. et al. Colchicine-containing nanoparticles attenuates acute myocardial infarction injury by inhibiting inflammation. *Cardiovasc. Drugs Ther.* **36**, 1075-1089 (2022).
172. Chu, T. et al. miR-146a contributes to atherosclerotic plaque stability by regulating the expression of TRAF6 and IRAK-1. *Mol. Biol. Rep.*, 1-12 (2022).
173. Chen, J. et al. Angiogenic and Osteogenic Synergy of Human Mesenchymal Stem Cells and Human Umbilical Vein Endothelial Cells Cocultured on a Nanomatrix. *Sci. Rep.* **8**, 15749 (2018).